

FOREWORD


This report is submitted by ARDE, INC. in fulfillment of contract NAS 1-10028 and covers the period from June 1970 to September 1972. The principal investigator was Mr. David Gleich.

Prepared by:



David Gleich

Approved by:



A. D. Cozewith

FEASIBILITY STUDY OF APPLYING AN
ADVANCED COMPOSITE STRUCTURE TECHNIQUE
TO THE FABRICATION OF
HELICOPTER ROTOR BLADES

by

D. Gleich

ABSTRACT

Feasibility of applying prestressed composite material design and construction methods to helicopter blade spars was demonstrated by the successful fabrication of two (2) composite spar specimens having prestresses in the selected design range. The composite spar configuration utilized consists of a compressively prestressed high strength ARDEFORM 301 stainless steel liner over-wrapped with pretensioned S-994 fiberglass. High liner strength and toughness together with the prescribed prestresses and final sizing of the part are achieved by means of cryogenic stretch forming of the fiber wrapped composite spar at -320°F , followed by release of forming pressure and warm up to room temperature. The prestresses are chosen to provide residual compression in the metal liner under operating loads. This prestressed construction presents significant potential crack propagation and fatigue life property improvements leading to increased structural performance at advantageous stiffness-weight trade-offs.

CONTENTS

	<u>Page</u>
SUMMARY	vii
1.0 INTRODUCTION	1
2.0 DESCRIPTION OF THE PRESTRESSED COMPOSITE SPAR.	4
3.0 TECHNICAL DISCUSSION	6
3.1 Composite Spar Structural Design Considerations . . .	6
3.2 Fiber Wrap Pattern and Composite Spar Head Closure Shape	31
3.3 Composite Spar Fabrication.	34
3.4 Evaluation of Composite Spar Prestressed State. . . .	61
3.5 Composite Spar Testing Requirements	64
4.0 CONCLUSIONS AND RECOMMENDATIONS.	66
4.1 Conclusions	66
4.2 Recommendations	67
5.0 REFERENCES	68
6.0 APPENDICES	70
6.1 Appendix 1 - Symbols.	70
6.2 Appendix 2 - Composite Spar Structural Design	74
6.3 Appendix 3 - Composite Spar Prestresses	98
6.4 Appendix 4 - Composite Spar Test Specification. . . .	113
7.0 DISTRIBUTION LIST.	120

LIST OF FIGURES

<u>Figure No.</u>	<u>Description</u>	<u>Page</u>
1	Prestressed Composite Spar Configuration.	5
2	Plasticity Relations.	9
3	Heat #76235 Long Cylinder Design Chart.	10
4	Spar Body Cross-Section Shapes.	12
5	Fiber Wrap Angle versus Prestress	13
6	Schematic - Fiber Torsional Resistance.	17
7	Composite Spar Initial and Operating State Stresses	18
8	Fiberglass Fatigue Data	20
9	Fiberglass Creep and Stress Rupture Data.	21
10	Metal Liner Fatigue Data.	22
11	Constrictive-Wrap Buckling Strengths for Cylindrical Tubes	24
12	Constrictive-Overwrapped Cylinder-Typical Buckling Mode Shape.	25
13	Variation of Natural Frequency Ratio with Frequency Parameter	29
14	Spar Metal Liner Head Shape	33
15	Liner Preform	35
16	Spar Liner Body Section	36
17	Liner Components.	37
18	Boss to Head Weld	38
19	Completed Liner Preform	39
20	Hydrostretch Die.	41
21	Hydrostretch Die.	42
22	Annealing Fixture	43
23	Flat Plate Cross-Section Element Buckled Shape. . .	45
24	Initial Fiber Wrap Configuration (Dry Wrap on Wooden Model)	48
25	Wet Winding of Final Fiber Wrap Configuration (On Wooden Model)	49
26	Completed Wooden Model Wound Final Fiber Wrap Configuration	50

LIST OF FIGURES

<u>Figure No.</u>	<u>Description</u>	<u>Page</u>
27	Start of Fiber Wrapping of Composite Spar Metal Liner Preform	51
28	Beginning Stage - Fiber Wrapping of Composite Spar Metal Liner Preform.	52
29	Intermediate Stage - Fiber Wrapping of Composite Spar Metal Liner Preform.	53
30	Final Stage - Fiber Wrapping of Composite Spar Metal Liner Preform	54
31	Completed Fiber Wrapped Composite Spar Preform Assembly.	56
32	Schematic - Cryogenic Stretch Facility.	57
33	Cryogenic Stretch Die	58
34	Cryogenic Stretch Die Components.	59
35	Composite Spar Cryogenic Stretch in Die	60
36	Composite Spar Postform Assembly.	62
37	Composite Spar Preform and Postform Assemblies. . .	63
A-1	Idealized Spar Cross-Section Contour.	75
A-2	Fiber Geometry and Load Components.	76
A-3	Spar Strains.	78
A-4	Mohr's Circle of Strain	82
A-5	Fiber Wrap Angle Change	90
A-6	Spar Deflection and Springback.	101
A-7	Spar and Die Geometry	104
A-8	Gage Points for Axial Strain.	108

LIST OF TABLES

<u>Table No.</u>	<u>Description</u>	<u>Page</u>
1	Heat #76235 Chemistry	8
2	Composite Spar Design Point	28
3	Weight and Stiffness Comparisons - Composite Vs. Homogeneous Material Spars.	30
4	Fiber Wrap Data	99
5	Hoop Strain Computation	102
6	Spar Measurement Data Correlation	105
7	Axial Strain Measurement Data	109
8	Measured Fiber Angles After Cryostretch and Spring- back to Room Temperature.	110
9	Strain Data Correlation	111

FEASIBILITY STUDY OF APPLYING AN
ADVANCED COMPOSITE STRUCTURE TECHNIQUE
TO THE FABRICATION OF
HELICOPTER ROTOR BLADES

by

D. Gleich

SUMMARY

A design, fabrication and experimental program was performed to prove the feasibility of applying prestressed composite metal-fiber material design and fabrication techniques to helicopter blade spars. The composite spar construction utilized consists of a high strength ARDEFORM 301 stainless steel liner overwrapped with S-994 fiberglass and resin. The metal liner is prestressed in compression and the fibers are pretensioned. Cryogenic stretch forming the fiber wrapped composite spar, followed by release of forming load and warm up to room temperature, is used to achieve high strength and toughness in the ARDEFORM 301 liner, together with the prescribed prestresses as well as final sizing of the spar. The prestresses are selected to provide a residual compression in the metal liner under operating service loads. This precompression, coupled with the fiber tensioning can suppress crack growth and provide considerable improvement in fatigue life properties with advantageous stiffness - weight options.

Design, analysis, fiberwrap pattern and compatible spar head shape determination and verification as well as composite spar fabrication and evaluation efforts were conducted during the program. Two (2) prestressed composite spars were successfully fabricated and their prestressed states determined. The prestress levels achieved were in the desired design range.

1. INTRODUCTION

1.1 Background

There is a need for improved operational life, "fail-safe" and structurally efficient helicopter blades. Considerable work (1), (2) has been done in applying composite material structures to meet this need. Stiffnesses can be tailored at good weight trade-offs compared to homogeneous material designs and redundant load carrying capability is inherent in this type of configuration. These composite structures generally consist of fiber-metal constructions in which the fibers, imbedded in a shear-tie resin matrix, are attached to the metal primarily by shear-type connections. The operational life of this construction (measured by fatigue and crack propagation rate considerations) is a strong function of the effectiveness of these shear-ties.

Another approach to composite metal-fiber material construction, aimed at providing even more improved operational life and fail-safe helicopter blade structures, consists of a high-strength and tough compressively prestressed metal liner overwrapped with pretensioned fibers. No shear-ties between the fibers and metal liner or between the fibers themselves are required. The fiber resin matrix merely provides protection against fiber abrasion and moisture. By regulating the magnitude of the metal liner compressive prestress so that the liner is always in compression under operational blade loads, liner crack propagation is theoretically eliminated and significant improvements in liner fatigue life should be obtained. Fiber pretensioning also should provide substantial increases in fiber fatigue cycle life compared to zero pretensioned fibers at the same maximum service stress levels. Theoretical considerations indicate that these crack propagation and fatigue life advantages should be attained at good stiffness-weight trade-offs compared to homogeneous material and other types of composite material blades. Finally, in addition to inherent redundant load carrying capability and relatively high structural damping capacity, the option exists to provide even more enhanced torsional and bending stiffness properties at little weight penalty by winding additional fibers at selected angles subsequent to the prestressing operation.

The design principles and fabrication techniques for prestressed metal-fiber structures have been successfully verified by previous ARDE work (3), (4) for NASA with 13 1/2 inch

diameter spherical shapes used for pressure vessels and by in-house effort with cylindrical shapes. Significant improvements in structural efficiency were demonstrated compared to homogeneous material and other composite constructions^{(3), (5)}. The composite spherical vessels consisted of a high strength ARDEFORM⁽⁶⁾ 301 stainless steel liner overwrapped with S-994 fiberglass wet with resin. The high liner strength and toughness, together with the prescribed prestresses in the liner and fiberglass as well as final sizing, were imparted by means of cryogenic stretch forming at LN₂ temperature, followed by release of load and warm up to room temperature.

Because of the aforementioned significant improvements potentially possible, the primary goal of the current program was to verify the feasibility of applying the prestressed composite construction technology to helicopter blade spars. The excellent structural performance of the ARDEFORM 301 stainless steel liner overwrapped with S-994 fiberglass (together with established fabrication techniques) dictated the use of these materials in the feasibility demonstration. The basic requirement was to effectively transfer this technology (initially developed for spherical and cylindrical shapes) to the relatively long and slender helicopter blade spar shape. A subscale oval-shaped cross-section spar structural model about three (3) feet long was selected for the demonstration. This report presents a detailed summary and discussion of all work performed during the program.

1.2 Program Description

The program objective was to demonstrate the feasibility of applying prestressed composite material design and construction technology to helicopter blade spars. The goals were 1, to show the suitability of prestressed composite spar fabrication technology for constructing spars and 2, to verify the theoretically predicted operational life and weight-stiffness advantages obtainable by virtue of enhanced crack propagation and fatigue properties of the prestressed composite construction compared to homogeneous material spars.

The program consisted of a five (5) task effort which included determination of fiber wrap pattern and compatible spar head shape, design and fabrication of prestressed composite spars (including special tooling) and spar testing and evaluation. The program was subsequently revised by deleting spar static and fatigue testing in order to concentrate on prestressed composite spar fabrication effort.

Prestressed composite spar design and fabrication techniques were verified. Suitable spar fiber wrap patterns, together with compatible spar liner head closure shapes needed to properly anchor the fibers, were determined and verified. A definitive test specification and test program, including both static and fatigue tests, was prepared for spar testing and evaluation purposes. Program effort culminated in the successful fabrication of two (2) prestressed composite spars. The prestressed state of these spars was determined and verified by means of structural theory coupled with inspection data taken during and after spar fabrication. The two (2) completed spars are being held for subsequent testing and evaluation.

2. DESCRIPTION OF THE PRESTRESSED COMPOSITE SPAR

The prestressed composite spar model considered herein consists of a relatively long and slender inner ARDEFORM 301 stainless steel member (liner) overwrapped with S-994 fiberglass impregnated in a resin matrix, Figure 1. The fibers are wrapped at a constant helix angle, α , on the spar body as shown. The head closure shape is chosen so that the fibers, under constant tensions, are anchored on the head and body by bearing forces alone. No shear stresses in the resin are needed to hold the fibers in place. Threaded bosses (loading adapters) with central holes are provided at each closure end to facilitate pressurization during spar fabrication and to permit test load application.

During fabrication, the composite spar is immersed in and pressurized internally with liquid nitrogen which plastically stretches the spar to its final configuration and material properties. The plastic straining operation is done in a closed die which controls the final spar shape. The cryogenic stretch forming transforms the initially annealed ARDEFORM 301 austenitic stainless steel inner member to martensite, imparting high strength and toughness to the material. After release of the cryogenic stretch forming pressure, the stainless steel liner and the fiberglass spring back elastically to their unpressurized room temperature state with the fiberglass under initial tension and the metal under initial compression due to the difference in extensional stiffness of the two spar materials. In operation, both the fiberglass and metal resist the applied loads, with the metal member designed to always be in compression and the fiberglass always in tension.

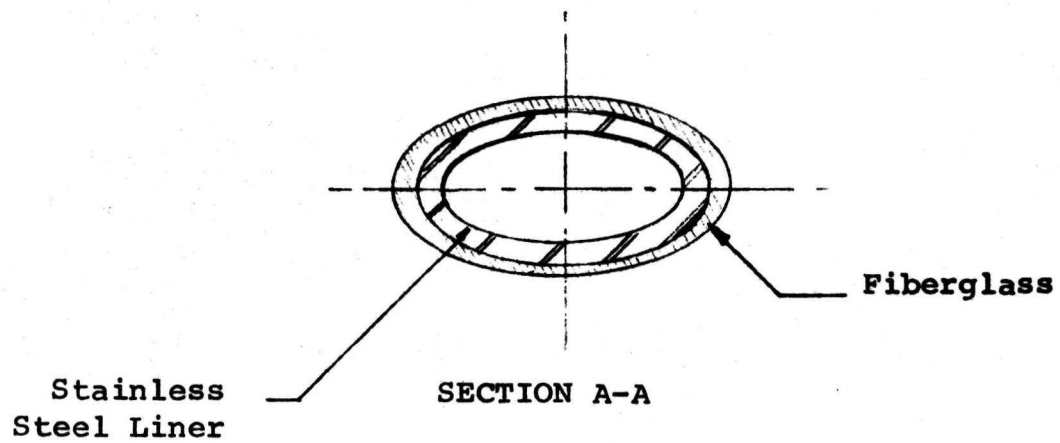
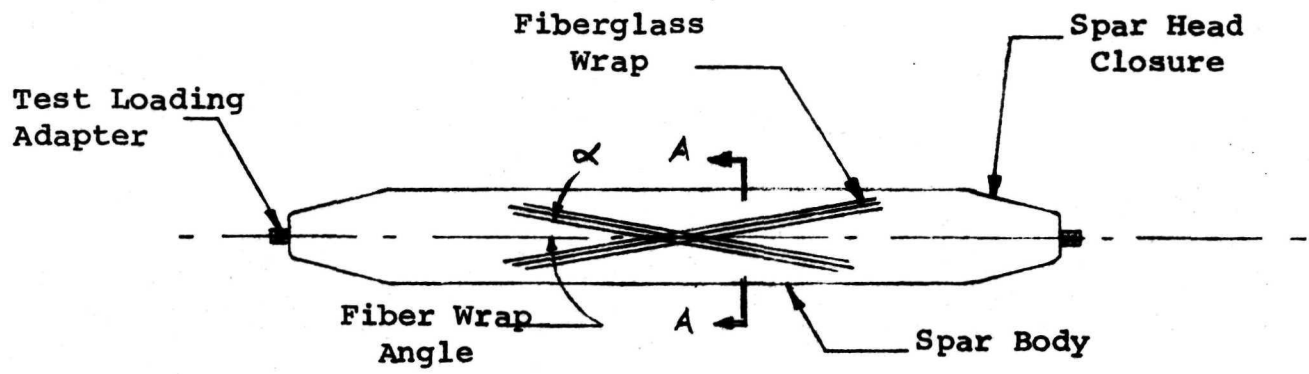


FIGURE 1
PRESTRESSED COMPOSITE SPAR CONFIGURATION

3. TECHNICAL DISCUSSION

This section describes the technical effort and accomplishments, presents analytic and test data, details problem areas encountered during the program and discusses approaches taken to resolve these problems. The program effort included determination of appropriate fiber wrap patterns and compatible spar model head closure shapes, design and fabrication of prestressed composite spar models (including required special tooling) as well as preparation of a test plan and test specification for static and fatigue testing of the spar models.

3.1 Composite Spar Structural Design Considerations

The basic design objective of the composite metal-fiberglass configurations considered herein is to provide a prestressed member with the high strength and tough liner always in compression and the fiberglass always in tension throughout the spar storage and operating life. In this manner, one should achieve significantly improved crack propagation and fatigue properties at good weight-stiffness trade-offs, as heretofore indicated. The structural design considerations related to achievement of this design goal are strongly coupled with spar fabrication. The magnitude of cryogenic strain imparted to the composite spar during fabrication not only determines the metal liner strength level, but together with fiberwrap angle, metal and fiberglass thickness and material properties, determines the spar prestresses and influences spar operational characteristics.

These factors are discussed in detail in this section. Calculations and data, given in the Appendices of Section 6, amplify and present additional depth of detail in support of this discussion.

3.1.1 Metal Liner Design Parameters

a) Heat Selection

An extra low interstitial ARDEFORM 301 stainless steel material (Heat 76235) was chosen for the metal liner. This heat has excellent properties and a successful application history including Apollo astronauts' backpack oxygen bottles, post boost propulsion tankage and Agena positive expulsion propellant tanks. Fatigue test data⁽⁷⁾, indicates

superior crack propagation and fatigue properties at the same weight compared to annealed 6Al-4Ti titanium. Heat 76235 data and chemistry is given in Table 1. Existing sheet stock, 28/30 mil initial thickness, was utilized in metal liner construction.

b) Room Temperature Design Yield Point and Corresponding Cryogenic Stress-Strain Requirements

As previously described, metal liner behavior and material properties are a function of the plastic strain imparted to it during the cryogenic stretch forming operation. Plasticity stress-strain relations, appropriate for tensile coupons, spheres and cylinders are given on Figure 2, assuming a Poisson's ratio of 1/2 compatible with an ideal plastic material. For an internally pressurized closed cylindrical membrane shape where the principle stress ratio is 2, (hoop stress twice the longitudinal stress) the plastic longitudinal (axial) strain is zero as indicated by the formulae of Figure 2. In order to minimize the effects of die friction during the cryogenic stretch forming operation, as well as simplify the composite spar design analysis, the spar metal liner body was accordingly designed as a cylindrical membrane.

Heat 76235 long cylinder design data, based on vessel tests are given on the curves of Figure 3. Here, nominal and true stresses are plotted versus final to initial radius ratio (equal to unity plus the nominal plastic hoop strain). S_1 and S_{1A} are the nominal room temperature .2% offset yield stresses (room temperature response) resulting from the cryogenic plastic hoop strains indicated. The aged stress values shown are for vessels aged at 800°F for 20 hours subsequent to cryogenic straining. σ_{1T} and S_2 are the true and nominal stresses at -320°F during cryogenic stretch forming at cryogenic stretch pressure p_s .

A conservative initial composite spar unaged liner design value of 220 ksi room temperature nominal .2% offset yield point was selected for composite spar feasibility demonstration purposes. As shown on Figure 3, a metal plastic cryogenic hoop strain of $\epsilon_{mo'} = 14.2\%$ and a true cryogenic hoop stress of $\sigma_{mo'} = 250$ ksi are required to produce this room temperature yield point value. The cryogenic longitudinal true stress in the "cylindrical" liner accordingly then is

$$\sigma_{mx'} = \frac{\sigma_{mo'}}{2} = 125 \text{ ksi.}$$

CERTIFICATE OF TEST

MANIFEST NO.

158

EASTERN STAINLESS STEEL COMPANY

DIVISION OF  CORPORATION

BALTIMORE, MARYLAND 21203

DATE 3-17-72

ARDE, INC.

ATTN: GENE BASILE
19 INDUSTRIAL AVE.

SHIP

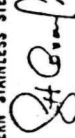
TO:

MAHEAH, N. J. 07430

MILL ORDER NO.		CUSTOMER ORDER NO.		SHIPPED VIA		CAR NUMBER		PREPAID COLLECT		F.O.B. BALTO. F.A																																																																											
S2-1993		14665		WILSON FT.				<input type="checkbox"/>		<input checked="" type="checkbox"/>																																																																											
ITEM	HEAT NO.	M.P.O. NO.	GAUGE	SIZE	S	DESCRIPTION	PLATES SOLLS SHEETS	GROSS	TARE	NET																																																																											
1	E76235	5818	48272	36-3/4 x 120	✓	Type 301-2D AES 252 STRETCHER LEVEL QUALITY SPV COATED BOTH SIDES AES 252 MECHANICAL TEST ONLY SKID BOX	54	2257	175	2092																																																																											
							54	2261	175	2086																																																																											
							51	2155	175	1980																																																																											
				SCRAP				470	90	380																																																																											
								7143	615	6528																																																																											
CUSTOMERS MATERIAL																																																																																					
HEAT NO.	TYPE	C	Mn	P	S	SI	Cr	Ni	Cu	Ti	Cl+Ta	Mo	CO																																																																								
E76235	301	0721	5602	2012	64	1707	777	27				30	.08																																																																								
<table border="1"> <thead> <tr> <th colspan="4">TRANSVERSE OR FRONT</th> <th colspan="4">LONGITUDINAL BACK OR AGED</th> <th colspan="2">HARDNESS</th> <th colspan="2">Bend</th> <th colspan="2">R/A</th> <th colspan="2">GR</th> <th colspan="2">C</th> <th colspan="2">S.R. LIFE</th> <th colspan="2">CODE</th> <th colspan="2">RATE</th> <th colspan="2">REMARKS</th> </tr> <tr> <th>HEAT NO.</th> <th>MPO</th> <th>TENSILE (X100)</th> <th>YIELD (X100)</th> <th>ELONG</th> <th>HARDNESS</th> <th>Bend</th> <th>R/A</th> <th>TENSILE (X100)</th> <th>YIELD (X100)</th> <th>ELONG</th> <th>HARDNESS</th> <th>Bend</th> <th>R/A</th> <th>GR</th> <th>C</th> <th>S.R. LIFE</th> <th>CODE</th> <th>RATE</th> <th>REMARKS</th> </tr> </thead> <tbody> <tr> <td>E76235</td> <td>P5818</td> <td>972</td> <td>410</td> <td>5630</td> <td>T66</td> <td>G</td> <td></td> <td></td> <td></td> <td></td> <td></td> <td></td> <td></td> <td></td> <td></td> <td></td> <td></td> <td></td> <td></td> <td></td> <td></td> <td></td> <td></td> <td></td> <td></td> </tr> </tbody> </table>														TRANSVERSE OR FRONT				LONGITUDINAL BACK OR AGED				HARDNESS		Bend		R/A		GR		C		S.R. LIFE		CODE		RATE		REMARKS		HEAT NO.	MPO	TENSILE (X100)	YIELD (X100)	ELONG	HARDNESS	Bend	R/A	TENSILE (X100)	YIELD (X100)	ELONG	HARDNESS	Bend	R/A	GR	C	S.R. LIFE	CODE	RATE	REMARKS	E76235	P5818	972	410	5630	T66	G																			
TRANSVERSE OR FRONT				LONGITUDINAL BACK OR AGED				HARDNESS		Bend		R/A		GR		C		S.R. LIFE		CODE		RATE		REMARKS																																																													
HEAT NO.	MPO	TENSILE (X100)	YIELD (X100)	ELONG	HARDNESS	Bend	R/A	TENSILE (X100)	YIELD (X100)	ELONG	HARDNESS	Bend	R/A	GR	C	S.R. LIFE	CODE	RATE	REMARKS																																																																		
E76235	P5818	972	410	5630	T66	G																																																																															

WE CERTIFY THAT THE CHEMICAL ANALYSIS AND MECHANICAL TEST RESULTS APPLYING ON THE ABOVE NUMBER ARE CORRECT AND TRUE TO THE BEST OF OUR KNOWLEDGE AND BELIEF.

EASTERN STAINLESS STEEL CO.



METALLURGICAL DEPT.

MARCH 22, 1972

SWORN AND SUBSCRIBED TO BEFORE ME



NOTARY PUBLIC

G - HUEY AVERAGE RATE.

E - PROPERTY BEFORE FORMING.

A - INTERGRAN CORR TESTS SATIS.

C - MAGNETIC PERM LESS THAN 1.02

PLASTICITY RELATIONS APPLIED TO TENSILE COUPONS AND INTERNALLY PRESSURIZED SPHERES AND CYLINDERS					
Line No.	Type of Member		Tensile Coupon Axial	Sphere Pressure	Cylinder Pressure
	Loading				
1	Given principal stresses, in terms of Maximum Principal Stress,	σ_1 σ_2 σ_3	σ_1 0 0	σ_1 σ_1 0	σ_1 $\frac{1}{2}\sigma_1$ 0
2	Stress invariant in terms of maximum principal stress, $\sigma^* = \sqrt{\frac{1}{2}[(\sigma_1 - \sigma_2)^2 + (\sigma_2 - \sigma_3)^2 + (\sigma_3 - \sigma_1)^2]}$		σ_1	σ_1	$\frac{\sqrt{3}}{2}\sigma_1$
3	Principal stresses in terms of stress invariant,	σ_1 σ_2 σ_3	$\sigma^* = \sigma_N(1+\epsilon)$ 0 0	$\sigma^* = \sigma_N(1+\epsilon)^3$ $\sigma^* = \sigma_N(1+\epsilon)^3$ 0	$\frac{2}{\sqrt{3}}\sigma^*$ $\frac{1}{\sqrt{3}}\sigma^*$ 0
4	Invariant stress-strain relation		$\sigma^* = D\epsilon^*$	$\sigma^* = D\epsilon^*$	$\sigma^* = D\epsilon^*$
5	Strain invariant relation		$\epsilon^* = \sqrt{\frac{2}{3}} \sqrt{\epsilon_1^2 + \epsilon_2^2 + \epsilon_3^2}$		
6	Principal strains in terms of stress invariant $D\epsilon_1 = \sigma_1 - .5(\sigma_2 + \sigma_3)$ $D\epsilon_2 = \sigma_2 - .5(\sigma_3 + \sigma_1)$ $D\epsilon_3 = \sigma_3 - .5(\sigma_1 + \sigma_2)$		σ^* $-.5\sigma^*$ $-.5\sigma^*$	$.5\sigma^*$ $.5\sigma^*$ $-\sigma^*$	$\frac{1}{2}\sqrt{3}\sigma^*$ 0 $-\frac{1}{2}\sqrt{3}\sigma^*$
7	Principal strains in terms of invariant strain, $\epsilon_1 = \ln L/L_0$ or $\epsilon_1 = \ln R/R_0$ $\epsilon_2 = \ln w/w_0$ $\epsilon_3 = \ln t/t_0$		ϵ^* $-.5\epsilon^*$ $-.5\epsilon^*$	$.5\epsilon^*$ $.5\epsilon^*$ $-\epsilon^*$	$\frac{1}{2}\sqrt{3}\epsilon^*$ 0 $-\frac{1}{2}\sqrt{3}\epsilon^*$

$\sigma_1^*, \sigma_1, \sigma_2, \sigma_3$ are true stresses (load \div actual area)
 σ_N^*, σ_2^N are nominal stresses (load \div initial area)
 $\epsilon_1^*, \epsilon_1, \epsilon_2, \epsilon_3$ are true strains (logarithmic)
 ϵ = engineering (nominal) strain,
 uniaxial or hoop strain as appropriate
 L_0, R_0, t_0, w_0 = initial values of length, radius, thickness, width
 L, R, t, w = final value of length, radius, thickness, width

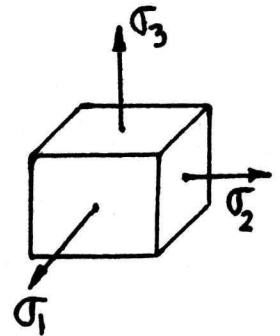


FIGURE 2

HEAT 76235 LONG CYLINDER DESIGN CHART

—○— BASED ON ACTUAL CYLINDER TESTS

12-27-67

--- APPROXIMATED FROM UNIAXIAL DATA

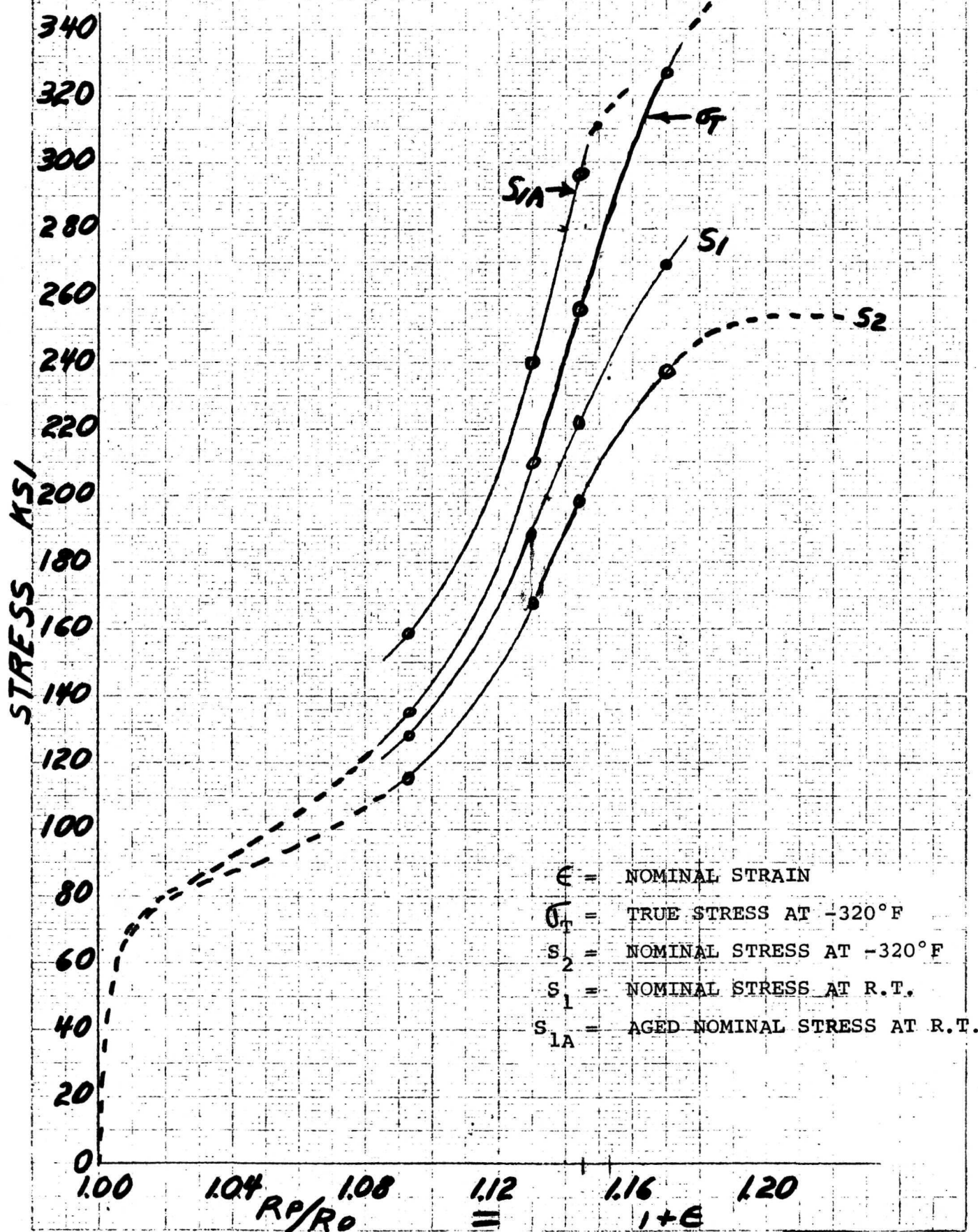


FIGURE 3

3.1.2 Spar Body Cross-Sectional Shape

A constant cross-section thin-walled spar body shape was selected for this composite spar feasibility demonstration program. The initial cross-section shape, Figure 4a, chosen primarily for simplicity and ease of fabrication, consisted of flat plate top and bottom elements joined together by hemispherical side members. The spar body cross-section shape was subsequently modified by changing the flat plate elements to curved members as shown on Figure 4b.

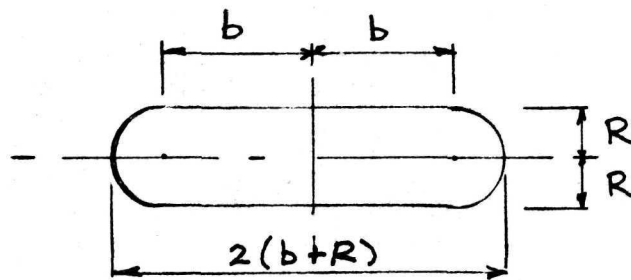
Initial .030/.028 inch thick metal liner preform cross-section dimensions selected (size prior to hydrostatic and cryogenic stretch forming) were $R = 1 \frac{1}{2}$ inches, $b = \frac{15}{16}$ inches, corresponding to overall cross-sectional dimensions of $4 \frac{7}{8}$ inches wide by 3 inches deep, see Figure 4a. Metal liner preform dimensions prior to fiber wrap for the revised cross-section (Figure 4b) were taken as,

$$R_A = 2.55", \quad R_B = 1.53", \quad 2b = 1.91, \quad \beta = 30^\circ.$$

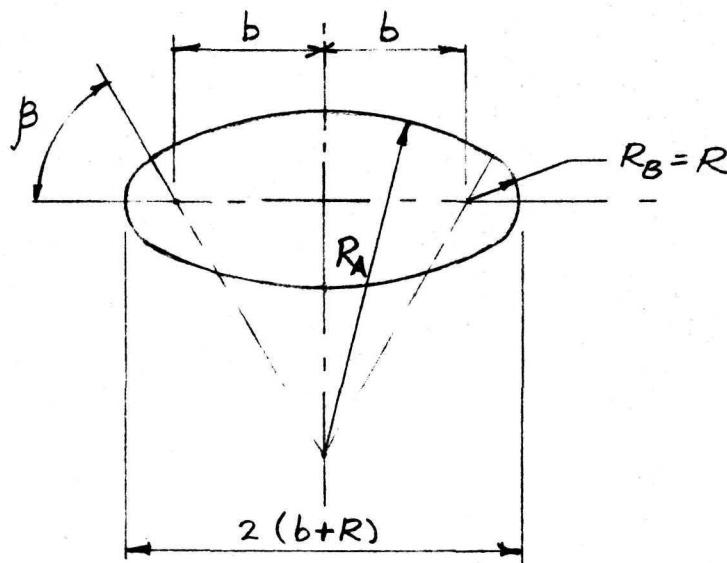
This cross-sectional sizing was achieved by means of room temperature hydrostatically stretch forming the initial cross-sectional shape (Figure 4a) in a closed die as discussed in Section 3.3.

3.1.3 Fiber Wrap Angle Versus Prestress

For a given cryogenic plastic hoop strain and accompanying metal liner stresses during stretch forming at liquid nitrogen temperature, equilibrium, geometric and strain compatibility requirements relate fiberglass and metal prestresses and fiber to metal thickness ratio to initial fiber wrap angle as shown on Figure 5. As the fiber wrap angle increases, prestresses increase and relative fiberglass thickness required decreases. This occurs because, for a given fiberglass thickness, as the fiber wrap angle is increased, more fiberglass hoop extensional stiffness is available to resist metal liner elastic springback from the cryogenic plastic hoop strain state. Maximum fiberglass hoop stiffness occurs at fiber wrap angle, $\alpha = \frac{\pi}{2}$, corresponding to a pure hoop fiber wrap. For our application, rather shallow fiber wrap angles (15° - 20°) are required in order to produce relatively high longitudinal compressive prestresses in the metal to overcome the effects of spar longitudinal tensile service loads (centrifugal plus



(a) Initial Spar Body Cross-Section Shape



(b) Revised Spar Body Cross-Section Shape

FIGURE 4
SPAR BODY CROSS-SECTION SHAPES

FIBER WRAP ANGLE VS. PRESTRESS

(for $\sigma_{MH} = 250$ Ksi and $\sigma_{ML} = 125$ Ksi)

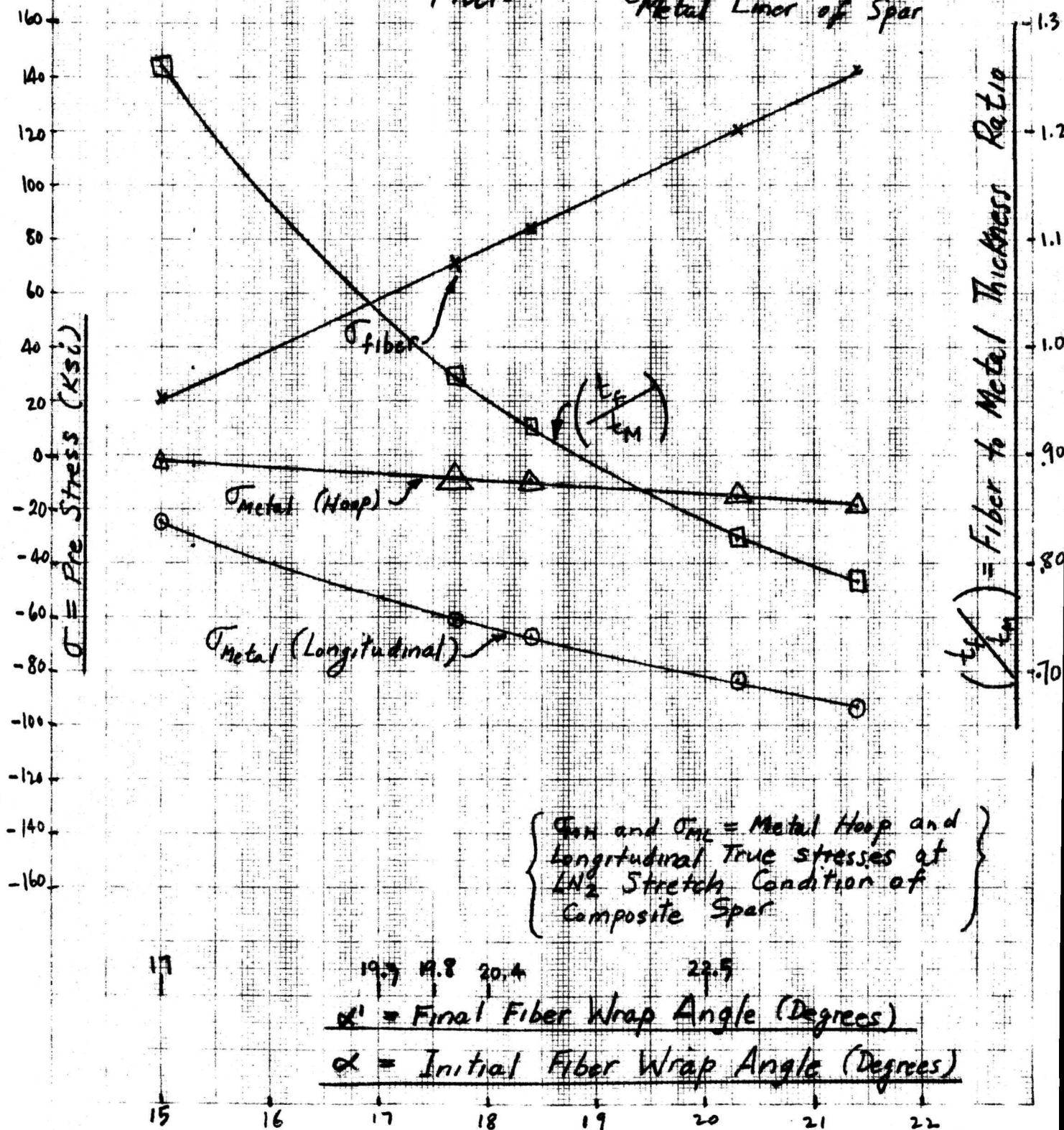


FIGURE 5

bending).

The plastic strains imparted to the fiber-wrapped composite spar metal liner during cryogenic stretch forming change the initial dimensions of the body. These dimensional changes produce an increase of fiber wrap angle from its initial wrapped value, α , to its final value, α' , as shown on figure 5. The initial and final fiber wrap angles are related by geometric and strain compatibility requirements to the fiber and metal strains as detailed in Appendix 2 and set forth in equations (1), (2) below. Here, ϵ_f is the fiber strain and ϵ_θ and ϵ_x are metal hoop and longitudinal strains, respectively.

$$\sin^2 \alpha = \frac{(\epsilon_f - \epsilon_x)(2 + \epsilon_x + \epsilon_f)}{(\epsilon_\theta - \epsilon_x)(2 + \epsilon_x + \epsilon_\theta)} \quad (1)$$

$$\sin \alpha' = \frac{(1 + \epsilon_\theta)}{(1 + \epsilon_f)} \times \sin \alpha \quad (2)$$

The numerical results given on figure 5 are based on the metal liner design point discussed in section 3.1.1b ($\epsilon_{Me}' = .145$, $\sigma_{Me}' = 250$ ksi, $\sigma_{MX}' = 125$ ksi) together with other appropriate metal and fiberglass material properties and the assumption that the width of the spar cross-section is large compared to its depth. Detailed derivations and calculations are given in Appendix 2, Section 6.2.

3.1.4 Bending, Axial and Torsional Load Effects for Composite Spar

3.1.4.1 Bending Effects

In composite spar construction, both the metal liner and fiberglass contribute to the bending stiffness and resist the applied bending moments. The relative bending stiffnesses per unit mass and bending stresses in fiber and metal, derived in Appendix 2, are given below in equations (3) to (5). For purposes of comparison, the results have been normalized on a thin-walled reference datum homogeneous metal spar with thickness t_0 , Young's Modulus E_M , density ρ_M , bending stress σ_{b0} and bending stiffness per unit mass \hat{K}_{b0} , having the same shape and perimeter and subjected to the same bending moments as the composite spar.

$$\frac{(\text{Bending Stiffness per unit mass})_{\text{composite}}}{(\text{Bending Stiffness per unit mass})_{\text{homogeneous}}} = \frac{\hat{k}_{bc}}{\hat{k}_{bo}} = \frac{\left(\frac{t_m}{t_o}\right) + \left(\frac{t_f}{t_o}\right) \left(\frac{E_f \cos^4 \alpha'}{E_m}\right)}{\lambda + (1-\lambda) \left\{ \left(\frac{t_m}{t_o}\right) + \left(\frac{t_{fc}}{t_o}\right) \left(\frac{E_f}{E_m}\right) \right\}} \quad (3)$$

$$\frac{(\text{Bending Stress in metal})_{\text{composite}}}{(\text{Bending Stress})_{\text{homogeneous}}} = \frac{\sigma_{mb}}{\sigma_{bo}} = \frac{(t_o/t_m)}{1 + \left(\frac{t_f}{t_m}\right) \left(\frac{E_f \cos^4 \alpha'}{E_m}\right)} \quad (4)$$

$$\frac{(\text{Bending Stress in fibers})_{\text{composite}}}{(\text{Bending Stress})_{\text{homogeneous}}} = \frac{\sigma_{fb}}{\sigma_{bo}} = \left(\frac{\sigma_{mb}}{\sigma_{bo}}\right) \left(\frac{E_f \cos^4 \alpha'}{E_m}\right) \quad (5)$$

Here t_f and t_{fc} are the fiber structural and composite thicknesses, respectively, t_m the metal thickness of the composite, ρ_c the composite density of the fibers (glass + resin), λ the blade non-structural mass ratio parameter, E_f the fiber Young's Modulus and the other terms are as previously defined. The composite fiber thickness and density are related to μ , the resin fraction by weight, as indicated in (6) and (7).

$$t_{fc} = \frac{t_f}{\text{Volume ratio of glass}} = \frac{t_f (1 + 1.19\mu)}{(1-\mu)} \quad (6)$$

$$\rho_{fc} = \frac{1}{10.9 + 12.96\mu} \quad (7)$$

3.1.4.2 Direct Axial Load Effects

The centrifugal tensile load is also shared by the metal and fiber components of the composite spar. Utilizing again, a reference datum homogeneous metal spar, we have (see Appendix 2) the direct axial stress ratios.

$$\frac{(\text{metal direct axial stress})_{\text{composite}}}{(\text{direct axial stress})_{\text{homogeneous}}} = \frac{\sigma_{mx}}{\sigma_{ox}} = \frac{1 + \left(\frac{t_{fc}}{t_m}\right) \left(\frac{\rho_{fc}}{\rho_m}\right) + \left(\frac{\lambda}{1-\lambda}\right) \left(\frac{t_o}{t_m}\right)}{\left\{ 1 + \left(\frac{t_f}{t_m}\right) \left(\frac{E_f \cos^4 \alpha'}{E_m}\right) \right\} \left(\frac{1}{1-\lambda}\right)} \quad (8)$$

$$\left(\frac{\sigma_{fx}}{\sigma_{ox}}\right) = \left(\frac{\sigma_{mx}}{\sigma_{ox}}\right) \left(\frac{E_f \cos^4 \alpha'}{E_m}\right) \quad (9)$$

3.1.4.3 Torsional Load Effects

When a torque is applied to the composite spar, the metal liner twists and the fibers are subjected to extensional strains. The resisting torque at a composite spar axial station contributed by the metal component is thus the shear flow times its lever arm integrated around the cross-section circumference the same as for a homogeneous metal spar. The extensional strains in the fibers produce incremental fiber loads in the pretensioned fibers; additional tension in those fibers which lengthen and reduction in tension in those fibers

which shorten as a result of the twist. As sketched in Figure 6, the tangential components of these incremental fiber loads times their lever arms, summed up around the cross-section, constitute the resisting torque contributed by the fibers. The fibers thus act like the inclined truss members of an engine mount which transmit the applied torque between their braced end planes by alternate tensile and compressive loads.

As derived in Appendix 2, the torsional stiffness ratio per unit mass of the composite compared to the reference homogeneous metal blade is given by,

$$\frac{k_{Tc}/M_c}{k_{To}/M_o} = \frac{\hat{k}_{Tc}}{\hat{k}_{To}} = \frac{\left\{ \left(\frac{t_M}{t_o} \right) + \left(\frac{I_{pM}}{GJ} \right) \left[\sigma_{Mx} + E_f \left(\frac{t_f}{t_M} \right) \left(\tan \alpha' \sin \alpha' + \frac{\sigma_f}{E_f} \cos \alpha' \right) \right] \right\}}{\left\{ \lambda + (1 - \lambda) \left[\left(\frac{t_M}{t_o} \right) + \left(\frac{\rho_{fc}}{\rho_M} \right) \left(\frac{t_{fc}}{t_o} \right) \right] \right\}} \quad (10)$$

In most cases, the term $\frac{\sigma_f}{E_f} \cos \alpha'$, the order of the fiber strain σ_f , may be neglected by comparison with the other terms in the numerator of (10) and we have the simplified relation,

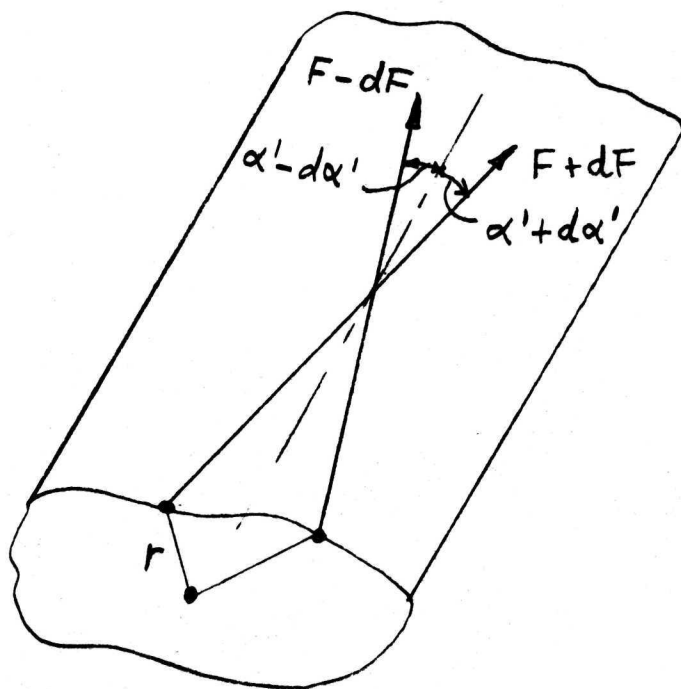
$$\frac{\hat{k}_{Tc}}{\hat{k}_{To}} \approx \frac{\left\{ \left(\frac{t_M}{t_o} \right) + \left(\frac{I_{pM}}{GJ} \right) \left[\sigma_{Mx} + E_f \frac{t_f}{t_M} \tan \alpha' \sin \alpha' \right] \right\}}{\left\{ \lambda + (1 - \lambda) \left[\left(\frac{t_M}{t_o} \right) + \left(\frac{\rho_{fc}}{\rho_M} \right) \left(\frac{t_{fc}}{t_o} \right) \right] \right\}} \quad (10A)$$

In (10), (10A), I_{pM} is the polar moment of inertia of the metal member of the composite cross-section, GJ the torsional stiffness of the reference homogeneous metal spar cross-section, σ_{Mx} the metal axial stress defined by (8), and the other quantities are as heretofore defined.

3.1.5 Fatigue, Creep and Buckling Considerations

a) General

In selecting composite spar prestress levels (tension in the fiberglass and compression in the metal liner) as well as operating stress state (see Figure 7) consideration must be given to limitations imposed by fatigue, creep and buckling effects. The fiberglass should not fail by fatigue when it cycles between its tensile prestress σ_{fi} , and operating tension, σ_o , nor should significant creep deformation and/or stress rupture occur while it is at prestress σ_{fi} for long periods of time during storage or other non-operating modes. The metal liner compressive prestress, σ_{mi} , should be low enough to preclude elastic buckling, compressive yielding



$$T_f = \sum dT_f = \sum r \{ (F + dF) \sin(\alpha' + d\alpha') - (F - dF) \sin(\alpha' - d\alpha') \}$$

FIGURE 6

SCHEMATIC - FIBER TORSIONAL RESISTANCE

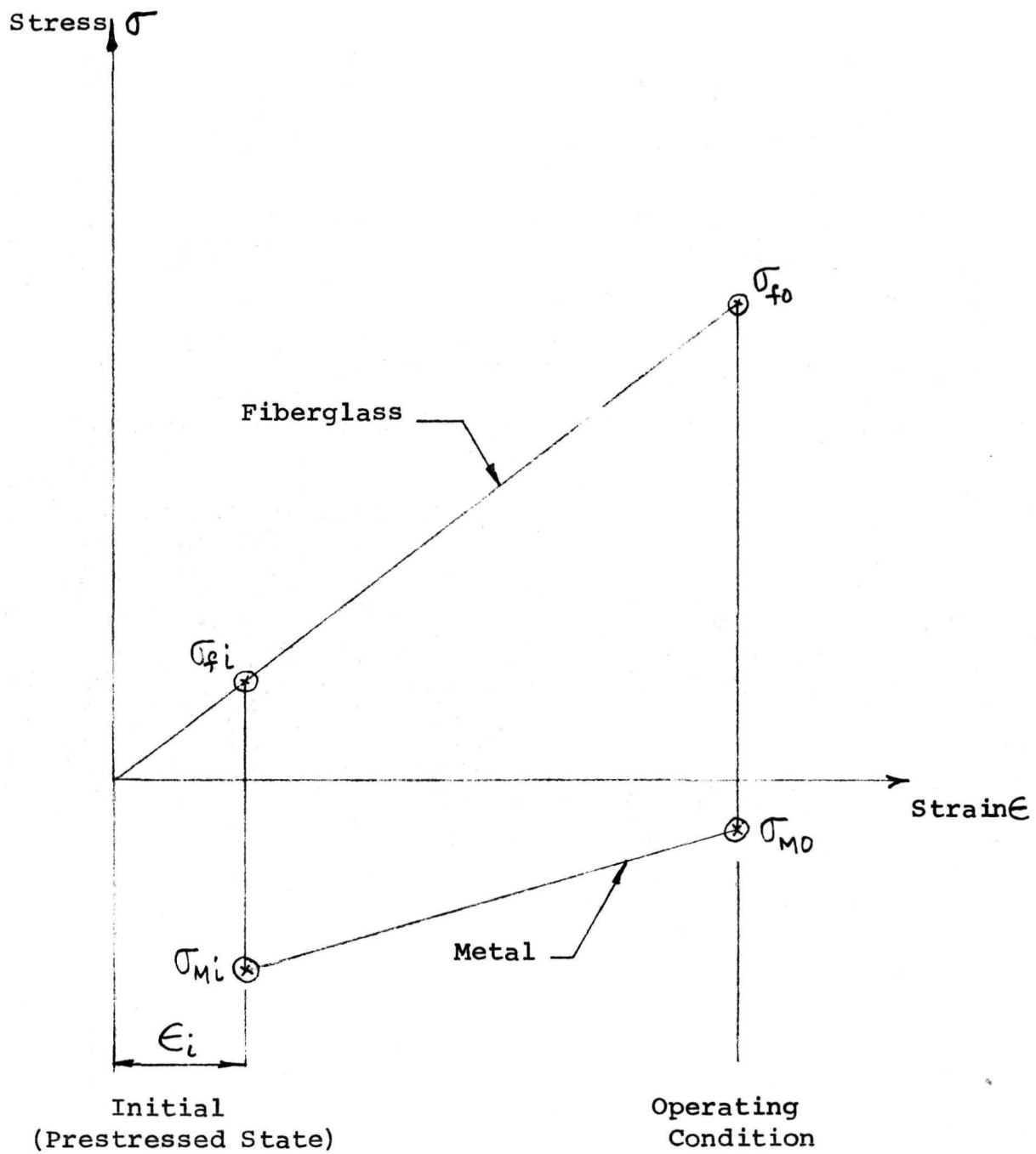


FIGURE 7
COMPOSITE SPAR INITIAL AND
OPERATING STATE STRESSES

or fatigue failure. At the same time, as previously discussed in Section 3.1, σ_{mi} should be large enough to maintain a residual compression in the metal liner under operating conditions in order to achieve enhanced crack propagation and fatigue properties.

b) Fiberglass Fatigue and Creep Values

Some fatigue and creep data for fiberglass are given on Figure 8 and 9. Emphasizing the conservative ASME Boiler and Pressure Vessel fatigue requirement (based on 15 years of data accumulation) we project for design purposes and infinite fiberglass fatigue life at a maximum of 1/4 of its ultimate tensile strength (for $R = \sigma_{min} = 0$) as sketched on Figure 8. Similarly, (see Figure 9) σ_{max} we project an infinite creep life at 1/3 the fiberglass ultimate tensile strength.

c) Liner Fatigue Data

Metal liner material fatigue data (ARDEFORM 301 stainless steel - Heat 76235) based on vessel and uniaxial tests are given on Figure 10. Infinite cycle life is at a maximum stress of 46% of ultimate tensile strength (for $R = 0$) corresponding to 30% of ultimate tensile strength (for $R = -1$), completely reversed bending).

d) Liner Buckling and Compressive Yielding Limitations

Compressive yielding of the liner leading to plastic buckling because of reduction in Young's Modulus is to be avoided at both the metal liner prestressed and operating load states. For design purposes, the liner .2% compressive yield point is taken conservatively at 2/3 the .2% tensile yield point (reference 4). However, fatigue allowables, with absolute values much less than 2/3 tensile yield point (See Figure 10) as well as the design objective of a small residual compression under operating load conditions, preclude liner yielding governing the design. The critical liner structural design limitation, therefore, is elastic buckling due to its compressive prestress.

The critical buckling loads for fiber overwrapped shells are much greater than the critical buckling loads for the same shells without the constrictive fiber overwrap. Test data for hoop fiberwrapped cylindrical tubes

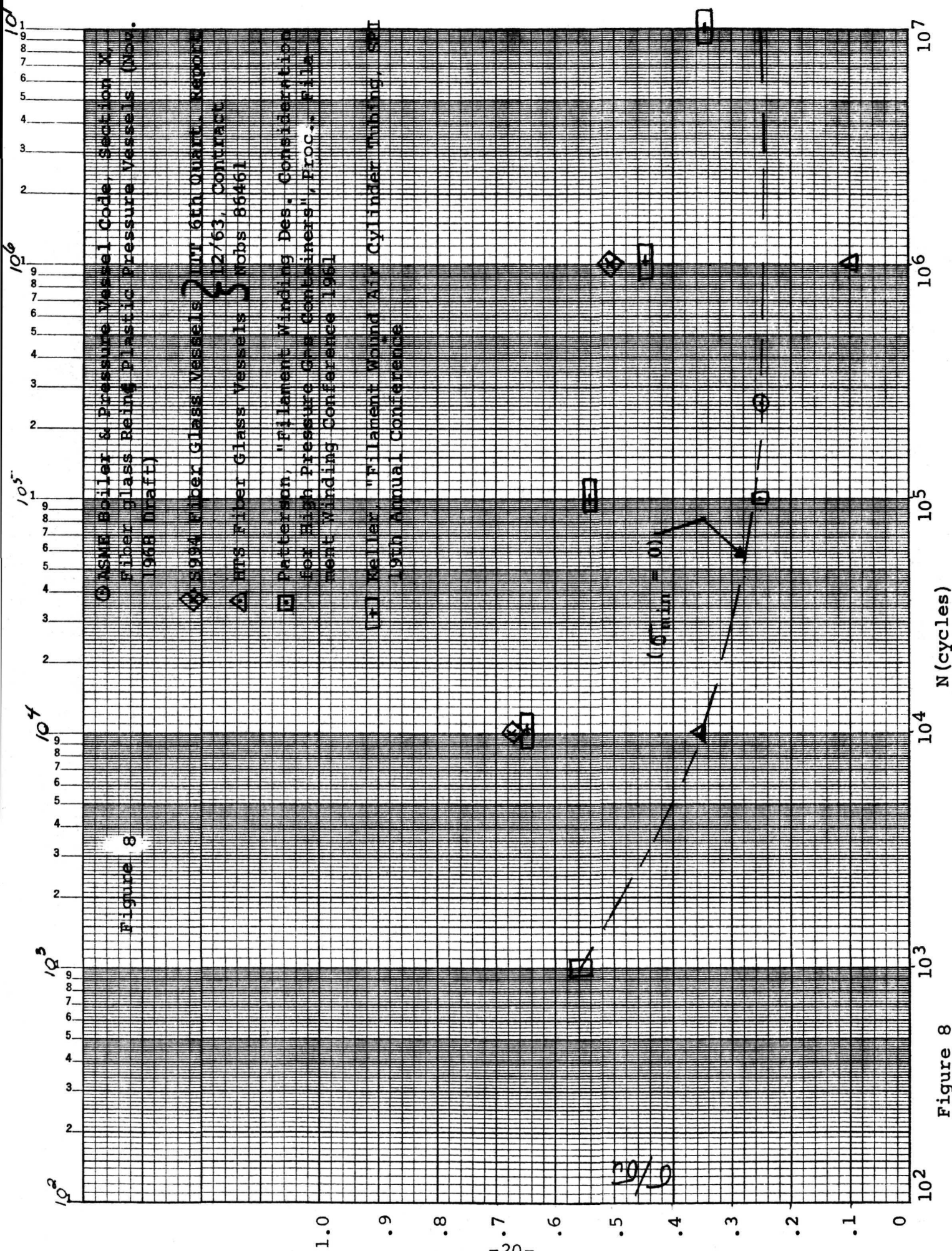


Figure 8

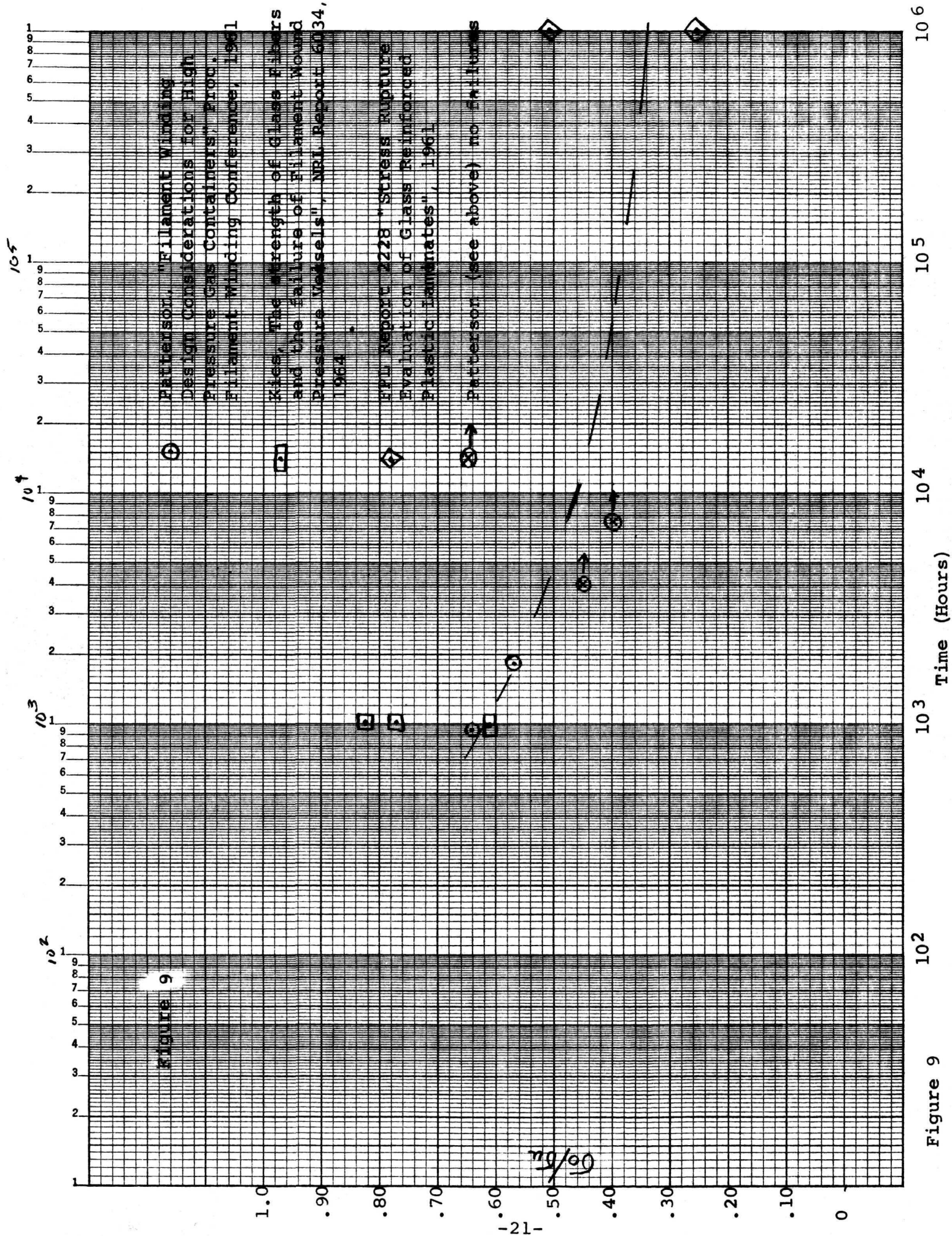


Figure 9

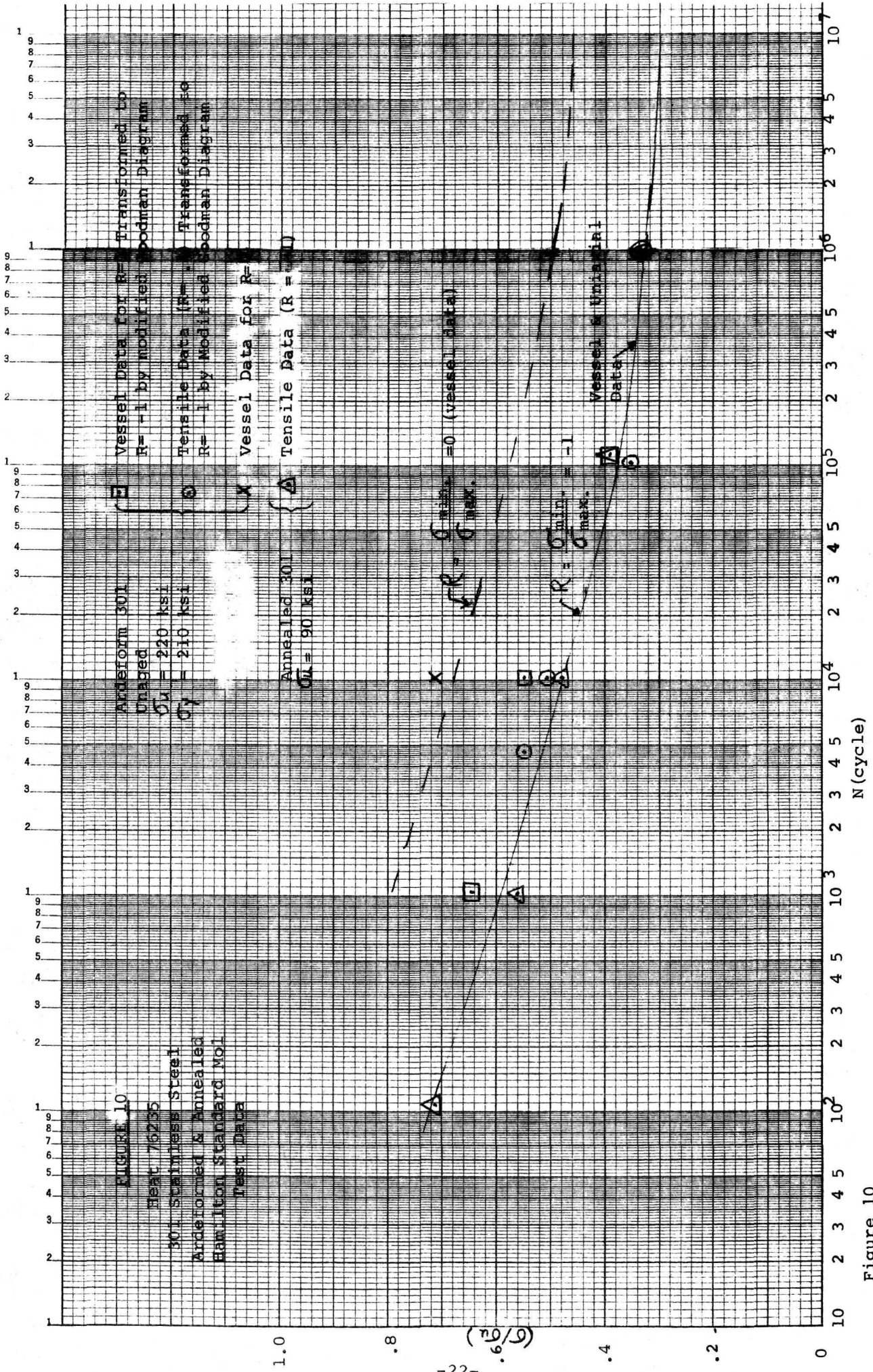


Figure 10

(references 5, 8) as well as a comparison with classical (unwrapped) cylindrical tube buckling strength, are given on Figure 11. Many orders of magnitude improvement in buckling strength due to the fiber overwrap is evident. ARDE has similar experience with fiber overwrapped spherical shells (reference 4) wherein compressive prestresses with absolute values as high as 72% of tensile yield point at a diameter-to-thickness ratio of 650 were applied without liner buckling occurring. The physical reason for this phenomenon is that the fibers act like spring supports which resist shell displacement under the applied compressive loads and thus rule out the "classical" buckling mode shapes consisting of outward as well as inward displacements. Local inward crisp-like buckling mode shapes, as sketched on Figure 12, have been observed. These buckling mode shapes correspond to much higher energy (or compressive load levels) compared to the classical buckling mode shapes. It is anticipated that similar improvement in composite spar fiber - overwrapped metal shell buckling loads will be experienced, even for the rather small helix angle fiber wrap pattern used for the composite spar configuration. Test data at various diameter-to-thickness ratios are needed to determine the magnitude of the improvement in buckling loads.

Buckling problems were encountered during fabrication of the composite spar metal liner preform. At this stage of the fabrication, no constrictive fiber overwrap is available to increase the buckling resistance. The unwrapped flat plate element of the initial spar body cross-sectional configuration (Figure 4a) buckled during the hydrostatic stretching operation in a closed die. Internal pressure of room temperature water was used to plastically deform the metal liner and force it up against the die. Upon removal of the pressure, the metal liner sprung back elastically from the die. The elastic spring back strains of the stiffer hemispherical shell portions of the cross-section, joined to the flat plate elements, compressed the flat plate members. It was "easier" for the flat plate to buckle than to shorten as a sheet in order to preserve deflection and strain continuity at the hemisphere - flat plate junctions of the cross-section. The preform buckling problem was solved by replacing the flat plate portions of the cross-section by curved elements as sketched in Figure 4b. Since actual spar cross-sections are composed of all curved members it would appear that metal liner preform

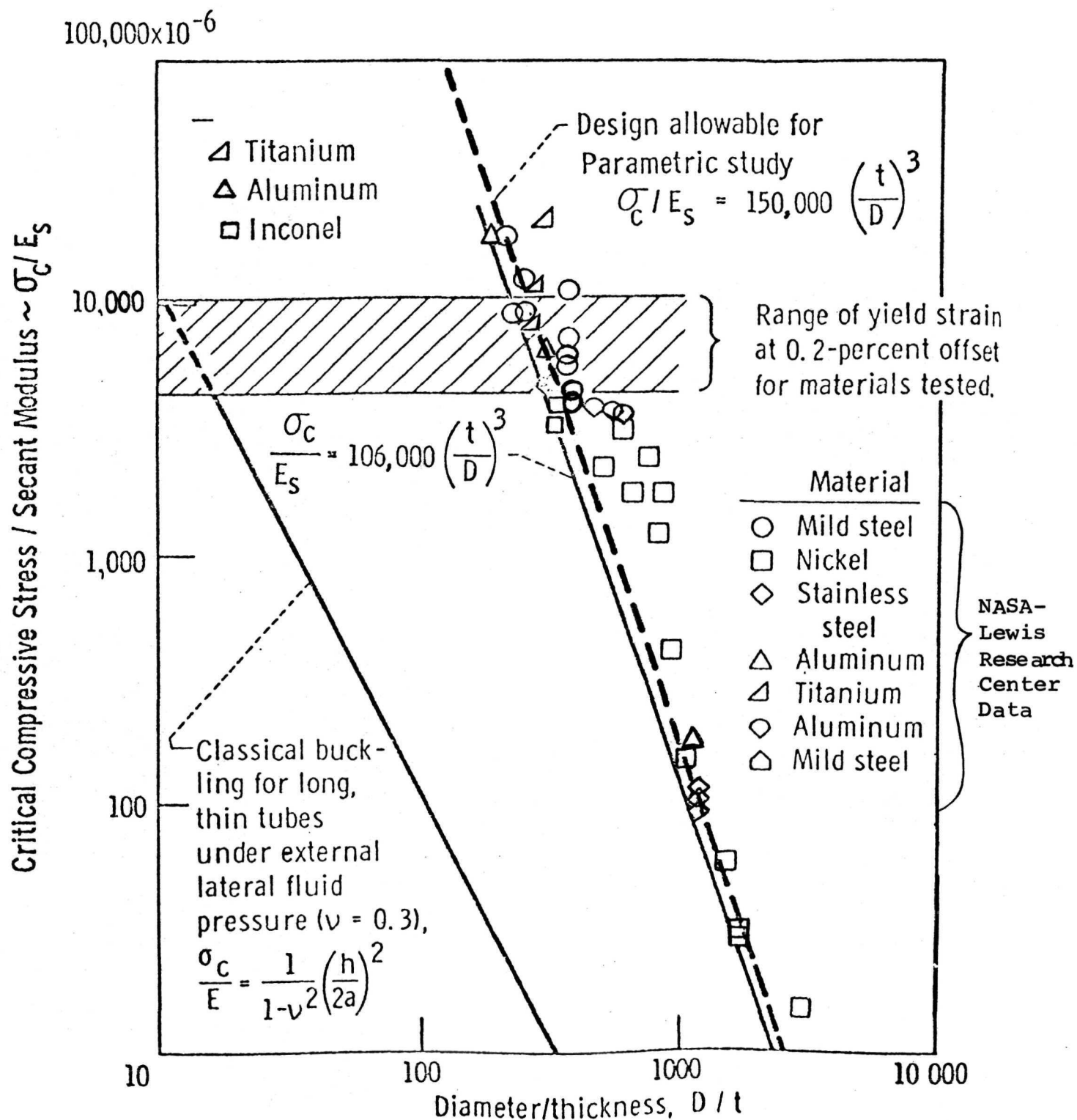
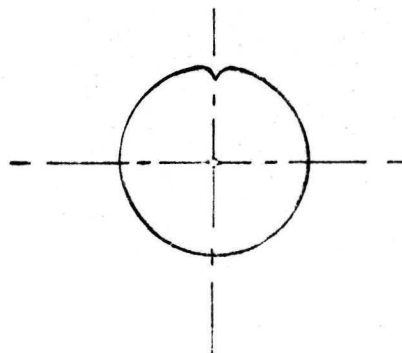
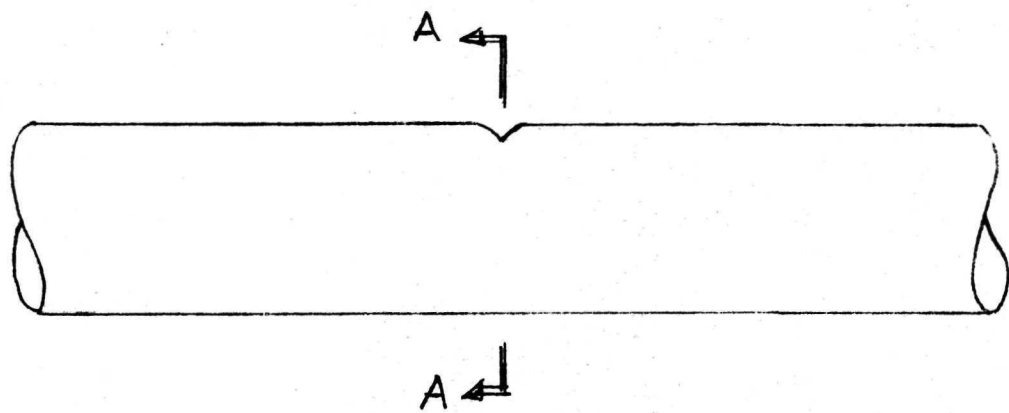


FIGURE 11

CONSTRUCTIVE-WRAP BUCKLING STRENGTHS
FOR CYLINDRICAL TUBES



SECTION A-A

FIGURE 12
CONSTRICTIVE OVERWRAPPED CYLINDER -
TYPICAL BUCKLING MODE SHAPE

buckling can be prevented in this matter. The preform buckling problem, including tests to determine its cause, is discussed in more detail in Section 3.3.

3.1.6 Selection of Composite Spar Design Point

A reference homogeneous metal spar was selected as a comparison datum design. Discussions with helicopter companies, reference 9, led to the choice of operating design stress range of 24 ± 17 ksi, compatible with a high structural efficiency homogeneous ferritic steel material spar. Test data, references 10, 11, show that the alternating stress level with a mean compressive stress can be considerably greater in magnitude than the conventional endurance limit value for completely reversed bending. Since the metal liner of the composite spar will always be in compression, a design value of ± 34 ksi (twice the homogeneous spar alternating stress allowable) was selected as the allowable bending stress for the composite spar metal liner.

Several composite spar design configurations, together with the reference homogeneous metal spar, are given in Table 2. The $17\ 1/2^\circ$ initial fiber wrap composite spar configuration was selected as the design point for the composite spars to be built and tested. The metal design operating stress range (-35.3 ± 34 ksi) always keeps the metal liner in compression with the lowest prestresses. Creep, buckling or fatigue problems are not anticipated at the stress values shown, as discussed in Section 3.1.5. In addition to anticipated crack propagation and fatigue property advantages, it is seen from Table 2 that the selected composite spar design configuration only weighs 49% of the homogeneous material reference spar.

The selected composite spar design point ($17\ 1/2^\circ$ initial fiber wrap angle) is indicated on Figure 5. The metal liner true hoop stress ($\sigma_T = \sigma_{M\theta} = 250$ ksi) during cryogenic stretch forming to 14.2% plastic hoop strain, compatible with the selected design point, is shown on Figure 3. These figures have been previously discussed in Sections 3.1.3. Detailed calculations are given in Appendix 2.

3.1.7 Weight and Stiffness Comparisons for Composite Versus Homogeneous Material Spars

Numerical calculations are presented in Appendix 2 to illustrate the type of favorable weight and weight-stiffness trade-offs offered by the composite prestressed spar compared to a homogeneous material spar. The 17 1/2° initial fiber wrap angle design point given in Table 2 and a simplified thin-walled rectangular cross-section of width four times its depth as well as a blade non-structural weight of 23% were chosen for the illustrative calculations. Formulas used have previously been discussed in Section 3.1.4.

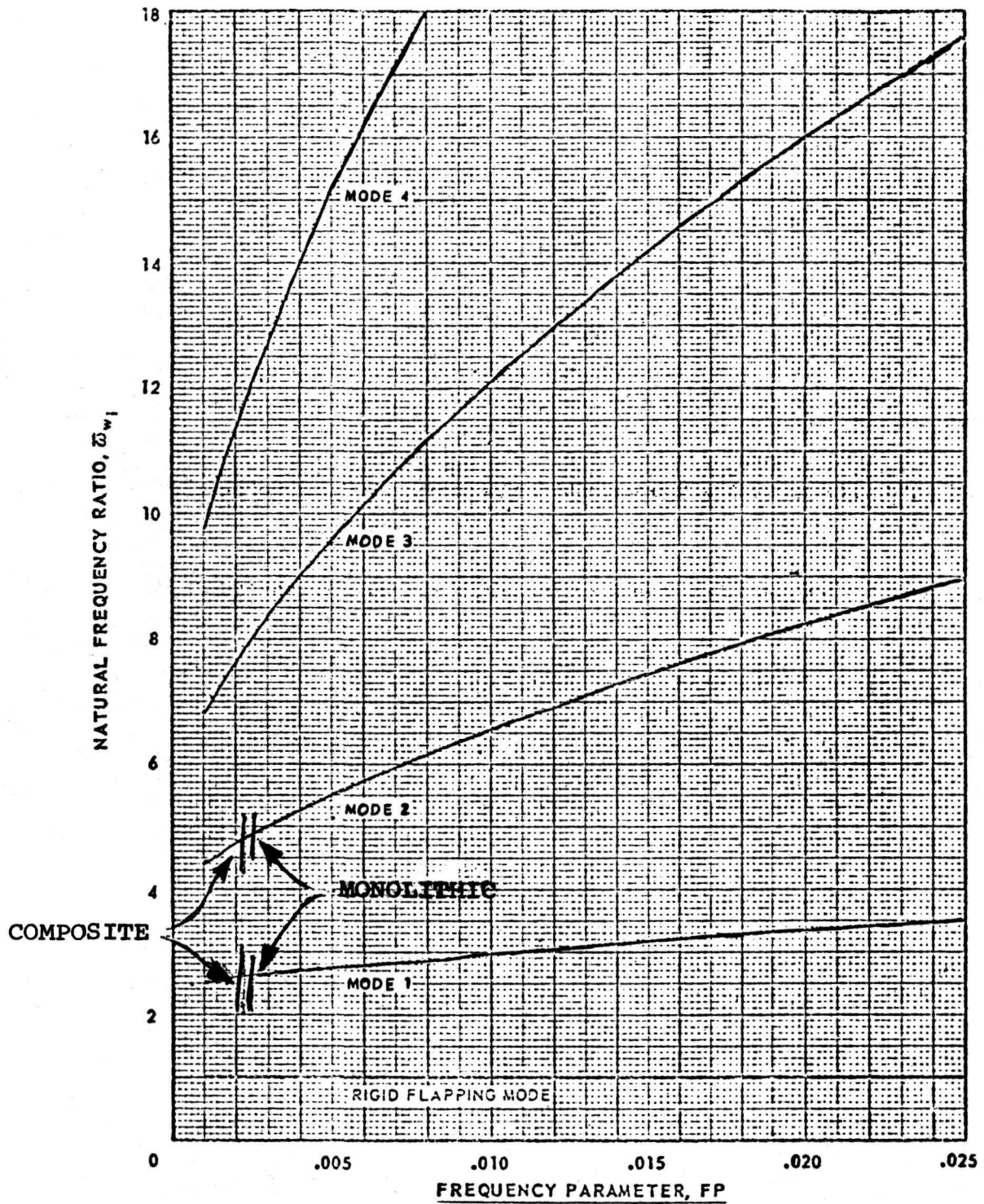
The numerical results given in Table 3 show that the composite spar at 49% the structural weight has bending and torsional stiffnesses of 50% and 54%, respectively, compared to the reference homogeneous metal spar. However, the bending and torsional stiffnesses per unit mass, significant for spar dynamic response and static deflection considerations, are 89% and 96%, respectively, of the homogeneous metal reference spar value. Using a frequency parameter, $FP = \left(\frac{EI}{M} \right) \times \frac{1}{l^4 r^2}$, of .0025 as

typical for homogeneous material blades (reference 12) we obtain a composite spar frequency parameter, $FP = .85 \times .0025 = .0021$. Here, EI/M is the spar bending rigidity per unit mass and l and r are the blade length and angular velocity, respectively. Figure 13, taken from reference 12, shows that the change in the blade flapwise bending natural frequency ratios is negligible due to the reduced bending rigidity per unit mass of the composite spar. The effect of the reduced composite spar torsional rigidity on torsional natural frequencies is also small.

The static "droop" of the composite spar blade would be increased due to the greater bending deflection under its own weight. At .89 relative bending rigidity per unit mass, the static deflection of composite construction blade would be about 11% greater than the reference homogeneous blade. To overcome this and/or "tune" the rigidities of the composite spar blade for dynamic response advantages, extra fibers at various helix angles may be added to the composite spar subsequent to the cryogenic stretching and prestressing operation. This will increase spar rigidities at only a small weight increase. Shallow helix angle fibers

TABLE 2 - COMPOSITE SPAR DESIGN POINT

Item	Homogeneous Metal Spar (Reference Spar)	Composite Spar (Metal and Fiberglass)		
α = Initial Fiber Wrap Angle ($^{\circ}$)	----	17	17.5	18
α' = Final Fiber Wrap Angle ($^{\circ}$)	----	19.3	19.8	20.4
σ'_{Mx} = Metal Longitudinal Prestress (ksi)	----	-52	-59	-64
σ'_f = Fiber Prestress (ksi)	----	58	67	76
t_f/t_M = Fiber to Metal Thickness Ratio	----	1.035	.987	.95
Relative Metal Thickness	1.0	.359	.361	.363
Relative Spar Weight	1.0	.498	.496	.493
Metal Centrifugal Stress (ksi)	24	23.6	23.7	23.8
Fiber Centrifugal Stress (ksi)	----	9.3	9.2	9.1
Metal Allowable Bending Stress (ksi)	± 17	± 34	± 34	± 34
Fiber Bending Stress (ksi)	----	± 13.4	± 13.2	± 13.1
Metal Operating Stress Range (ksi)	24 ± 17	-28 ± 34	-35.3 ± 34	-40.2 ± 34
Fiber Operating Stress Range (ksi)	----	67.3 ± 34	76.2 ± 13.2	85.1 ± 13.1



(a) Articulated blades.

FIGURE 13

VARIATION OF NATURAL FREQUENCY RATIO WITH FREQUENCY PARAMETER

TABLE 3 - WEIGHT & STIFFNESS COMPARISONS
PRESTRESSED COMPOSITE VERSUS
HOMOGENEOUS MATERIAL SPARS

	CONFIGURATION		
	(1)	(2)	(3)
	Basic 17 1/2° wrap angle design point (see Table 2)	Basic + 100% added 15° bending fibers + 30% added 45° torsion fibers	Same as configuration (2) except added fibers are high modulus graphite material. Graphite fibers added
Parameter Ratio: <u>Composite Spar</u> <u>Homogeneous Spar</u>	All glass		
Bending Stiffness	.50	.67	1.17
Torsional Stiffness	.54	.95	2.20
Structural Mass	.49	.67	.65
Total Blade Mass*	.56	.68	.66
Bending Stiffness/Unit Mass*	.89	.99	1.77
Torsional Stiffness/Unit Mass*	.96	1.41	3.32

* Includes effect of 23% added non-structural blade mass.

are effective in bending, and inefficient in torsion and conversely, larger helix angle fibers are effective in torsion and inefficient in bending. The use of high Young's Modulus fibers, high modulus graphite for example, are especially effective in increasing spar bending and torsional rigidity per unit mass.

Table 3 shows the effect of adding 100% of basic fiber thickness 15° bending fibers and 30% of basic fiber thickness 45° torsion fibers to the datum 17 1/2° fiberglass wrap angle prestressed composite spar design configuration. For the all-fiberglass construction, configuration 2 of Table 3, at only 68% of the homogeneous blade mass, the torsional and bending stiffnesses per unit mass are increased to 1.41 and .99, respectively from their corresponding composite datum values of .96 and .89. Use of high modulus graphite material for the added fibers (Young's Modulus increased by factor of four, reference 13) has an even more pronounced effect on rigidity per unit mass. As set forth under configuration 3 in Table 3, at only 66% of datum homogeneous material blade mass, torsional and bending stiffness per unit mass have been significantly increased to 3.32 and 1.77 times the reference homogeneous spar values. Even more optimum weight - stiffness trade-offs are possible. Each configuration can be "tailored" to the particular application.

3.2 Fiber Wrap Pattern and Head Closure Shape

The fiber wrap pattern used for the composite prestressed spar was a constant helix angle winding configuration. Rather shallow helix angles, \mathcal{L} , with respect to the spar longitudinal axis were required for high longitudinal precompression in the metal liner. As discussed in Section 3.1, $\mathcal{L} = 17\ 1/2^\circ$ initial fiber wrap angle was selected for the composite spar configurations built during the program.

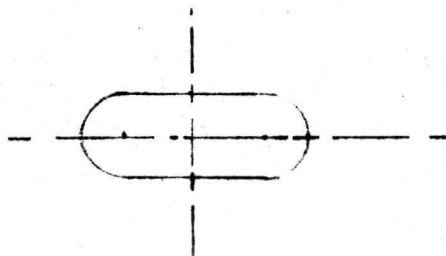
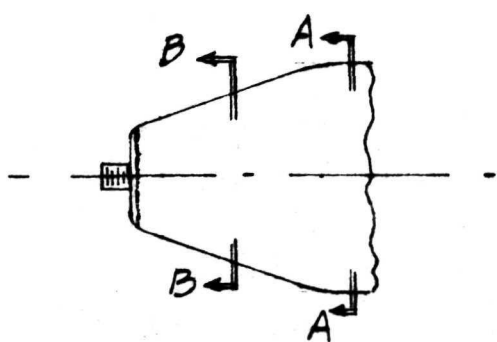
As heretofore indicated, the fiber wrap pattern design objective was to support each fiber on the metal spar liner without the need to develop shear stresses in the resin to prevent the fibers from slipping. The liner has to act like a pulley, with each fiber under constant tension supported by bearing on the "pulley". To achieve this,

objective, the fibers must be wrapped along geodesics* on the liner surfaces. For the constant cross-section spar liner cylindrical body region (Figures 1 and 4) the geodesics are constant angle helices. Consequently, the selected constant helix angle wrap pattern automatically satisfies the wrap design criteria in this region of the liner. The problem then was to evolve a proper head shape which would permit anchoring of each fiber on the head by bearing forces. The head shape selected also had to be compatible with the need to achieve large plastic strains during the spar fabrication process. Restraint of the body section by the head, resulting in material rupture or failure of all parts of the spar to reach the die during the hydrostretching or cryogenic stretch forming operation must be avoided. Finally, the head shape must permit ready fabrication by standard manufacturing techniques.

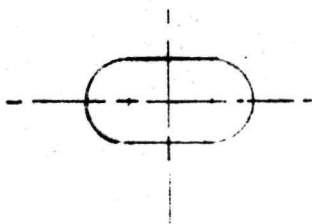
A spar head shape compatible with the fiber wrapping and plastic straining requirements coupled with ease of fabrication, was successfully developed. This spar head configuration appears also to be appropriate for rotor attachment purposes. The head evolved consists of a truncated conical prism shape with blend radii transition sections at either end. The head was fabricated by hydroforming it from flat sheet stock. Figure 14 shows sketches of the head preform shapes prior and subsequent to the hydrostretching operation. The flat elements of the initial head preform cross-section were changed to curved members by the hydrostatic sizing and shaping operation in a closed die to achieve a controlled dimensional and shaped part prior to fiber wrapping.

Head shapes and fiber wrapping patterns evolved during the program were checked by wrapping on wooden spar models. Dry winding was used first to check for fiber slippage and wrap pattern appearance. Head shapes and wrap patterns were revised as required and the final configuration selected was then checked out by wet winding and curing to ascertain the effect of these processing variables. The fiber wrap pattern and spar head configuration efforts are discussed in more detail in Section 3.3 which follows.

* A geodesic is a curve of minimum length between two points on the surface. The geodesic curve contains the principal normals to the surface, so that normal forces alone can hold the constant tension fiber in equilibrium.

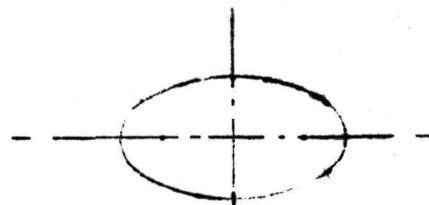
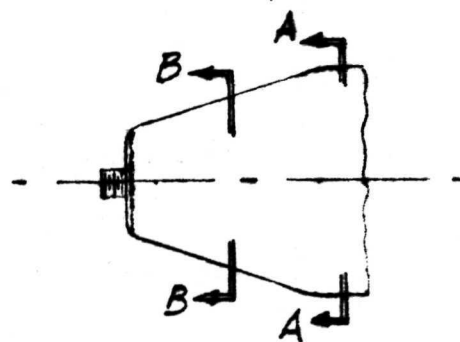


SECTION A-A

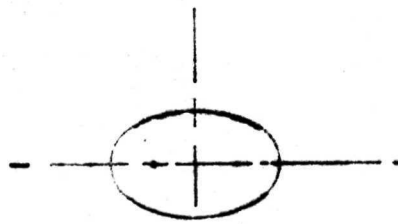


SECTION B-B

a) Head Preform Shape
(Prior to Hydrostretching)



SECTION A-A



SECTION B-B

b) Head Preform Shape
(After Hydrostretching)

FIGURE 14
SPAR METAL LINER HEAD SHAPE

3.3 Composite Spar Fabrication

3.3.1 Fabrication Steps

The primary fabrication steps for construction of the prestressed composite spar are outlined below.

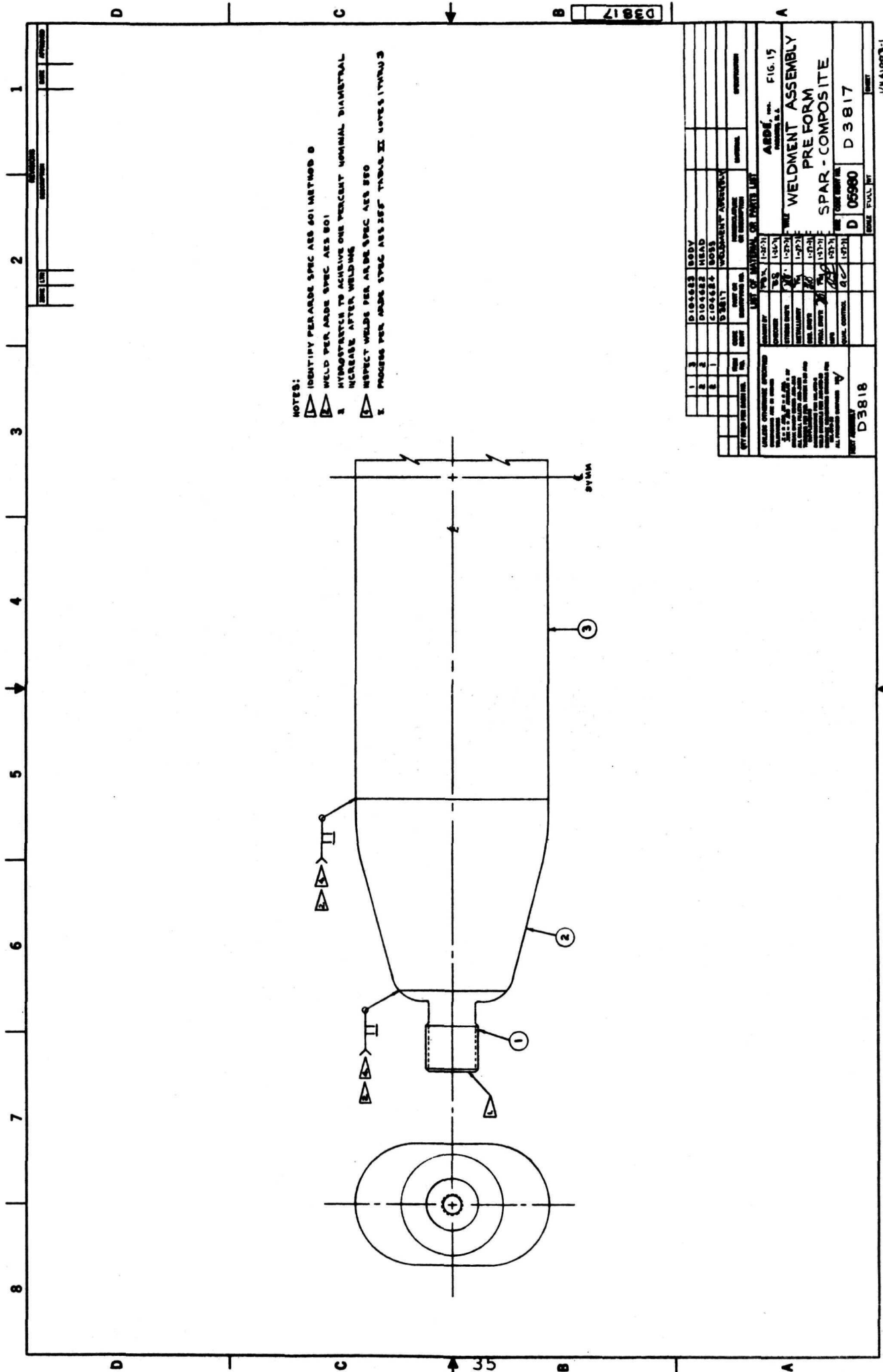
- a) Spar metal liner preform fabrication.
- b) Spar metal liner preform hydrostatic sizing.
- c) Spar metal liner preform fiber wrapping.
- d) Cryogenic stretch forming of fiber wrapped preform to obtain composite spar postform.

Each of these fabrication steps is discussed in detail in this section. Fiber wrapping was performed by Hercules, Inc., Alleghany Ballistics Laboratory. All other fabrication was done by ARDE.

3.3.2 Composite Spar Metal Liner Preform Fabrication

The composite spar metal liner preform consists of a constant cross-section region attached to truncated conical heads as shown on ARDE drawing (Figure 15). Both the body section and heads were fabricated from .030/.028 annealed extra low interstitial ARDEFORM 301 stainless steel flat sheet stock (heat #76235). The body section was press-brake formed in two half sections using appropriate tooling. The two half sections were then welded together by longitudinal welds as shown on Figure 16. The heads were fabricated by the hydroforming process using a male hydroform plug tool. Two forming passes, followed by interpass anneals were used to form the part. Holes for boss attachment were punched in the heads subsequent to forming.

Bosses, used for longitudinal load application and to facilitate pressurization during spar fabrication, were machined from bar stock. The bosses were welded to the heads to form the head sub-assembly detail. The head sub-assemblies were then girth welded to the body sections to make the liner preform assembly. The liner preform assembly was then solution annealed. Figure 15 describes the liner preform. The photographs of Figures 17 to 19 show the liner preform components, boss to head welding and a completed part.



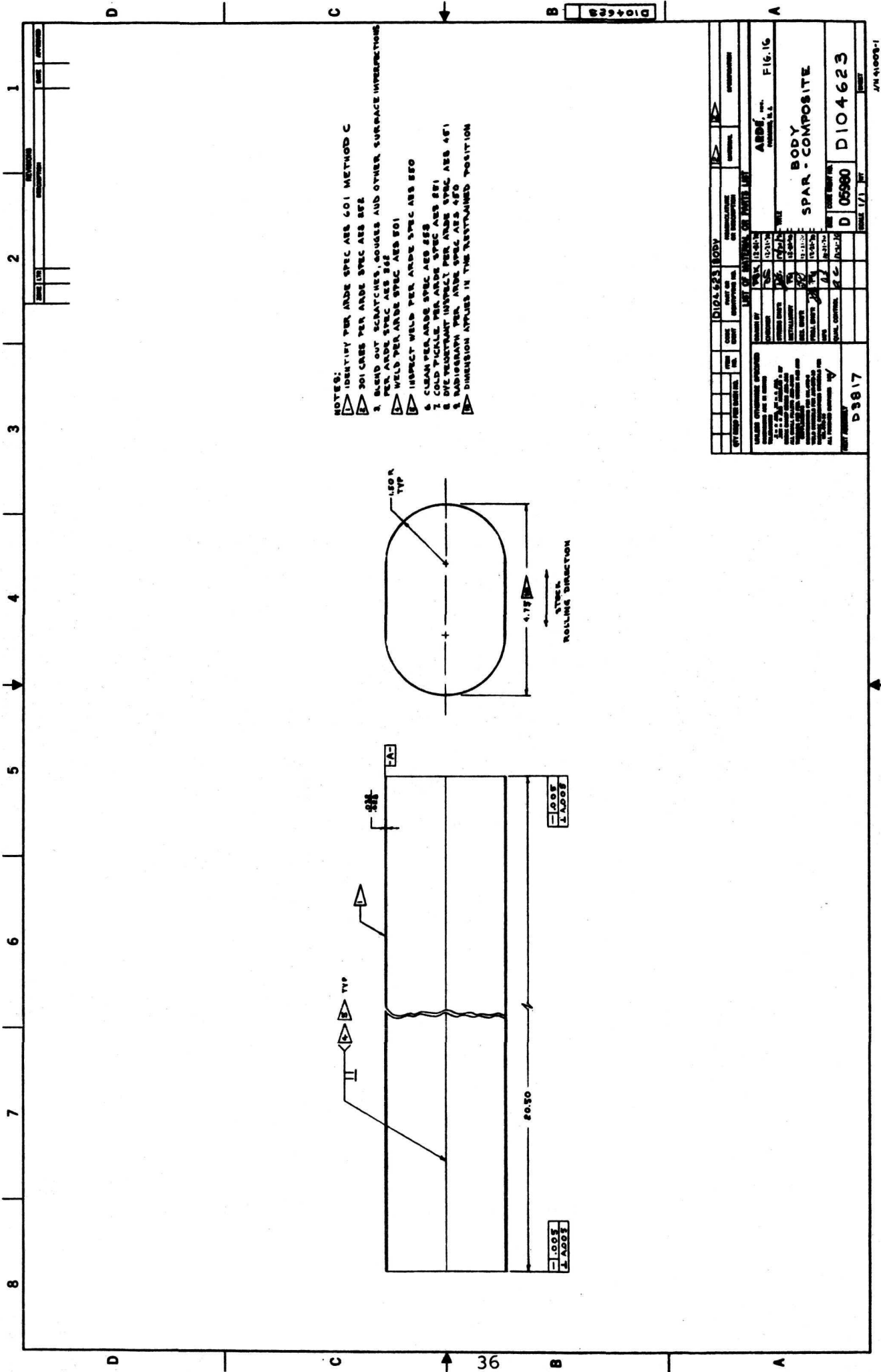


FIGURE 16

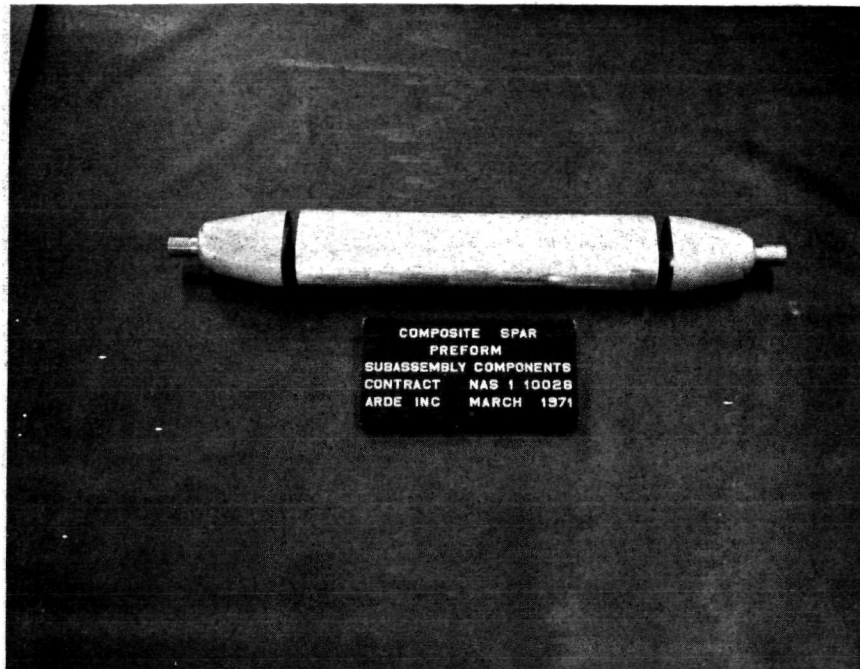


FIGURE 17

LINER PREFORM COMPONENTS

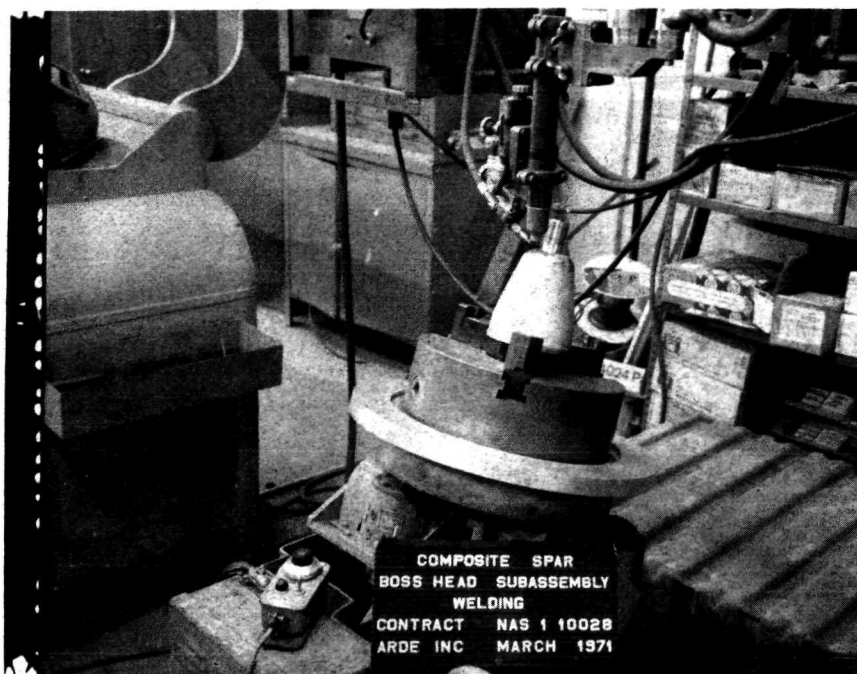


FIGURE 18

BOSS TO HEAD WELD

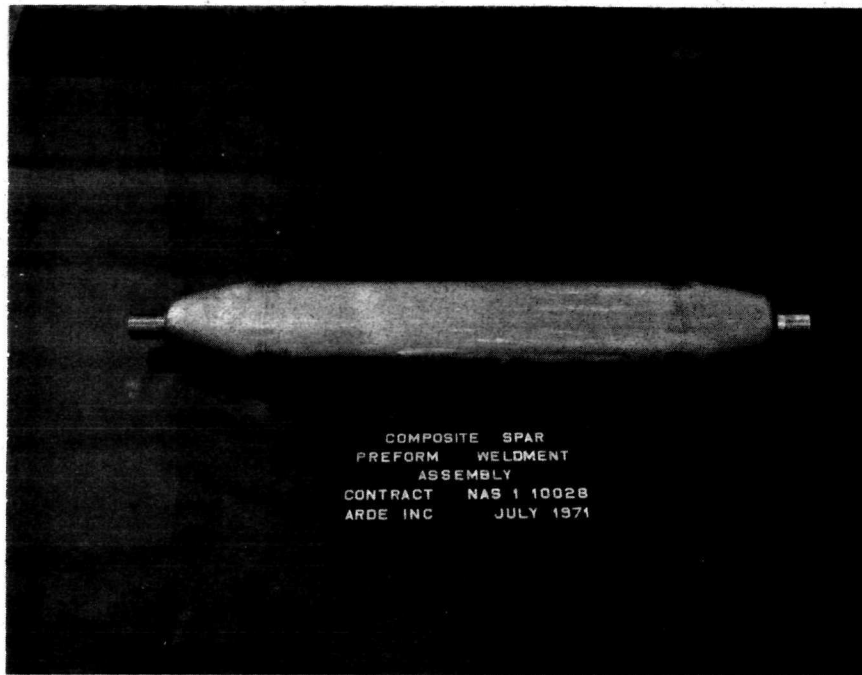
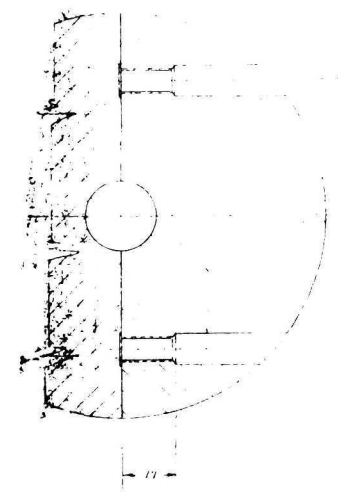


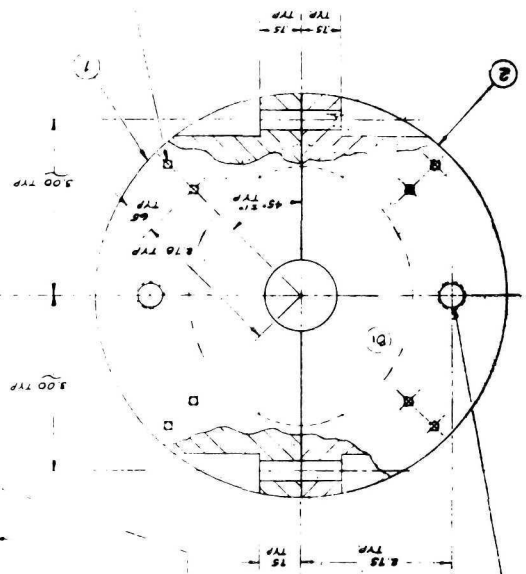
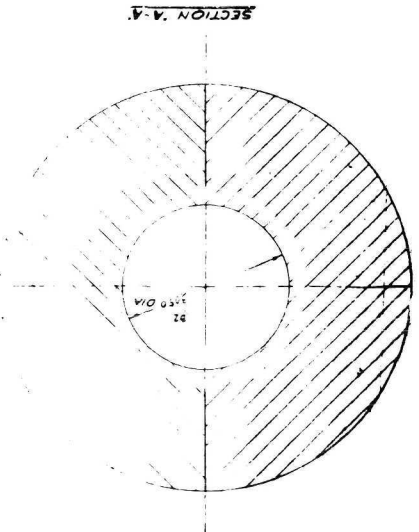
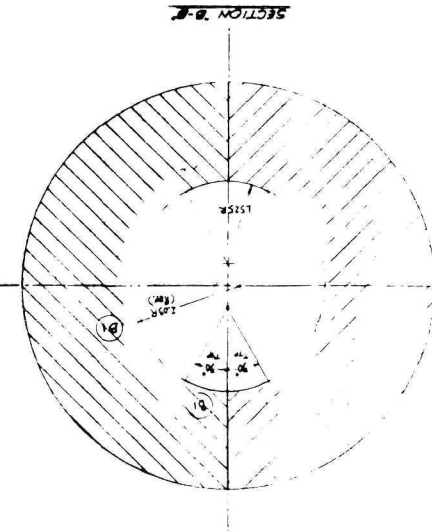
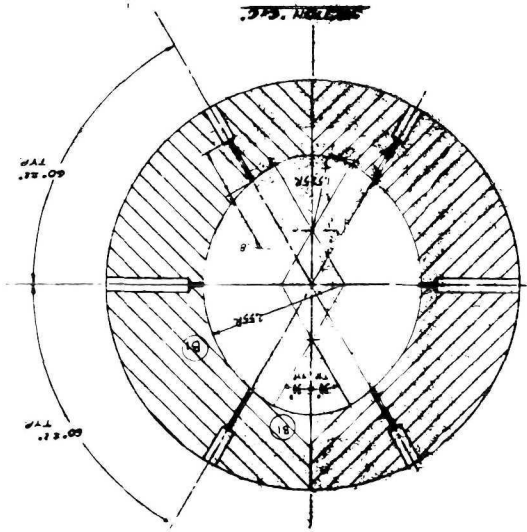
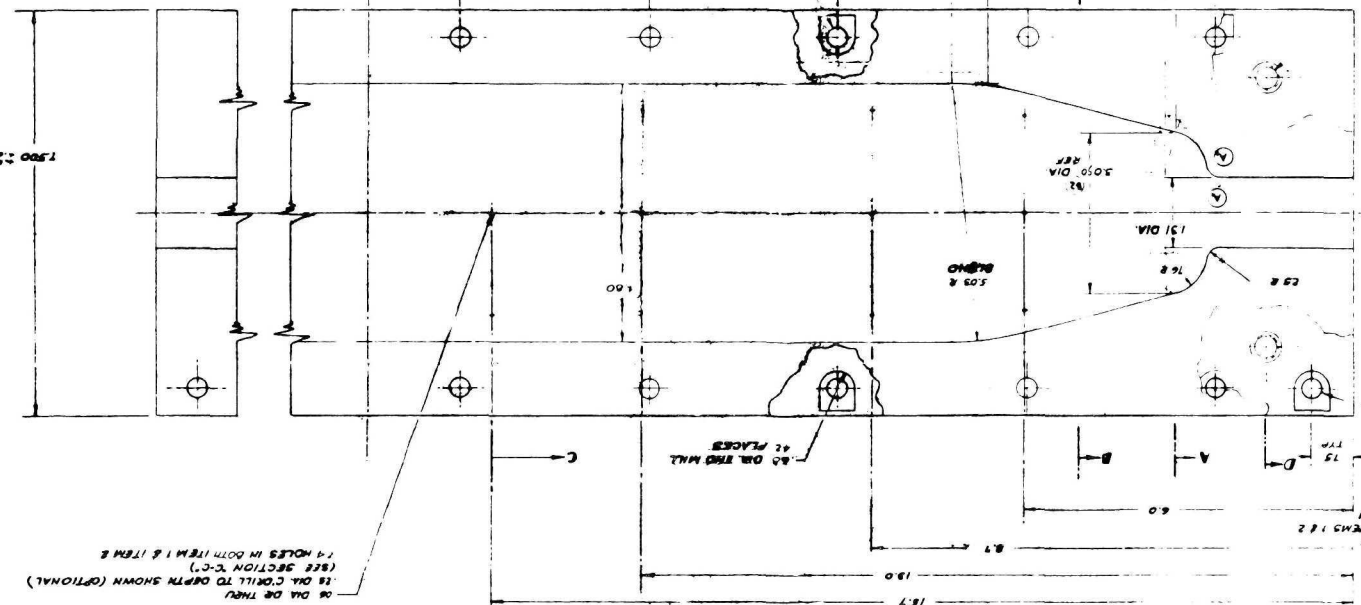
FIGURE 19

COMPLETED COMPOSITE SPAR PREFORM
WELDMENT ASSEMBLY

A	1) REMOVED TO 1) 100% CONTROL
B	1) CHANGED CONTROL (FROM 100% TO 100%) 2) 100% DIA W/ 100% DIA



06 DIA DE THER
15 DIA C ORILL TO DEPTH SHOWN (OPTIONAL)
(SEE SECTION C-C)
1-4 HOLES IN BOTH ITEM 1 & ITEM 2



3.3.3 Spar Metal Liner Preform Hydrostatic Sizing

3.3.3.1 Processing Steps

The spar metal liner preform was hydrostatically sized using room temperature water as the internal pressurant to stretchform it in a closed die. The hydrostatic sizing operation is performed to smooth out the welding distortions and to provide a liner preform with controlled and repeatable dimensions needed for subsequent fiber wrapping operation. A nominal plastic hoop strain of 2% was used in the hydrostatic sizing operation. The hydrostatically stretched preform was then solution annealed to remove the work hardening so as to maximize the amount of strain induced austenite to martensite transformation during the subsequent cryogenic stretch forming operation. A second "small strain" hydrostatic sizing in the die was then performed to remove the annealing distortions.

The composite spar liner hydro-stretch die is shown on ARDE drawing (Figure 20) and the photograph of Figure 21. It consists of two halves held together by pins for location and shear attachment and external aluminum rings which resist the hoop loads. A fiberglass insert, supported by an outer steel cylinder is used to form the internal die contour which shapes and sizes the composite spar metal liner. The fiberglass insert was layed up on a male wooden spar model and then machined on its outside diameter to fit the inside diameter of the outer metal die cylindrical support shell.

The annealing fixture with the metal liner preform installed is shown on the photograph of Figure 22. The liner preform is placed vertically in the furnace in order to minimize annealing distortions due to sag under part weight at the high solution annealing temperatures ($1950^{\circ}\text{F} \pm 25^{\circ}\text{F}$).

Three (3) composite spar metal liner preforms were successfully hydrostatically sized during the program effort rising the aforementioned processing steps.



FIGURE 21

HYDROSTRETCH DIE

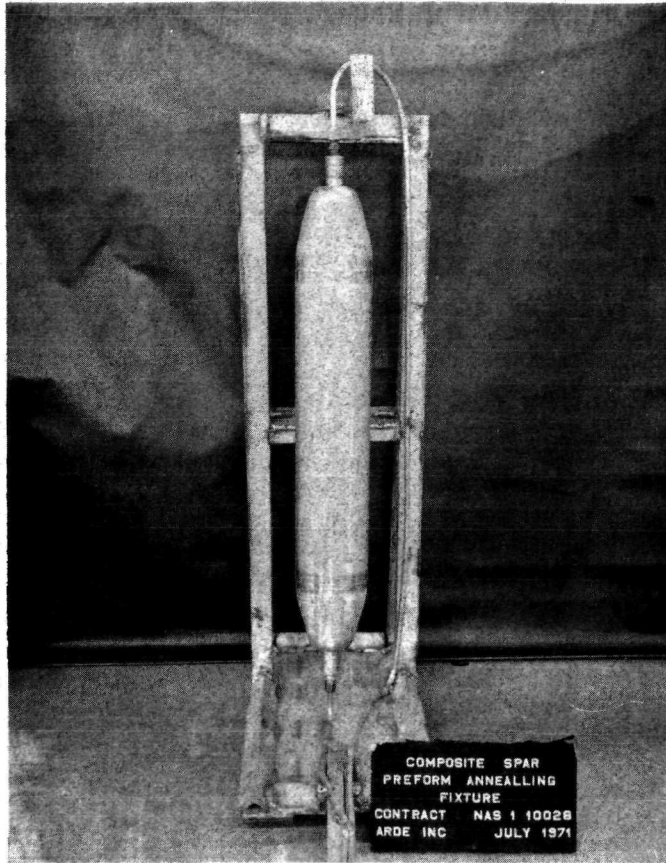


FIGURE 22

ANNEALING FIXTURE

3.3.3.2 Liner Preform Buckling

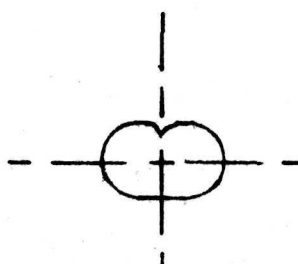
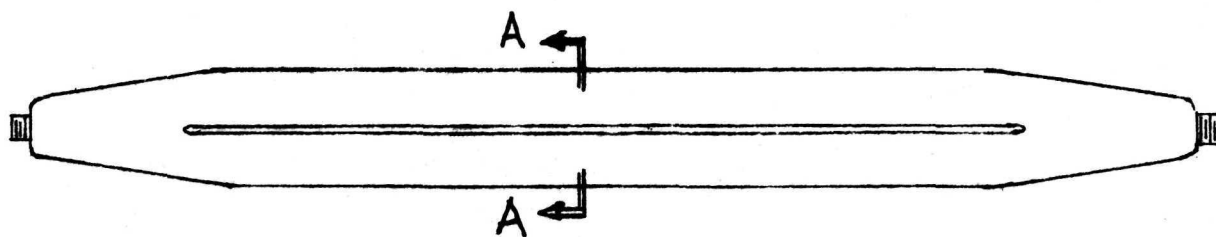
Buckling of one (1) of the flat plate elements of the unwrapped metal liner preform. (figure 4a) was noted upon part removal from the hydrostretch die subsequent to the room temperature hydrostatic sizing operation. The buckled mode shape consisted of a longitudinal "crease" traversing the body section and part way into the heads as shown on figure 23. Hydrostatic forming pressures were then significantly reduced. However, the buckling still persisted. Reduction of forming pressure just decreased the sharpness of the "crease" and its length.

Several possible causes for the buckling were formulated and corrective actions and/or failure mode tests were undertaken to resolve the problem as described below.

a) Elastic springback of the fiberglass die component at release of forming pressure was postulated as a possible buckling cause. The actual fiberglass content of the plastic member was much less than specified leading to a large reduction in stiffness. The plastic member was machined down and an outer cylindrical steel support liner was attached to it by bonding and screws as shown on figure 20. Liner buckling still occurred using the stiffened hydrostretch die, ruling out this failure mechanism.

b) Propagation of local bending disturbances due to head restraint or effect of concentrated forces due to initial local die contact at the center of the flat plate element spar were also postulated as possible buckling causes. These effects, if causitive, would occur at relatively low pressure levels (100 psi or less). These possible failure modes were eliminated by means of two simple tests.

A spar liner preform was pressurized in the open to 100 psi and the pressure then released. No head restraint bending disturbances were observed or propagated and no part buckling occurred. The flat plate elements, without any die restraint, just became curved elements under pressure load and upon release of pressure, returned to their original unbuckled flat plate shape.



SECTION A-A

FIGURE 23

FLAT PLATE CROSS-SECTION
ELEMENT BUCKLED SHAPE

A spar liner preform was pressurized in a rectangular cross-section hollow cylindrical member with open ends to simulate hydrostretch die restraint on the original flat plate elements of the spar cross-section. Upon internal pressurization, the liner preform flat plate elements bulged and touched the simulated die initially as anticipated at the center spar region. Pressure was increased to 100 psi and the liner die contact area increased. No buckling was observed. Upon release of pressure, the bulged spar liner cross-section elements returned to their original flat plate shape.

c) It was assumed that buckling of the flat plate elements was caused by forced elastic springback strains subsequent to plastic deformation and release of pressure loads imposed by continuity with the stiffer hemispherical cross-section members. It was easier for the flat plate member to buckle than to shorten as a "membrane" sheet. Calculations given in Appendix 2 indicate that the hoop compressive elastic springback strain required by continuity could exceed the critical compressive flat plate strain, leading to buckling. In view of this, the corrective action taken was to change the flat plate elements to curved surfaces, shown on Figure 4b, having the dimensions previously given in Section 3.1.2. Since actual spar cross-sections have all curved elements, this approach was considered an admissible solution.

The hydrostretch die contour was reworked by machining the fiberglass insert to the appropriate curved cross-section contour as described by Figure 20. The specified curved cross-sectional contour was obtained by stretch forming the flat plate element liner preform, Figure 15, in the revised curved cross-section hydrostretch die. Liner preform buckling was eliminated by this technique. No further buckling problems were encountered during the program. Although some analytic guidelines may be used, specification of the precise limiting values of spar cross-sectional radius to thickness and length to thickness ratios needed to rule out buckling of the unwrapped metal liner preform during the hydrostretch operation must await future work on subsequent programs. Reducing the magnitude of the hydrostretch sizing strain from 2% to say 1 1/2% would, of course, increase the size of "permissible" liner preform cross-sectional radii of curvature.

3.3.4 Spar Metal Liner Preform Fiber Wrapping

3.3.4.1 Fiber Wrap Pattern Development and Verification

As discussed in Section 3.2, constant 17 1/2% helix angle fiber wrap patterns and compatible head shapes to provide the desired fiber anchoring by bearing on the spar heads and body, were developed and verified by wrapping on wooden spar models. The fiber wrapping was first done dry (without resin) to check for fiber slippage and fiber distribution on the spar contour. Several iterations in head shape with accompanying wooden model modifications were required before a satisfactory wrap pattern without any fiber slippage was achieved. The fibers were then wet wound on the modified spar contour wooden model and cured to check the effect of wet winding and curing on the wrap pattern and to establish fiber wrapping processing variables. Wet winding and curing had no effect on the selected head shape and fiber wrap pattern.

The photograph of Figure 24 shows an early head configuration wooden model after dry fiber wrapping. Slippage of fibers over the relatively short head "knuckle" region is apparent. Subsequent head configurations featured longer conical transitions and larger body section to head blend radii as illustrated in Figures 14, 15 and 19. Fiber wrapping of the finalized spar contour wooden model is shown on Figure 25 and the cured and completed wrapped wooden model is depicted in Figure 26.

The spar head shape and contour developed and verified by the aforementioned wooden model fiber wrapping effort was used to finalize the metal liner preform shape and the hydrostretch and cryostretch die contours.

3.3.4.2 Fiber Wrapping of Composite Spar Metal Liner Preforms

Composite spar metal liner preforms, fabricated as previously described in Section 3.3.3, were wrapped using the same fiber pattern and processing variables that were developed and verified by the spar wooden model wrapping effort. Figures 27 through 30 show photographs of

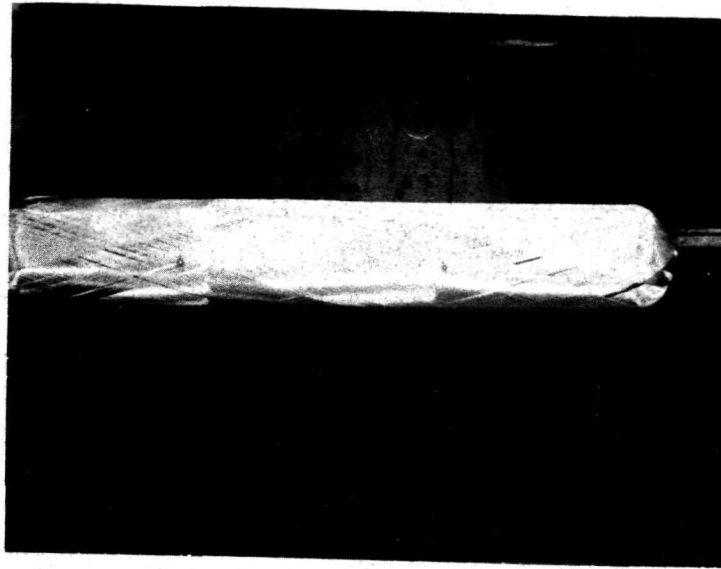


FIGURE 24

INITIAL FIBER WRAP CONFIGURATION -
DRY WRAP ON WOODEN SPAR MODEL

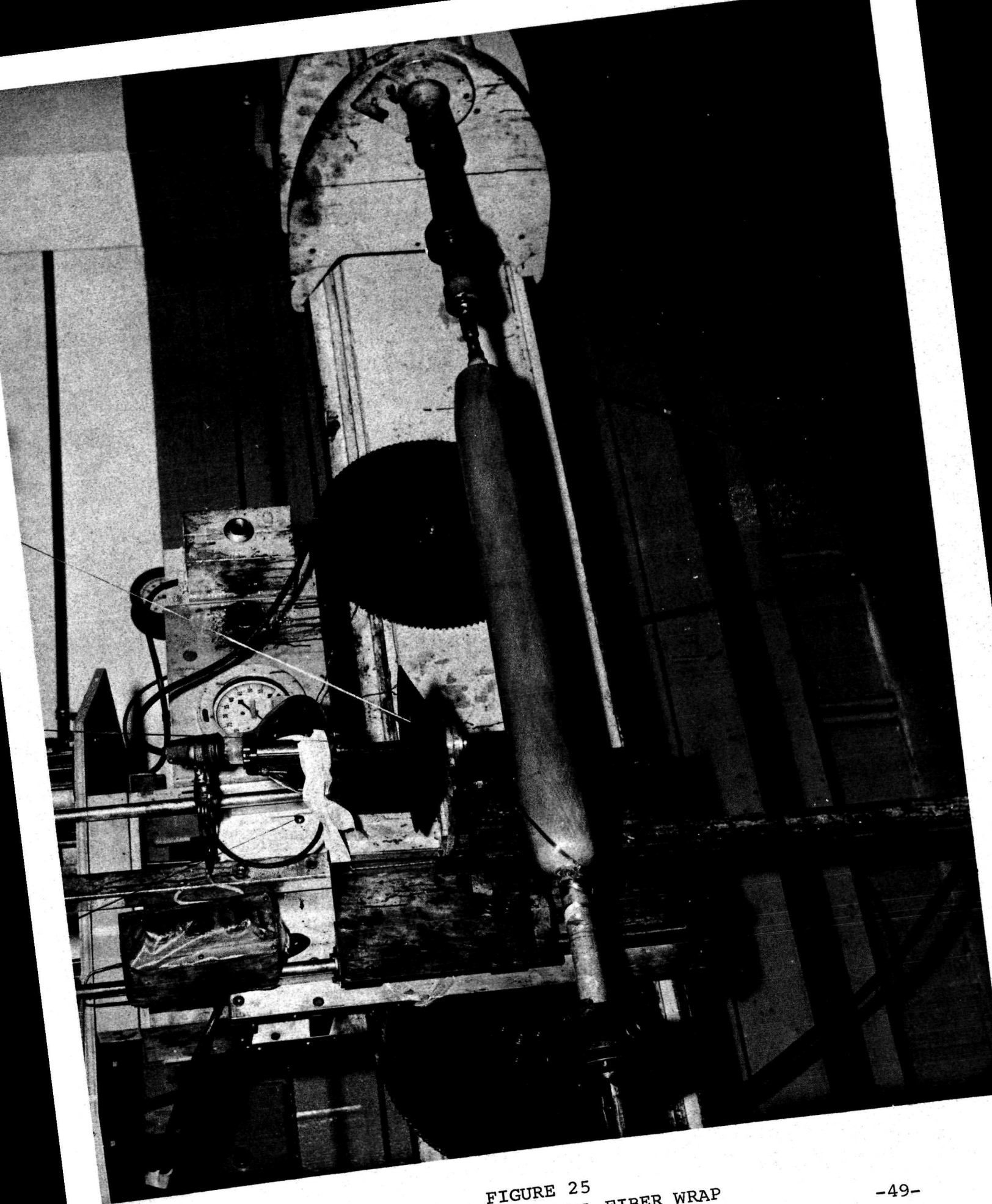


FIGURE 25
WET WINDING OF FINAL FIBER WRAP
CONFIGURATION ON WOODEN SPAR MODEL

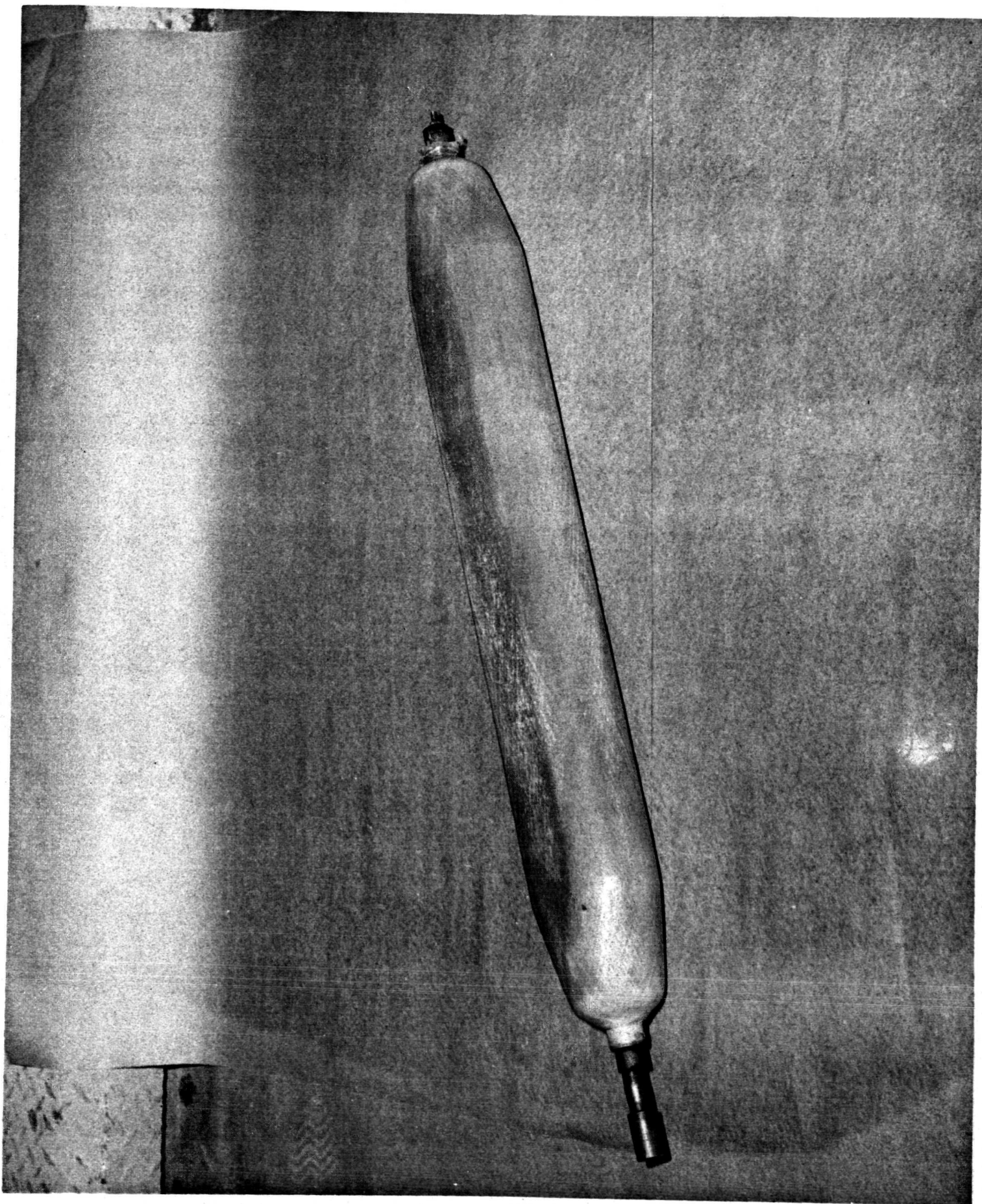


FIGURE 26
COMPLETED FINAL FIBER WRAP
CONFIGURATION WOUND ON WOODEN SPAR MODEL

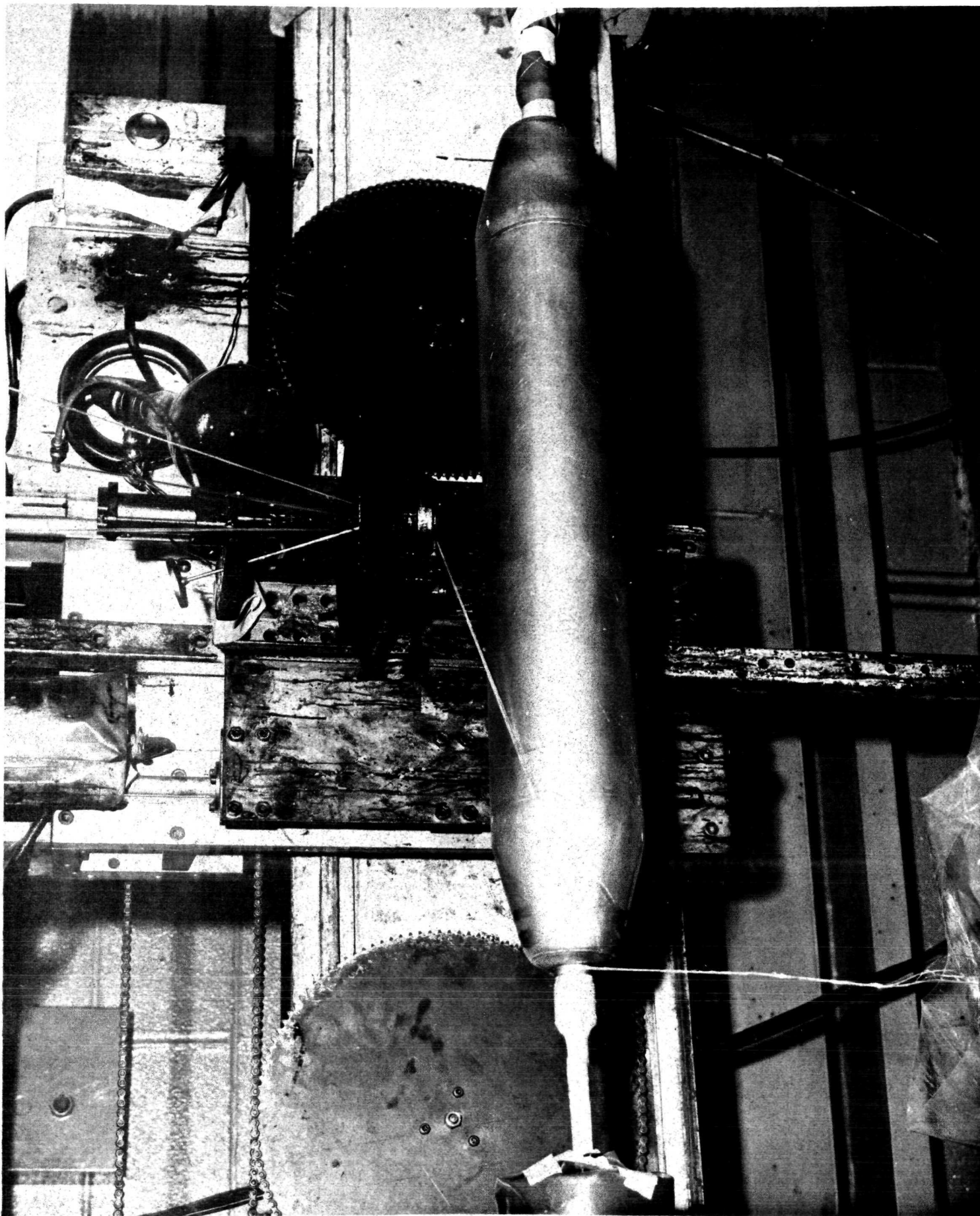


FIGURE 27
START OF FIBER WRAPPING OF COMPOSITE
SPAR METAL LINER PREFORM

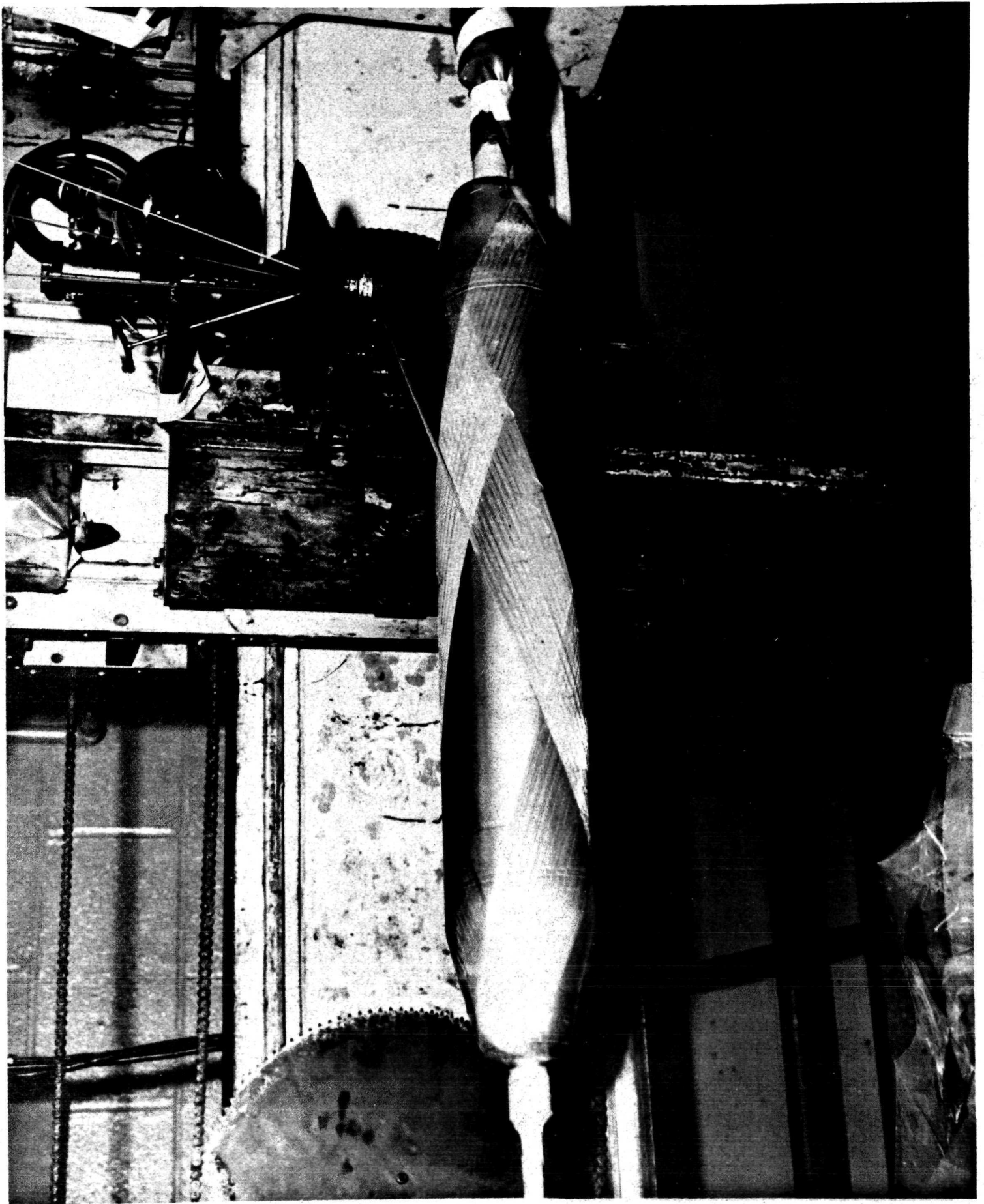


FIGURE 28
BEGINNING STAGE - FIBER WRAPPING
OF COMPOSITE SPAR METAL LINER PREFORM

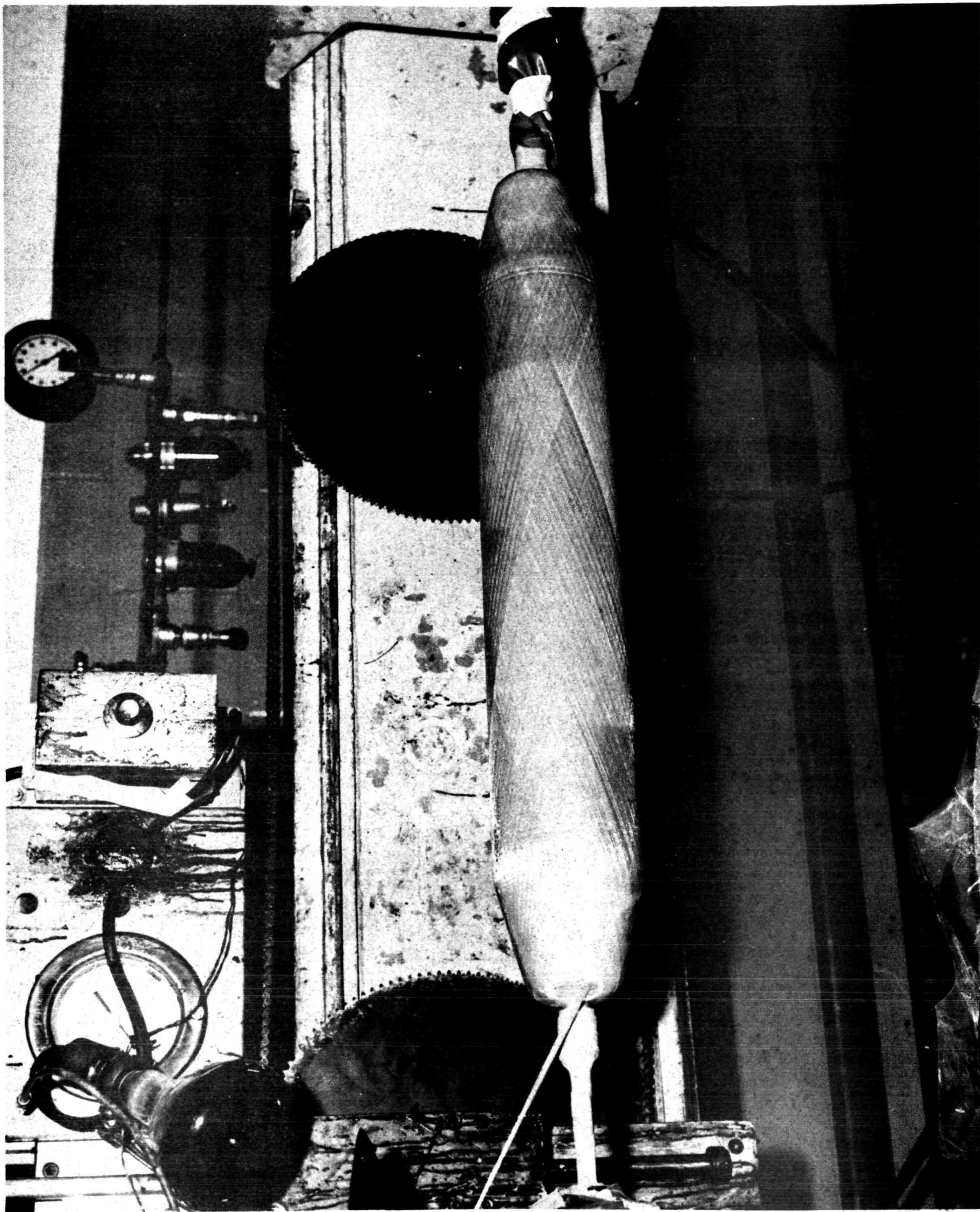


FIGURE 29
INTERMEDIATE STAGE - FIBER WRAPPING OF
COMPOSITE SPAR METAL LINER PREFORM

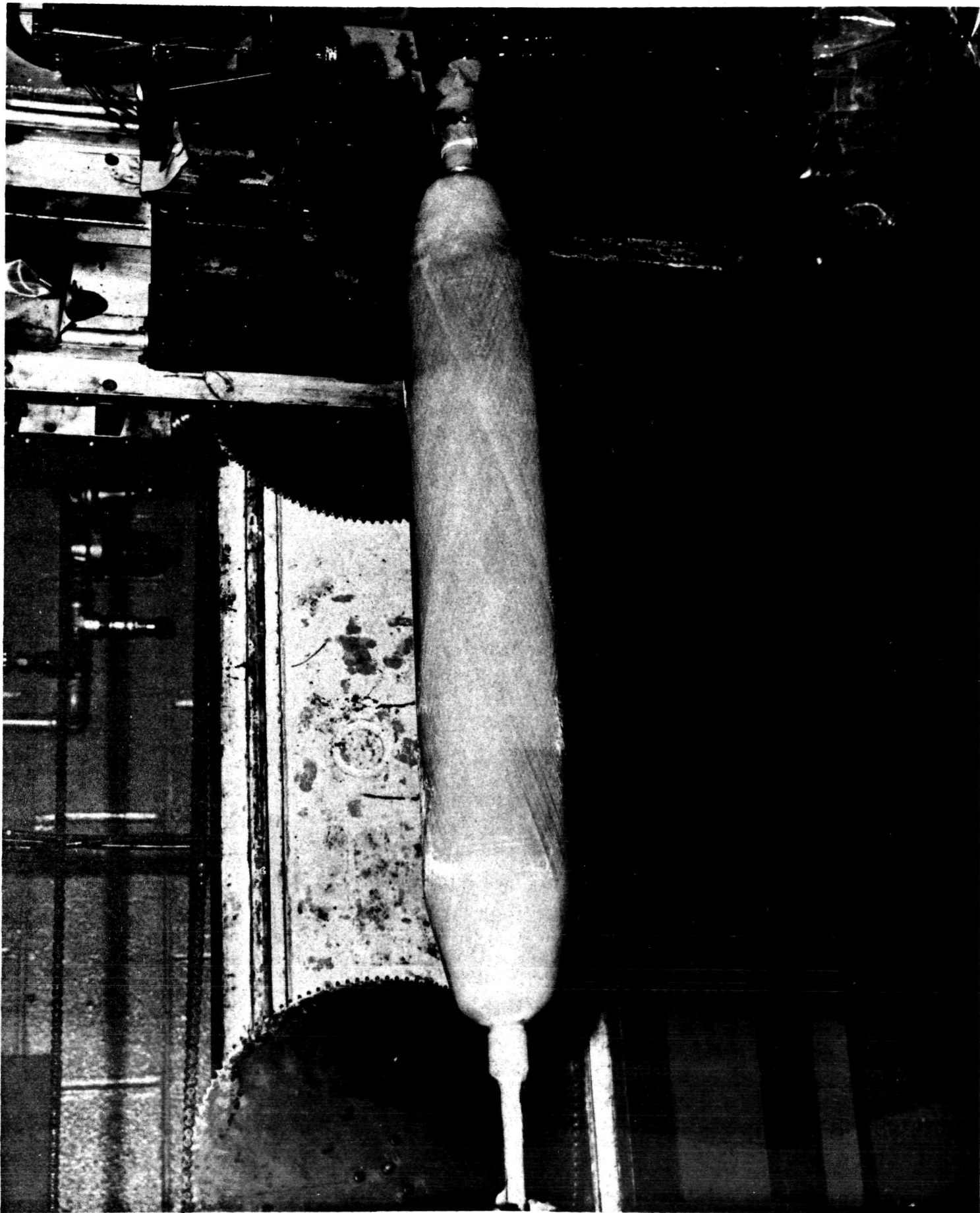


FIGURE 30
FINAL STAGE - FIBER WRAPPING
COMPOSITE SPAR METAL LINER PREFORM

successive stage of the fiber wrapping operation prior to curing. A cured and completed fiber wrapped composite spar preform assembly is depicted on the photograph of Figure 31. Three (3) composite spar preform assemblies were successfully fiber wrapped on the program using the techniques heretofore described.

The composite spar preforms were wet wound with S-994 glass fibers grouped together to give a 12 mil glass thickness per layer. The resin system used, developed especially for cryogenic applications under NASA funding, reference 4, consisted of Epon 8 28/DSA/Empol 1040/BDMA with the distribution in parts by weight of 100/115.9/20/1. The elevated temperature cure cycle employed was two hours at 150°F followed by four hours at 300°F.

3.3.5 Cryogenic Stretch Forming of Fiber Wrapped Composite Spar Preform

The fiber wrapped composite spar preform was assembled in the cryogenic stretch die and immersed in and pressurized with liquid nitrogen (LN_2) to a prescribed stretch pressure utilizing ARDE's cryogenic stretch forming facility. The stretch pressure is selected to impart the required 14.2% plastic hoop strain to the fiber wrapped composite spar (see Section 3.1.1). The cryogenic stretch forming facility, schematically shown on Figure 32, consists in general, of a stretch pit, LN_2 supply, LN_2 pumps, cryostat, associated instrumentation and controls and a stretch die.

Figure 33, gives the details of the cryogenic stretch die. Die components, with a fiber wrapped composite spar preform inserted in the die body section, are shown on the photograph of Figure 34. The aluminum rings, used for resisting hoop pressure loads, are the same rings utilized on the hydrostretch die. At room temperature, the aluminum rings are a slip fit on the stainless steel die body outside diameter facilitating assembly and disassembly operations. At LN_2 temperature, due to different thermal expansion coefficients of stainless steel and aluminum, the rings fit tight on the die body, holding the two halves firmly together. Figure 35 shows a photograph of the cryogenic stretch die containing the spar subsequent to the LN_2 stretch operation and prior to die disassembly for part removal. Ice (frozen water vapor from the ambient environment) is evident on the dies cold exterior surfaces. A completed prestressed composite spar

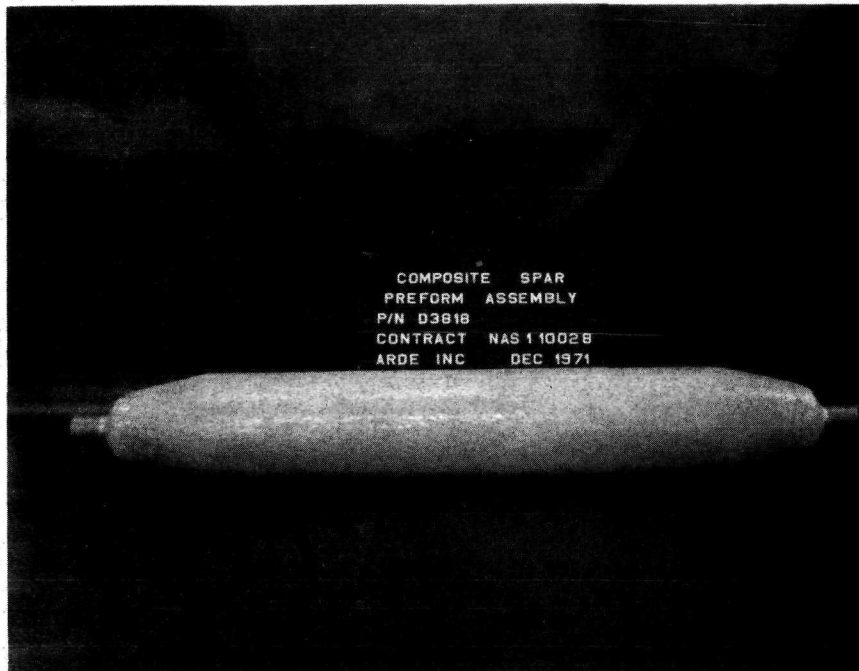


FIGURE 31

COMPLETED FIBER WRAPPED COMPOSITE SPAR
PREFORM ASSEMBLY

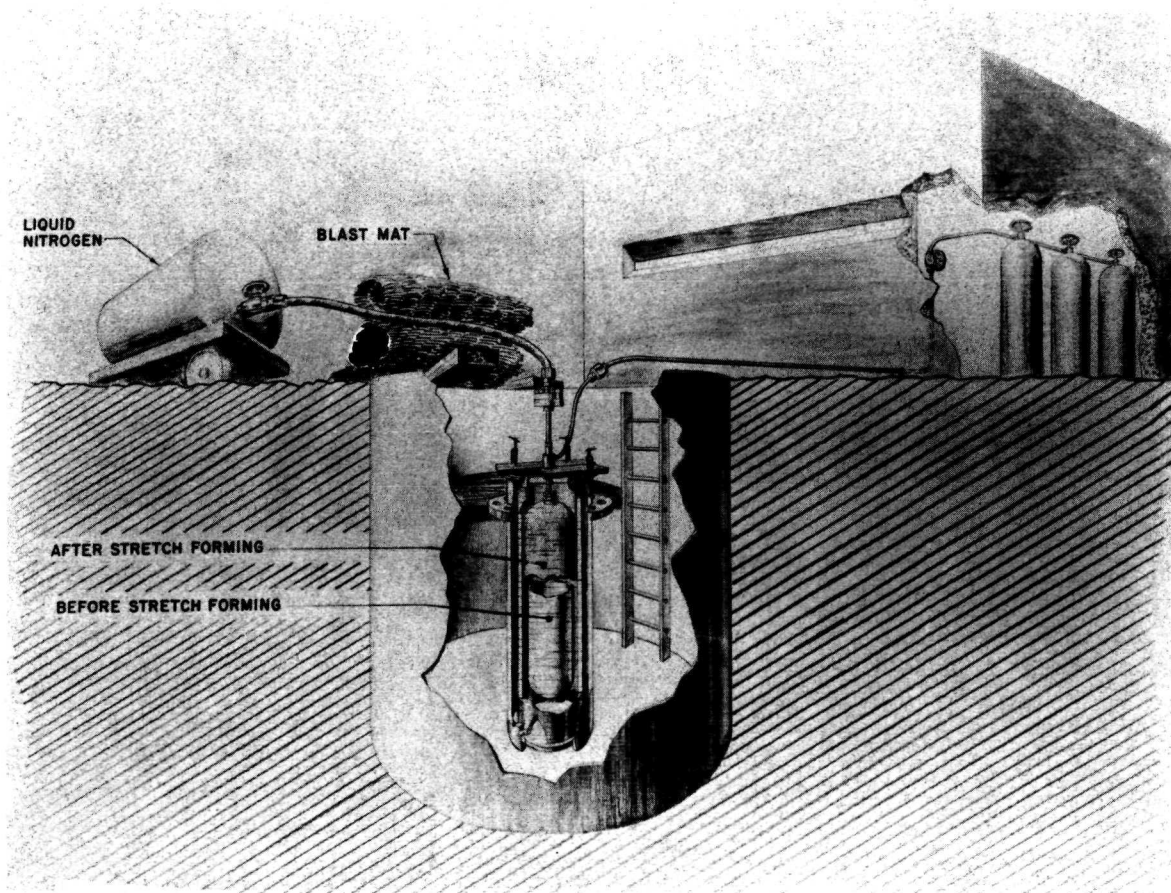


FIGURE 32

SCHEMATIC-CRYOGENIC
STRETCH FACILITY

A	REVISED CONTROLE; ADDRESS 30° TYP 2.48 R (REF) 2) ADDRESS BLEND
---	---



FIGURE 34

CRYOGENIC STRETCH DIE COMPONENTS



FIGURE 35

COMPOSITE SPAR CRYOGENIC STRETCH IN DIE

postform assembly is shown on Figure 36. For comparison purposes, a completed composite prestressed spar preform and postform are grouped together on Figure 37. The growth in size of the postform due to the cryogenic stretch forming is evident. The increase in fiber wrap angle due to the cryogenic straining (see Section 3.1.3) can also be noticed. Some fiber spreading occurred in the head knuckle region. This was caused by the considerable rounding of the local head knuckle region under the cryogenic stretch overpressure required to move the head out to the die contour. Revising the local cryogenic die contour to provide a flatter and longer transition in the spar knuckle region with less hoop strain required, should eliminate this problem.

Two (2) prestressed composite spar postform assemblies were successfully fabricated during the program. These completed parts will be held for testing in a projected subsequent program.

3.4 Evaluation of Composite Spar Prestressed State

Inspection measurements, consisting of spar axial lengths, diameters and fiber wrap angles taken prior and subsequent to the cryogenic stretch forming operation, were utilized together with structural theory and appropriate material properties to determine the prestresses in the fabricated composite spars. Gage lines were established and marked on the fiberglass exterior surfaces to facilitate these measurements. Diameters were measured with micrometers and lengths were determined with vernier calipers. Fiber wrap angles were determined by tracing fibers on tracing paper and measuring the angles between fibers with a protractor.

As detailed in Appendix 3 of Section 6, composite spar prestresses determined from these inspection measurements were,

$$\sigma_{fi} = 40 \text{ ksi (fiberglass tensile prestress)}$$

$$\sigma_{mxi} = -50 \text{ ksi (metal longitudinal compressive prestress)}$$

$$\sigma_{m\theta i} = -7 \text{ ksi (metal hoop compressive prestress)}$$

The data evaluation described in Appendix 3 indicated the need for improved measurement techniques, primarily for axial length used for longitudinal strain determination and to

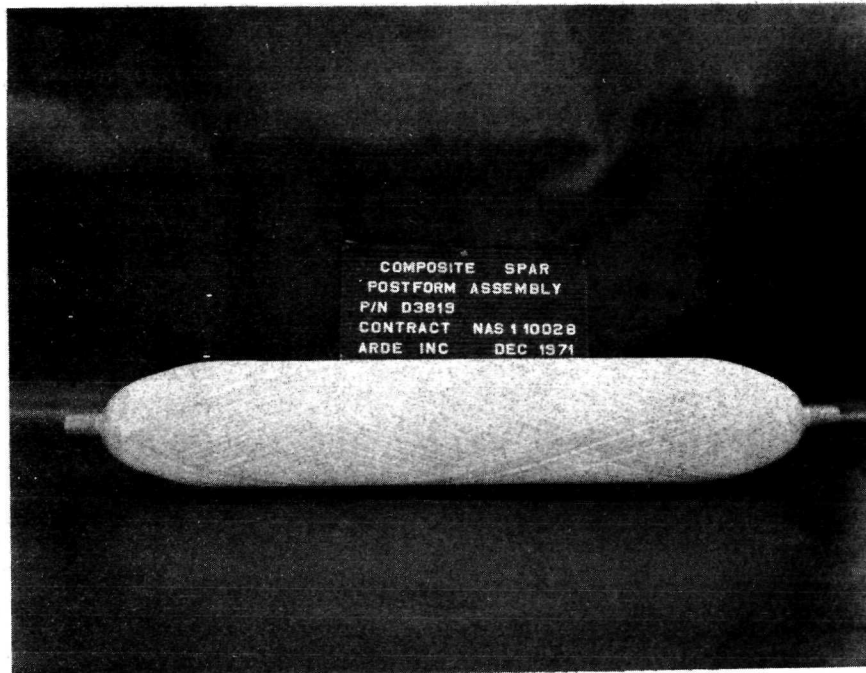


FIGURE 36

COMPOSITE SPAR POSTFORM ASSEMBLY

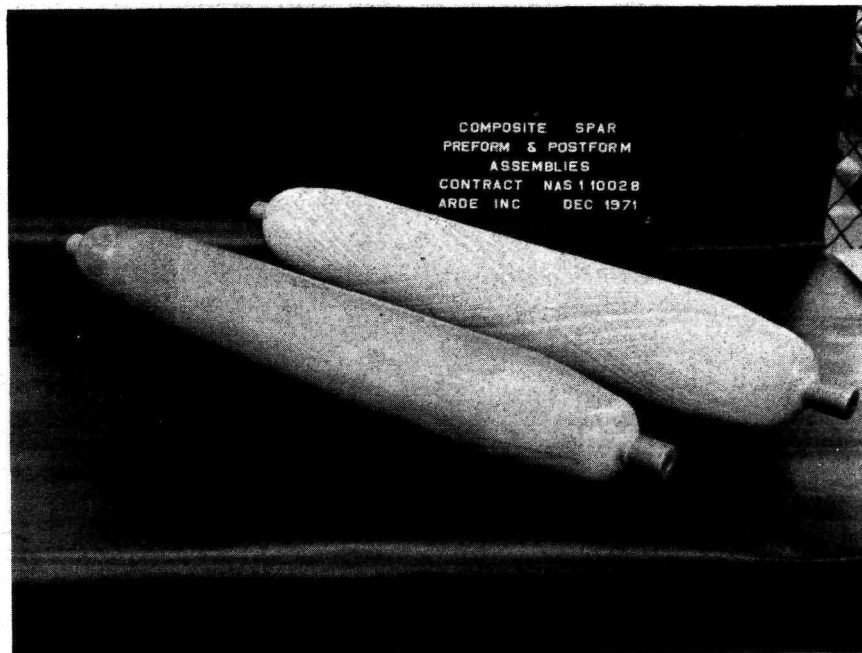


FIGURE 37

COMPOSITE SPAR PREFORM AND POSTFORM ASSEMBLIES

a much lesser degree, for spar fiber angle measurement. Interior metal surfaces were not accessible for measurement and use of strain gages or other "standard" techniques were ruled out because of the large plastic strains of the spar at cryogenic temperatures in a closed die. The measurement difficulty experienced was due to the problem of properly marking reference measurement lines on the exterior fiberglass surfaces. It is projected that required measurement technique refinements can be accompanied in a straight forward manner without any significant problems.

3.5 Composite Spar Testing Requirements

Tests are required to verify the theoretically anticipated crack propagation, fatigue life, and weight advantages of the prestressed composite spar. Three (3) types of tests were projected:

- a) Static bending and torsion tests
- b) Smooth spar specimen bending fatigue tests
- c) Notched spar specimen bending crack propagation tests

The static bending and torsion tests would determine stiffness, deflection mode shapes and static ultimate strength to be used as basic data and employed in the analysis of the dynamic test results.

The smooth and notched spar specimen dynamic bending tests planned would define fatigue life and crack propagation rates for the spars and give bending natural frequency and damping factor information. An unstressed spar metal liner processed in the same manner as the prestressed composite spar liner would also be tested for verification of the effect of liner compressive prestress. Comparison with existing fatigue and crack propagation data for other homogeneous material spars would also be made.

The selected composite spar design point would be simulated in the dynamic bending tests (see section 3.1.6). An alternating bending stress of ± 34 ksi in the liner (twice the reference homogeneous material spar value) would be employed. An axial tensile load to simulate the centrifugal

force equivalent to +24 ksi axial tensile stress in the reference homogeneous spar would be applied in all tests (static as well as dynamic).

A detailed test specification, ARDE Test Specification (ATS-100), describing the requirements for the spar testing outlined above was defined. This specification is given in Appendix 4, of section 6. During the course of the program effort, helicopter companies and other potential testing sources were contacted and testing bids were solicited based on the ARDE test specification. Testing of prestressed composite spar specimens is projected for a subsequent program.

4. Conclusions and Recommendations

4.1 Conclusions

a) The program objective was achieved. Composite prestressed spar fabrication techniques were developed and verified. Two (2) composite prestressed spar specimens were successfully fabricated.

b) An appropriate fiber wrap pattern and a compatible head shape to anchor the fibers on the spar without the need for shear stresses in the resin have been evolved and checked out. Three (3) composite spar specimens, together with several wooden spar models, were successfully fiber wrapped. The fiber wrap patterns were uniform, met helix angle tolerances, and did not slip off the spar even when wrapped dry (without resin). The head shape evolved appears to be appropriate for future root attachment requirements.

c) Composite prestressed spar structural design theory was verified. Hoop strains and fiber angle changes predicted by theory were achieved. Prestresses, based on structural design theory and dimensional measurements taken during and subsequent to cryogenic stretch forming, were obtained for the two spars successfully fabricated during the program. The prestress values (compression in the metal liner and tension in the fibers at zero external load state) were in the desired design range. The need for improved measurement techniques for spar strain determination was indicated by this work.

d) Buckling problems with the flat plate elements of the unwrapped metal liner during the intermediate hydrostatic stretching operation were successfully resolved. Curved elements, compatible with actual spar cross-sectional shapes were substituted for the flat plate portions. Additional effort is required to determine the limiting values of radius to thickness ratios to prevent buckling.

e) Rework of the head knuckle contour of the cryogenic stretch die should eliminate excessive head knuckle rounding and accompanying local fiber spreading during cryogenic stretch forming.

4.2 Recommendations

a) Fabricate additional spar specimens and test as defined by ARDE Test Specification ATS-100 to verify the projected advantages of the prestressed composite spar construction.

b) Improved measurement techniques for composite spar dimensional changes (needed to verify spar prestresses) should be investigated.

5.0 REFERENCES

- 1) Meredith, Seiferth and Rummel, "A Graphite/Epoxy Compression Panel for the Space Shuttle", p. 99, Society of Aerospace Material and Process Engineers, Space Shuttle Materials, Volume 3, National SAMPE Technical Conference, October 5-7, 1971, Huntsville, Alabama.
- 2) Lager, J. R., "Composite Space Shuttle Engine Support Structure", p. 149, Society of Aerospace Material and Process Engineers, Space Shuttle Materials, Volume 3, National SAMPE Technical Conference, October 5-7, 1971, Huntsville, Alabama.
- 3) Gleich, D., "Cryogenically Formed Prestressed Fiber-Metal Structures for O₂/H₂ High Pressure Gas Tanks", p. 527, Society of Aerospace Material and Process Engineers, Space Shuttle Materials, Volume 3, National SAMPE Technical Conference, October 5-7, 1971, Huntsville, Alabama.
- 4) Gleich, D., Development of a Filament Overwrapped Cryoformed Pressure Vessel, NASA CR-72753, ARDE, INC. under Contract NAS 3-11194, January 1971.
- 5) Morris, E. E., Glass-Fiber Reinforced Metallic Tanks for Cryogenic Service, NASA CR-72224, Aerojet-General Corporation under Contract NAS 3-6292, June 1967.
- 6) U. S. Patent Number 3,197,851.
- 7) Sikorsky Aircraft Corporation Fatigue Test Data.
- 8) Johns & Kaufmann, Filament Overwrapped Metallic Cylindrical Pressure Vessels, NASA TMX-52171, Lewis Research Center, 1966.
- 9) Discussions with Sikorsky Aircraft and Boeing, Vertol Division.
- 10) Dolan, T. J., "Stress Range", p. 82, ASME Handbook - Metals Engineering Design, McGraw-Hill Book Company, 1963.

- 11) Burck, Sullivan and Wells, "Fatigue of Glass Bead Blasted Nickel Base Superalloy", Metallurgical Transactions, Volume 1, No. 6, June 1970.
- 12) Landgrebe, A. J., Simplified Procedures for Estimating Flapwise Bending Moments on Helicopter Rotor Blades, NASA CR-1440 and 1441, October 1969.
- 13) Hercules, Inc. Product Data Numbers 815 and 816.
- 14) Flugge, Handbook of Engineering Mechanics, p. 36-15, McGraw-Hill Book Company, 1962.
- 15) Bruhn, Analysis and Design of Flight Vehicle Structures, p. C5.2, Tri-State Offset Company, January 1965.

6.0 APPENDICES

6.1 Appendix 1 - Symbols

Symbols used in the text are listed and defined in this section.

A	=	Enclosed cross-sectional area
A_f	=	Fiber area
A_M	=	Metal area
a	=	Element length prior to straining
a^1	=	Element length after straining
b	=	Spar cross-section dimension or element length before straining
b^1	=	Element length after straining
c	=	Element length before straining
c^1	=	Element length after straining
d	=	Cross-section depth or differential
ds	=	Arc length
E	=	Young's modulus
E_f	=	Fiber Young's modulus
E_g	=	Graphite fiber Young's modulus
E_M	=	Metal Young's modulus
F	=	Force, axial or fiber
F_O	=	Axial force of reference homogeneous metal spar
g	=	Acceleration of gravity
G	=	Shear modulus
(GJ)	=	Torsional stiffness of reference homogeneous metal spar
$(GJ)_M$	=	Torsional stiffness of metal liner
I	=	Moment of inertia
I_O	=	Moment of inertia of reference homogeneous metal spar
I_P	=	Polar moment of inertia
I_{pM}	=	Metal polar moment of inertia

I_{pf}	=	Fiber polar moment of inertia
J	=	Torsion constant for cross-section
k_b	=	Bending stiffness
k_{bc}	=	Bending stiffness of composite spar
k_{bo}	=	Bending stiffness of reference homogeneous metal spar
\hat{k}_{bc}	=	Bending stiffness per unit mass of composite spar
\hat{k}_{bo}	=	Bending stiffness per unit mass of reference homogeneous metal spar
k_T	=	Torsional stiffness
k_{Tc}	=	Torsional stiffness of composite spar
k_{To}	=	Torsional stiffness of reference homogeneous metal spar
\hat{k}_{Tc}	=	Torsional stiffness per unit mass of composite spar
\hat{k}_{To}	=	Torsional stiffness per unit mass of reference homogeneous metal spar
L	=	Length
M_b	=	Blade mass
M_c	=	Composite spar mass
M_o	=	Mass of reference homogeneous metal spar
M_{ns}	=	Non-structural mass
M_s	=	Spar mass
N_θ	=	Hoop membrane stress resultant
N_x	=	Longitudinal membrane stress resultant
P_s	=	Cryogenic stretch forming pressure
R	=	Radius
R_A, R_B	=	Spar cross-sectional radii
R_{die}	=	Die radius
R_o	=	Initial radius of spar
r_i	=	Radius of i^{th} fiber to shear center of cross-section
S	=	Fiber width
S_1	=	Nominal room temperature .2% offset hoop yield stress of metal
S_{1A}	=	Nominal aged room temperature .2% offset hoop yield stress of metal
S_2	=	Nominal metal hoop stress at $-320^\circ F$ during cryogenic stretch forming

ΔT	=	Temperature change
T_c	=	Resisting torque of composite spar
T_f	=	Fiber resisting torque
T_M	=	Metal resisting torque
T_o	=	Resisting torque of homogeneous reference metal spar
t_f	=	Fiber structural thickness (glass less resin)
t_{fc}	=	Fiber composite thickness (glass plus resin)
t_{cx}	=	Fiber composite thickness at cross-section minor diameter
t_{cy}	=	Fiber composite thickness at cross-section major diameter
t_o	=	Thickness of reference homogeneous metal spar
t_M	=	Metal thickness
t_{ns}	=	Thickness of non-structural spar material
W_c	=	Composite spar weight
W_o	=	Reference homogeneous metal spar weight
w_{sp}	=	Elastic springback deflection
X, Y	=	Spar cross-section minor and major diameters
X_o, Y_o	=	Initial spar cross-section minor and major diameters
x	=	Coordinate
z	=	Thickness coordinate
α	=	Initial fiber wrap helix angle
α^1	=	Final fiber wrap helix angle
α_f	=	Fiber thermal expansion coefficient
α_M	=	Metal thermal expansion coefficient
β	=	Spar cross-section angular dimension
P	=	Perimeter
γ	=	Mass per unit length
Δ	=	Increment
E_{cr}	=	Critical compressive strain
E_f	=	Fiber strain
E_o	=	Bending strain parameter

$\epsilon_{M\theta}^1$	=	Metal cryogenic plastic hoop strain
ϵ_{sp}	=	Elastic springback strain
ϵ_{θ}	=	Metal hoop strain
ϵ_x	=	Metal longitudinal strain
λ	=	Blade non-structural mass ratio parameter
μ	=	Resin fraction by weight
ρ_{fc}	=	Composite fiber density
ρ_{gc}	=	Composite graphite fiber density
ρ_M	=	Metal density
ρ_{ns}	=	Density of non-structural weight material
σ	=	Stress
σ_{cr}	=	Critical compressive stress
σ_f	=	Fiber stress
σ_f^1	=	Fiber prestress
σ_{fb}	=	Fiber bending stress
σ_{fo}	=	Fiber operating stress
$\sigma_{f\theta}$	=	Fiber hoop stress
$\sigma_{f\theta}^1$	=	Fiber hoop prestress
σ_M	=	Metal stress
σ_{Mb}	=	Metal bending stress
σ_{Mi}	=	Metal prestress
σ_{Mx}	=	Metal direct longitudinal stress
σ_{Mxi}	=	Metal longitudinal prestress
σ_{Mx}^1	=	Metal true cryogenic longitudinal stress or longitudinal prestress
$\sigma_{M\theta}$	=	Metal hoop stress
$\sigma_{M\theta i}$	=	Metal hoop prestress
$\sigma_{M\theta}^1$	=	Metal true cryogenic hoop stress or hoop prestress
σ_{ox}	=	Direct longitudinal stress in reference homogeneous metal spar
θ	=	Angle of twist of spar cross-section
$\Phi(x)$	=	Function of x
Ω	=	Blade angular velocity

6.2 Appendix 2 - Composite Spar Structural Design

Composite prestressed spar structural analysis theory and calculations are presented in this section.

6.2.1 Fiber and Metal Prestresses Versus Fiber Wrap Angle

Fiber and metal prestresses (initial stress state at zero external load) are derived herein based on equilibrium, strain compatibility, geometric and stress-strain relations at cryogenic and room temperatures. Numerical calculations for one (1) design point are presented as an illustrative example.

6.2.1.1 Membrane Stress Resultants

Idealizing the spar of length, L , with a cross-section as sketched in Figure A-1, equilibrium requirements determine the spar hoop and longitudinal membrane stress resultants N_θ and N_x as follows:

$$\begin{aligned} 2N_\theta L &= 2 \text{ RLP or,} \\ N_\theta &= PR \end{aligned} \tag{A-1}$$

$$\begin{aligned} N_x (2\pi R + 4b) &= P (\pi R^2 + 4bR) \text{ or,} \\ N_x &= PR \left(\frac{1 + \frac{\pi}{4} R/b}{1 + \frac{\pi}{2} R/b} \right) \end{aligned} \tag{A-2}$$

For a wide spar ($R/b \ll 1$) and we have the approximate relation,

$$N_x \approx PR \tag{A-3}$$

6.2.1.2 Fiber Stress Components

From fiber stress, fiber tensile load components and fiber widths sketch in Figure A-2, noting that fiber area is width times thickness, we have,

$$\sigma_f = \text{fiber stress} = \frac{\text{fiber load}}{\text{fiber area}} = \frac{T}{t_f s \sin \alpha' \cos \alpha'} \tag{A-4}$$

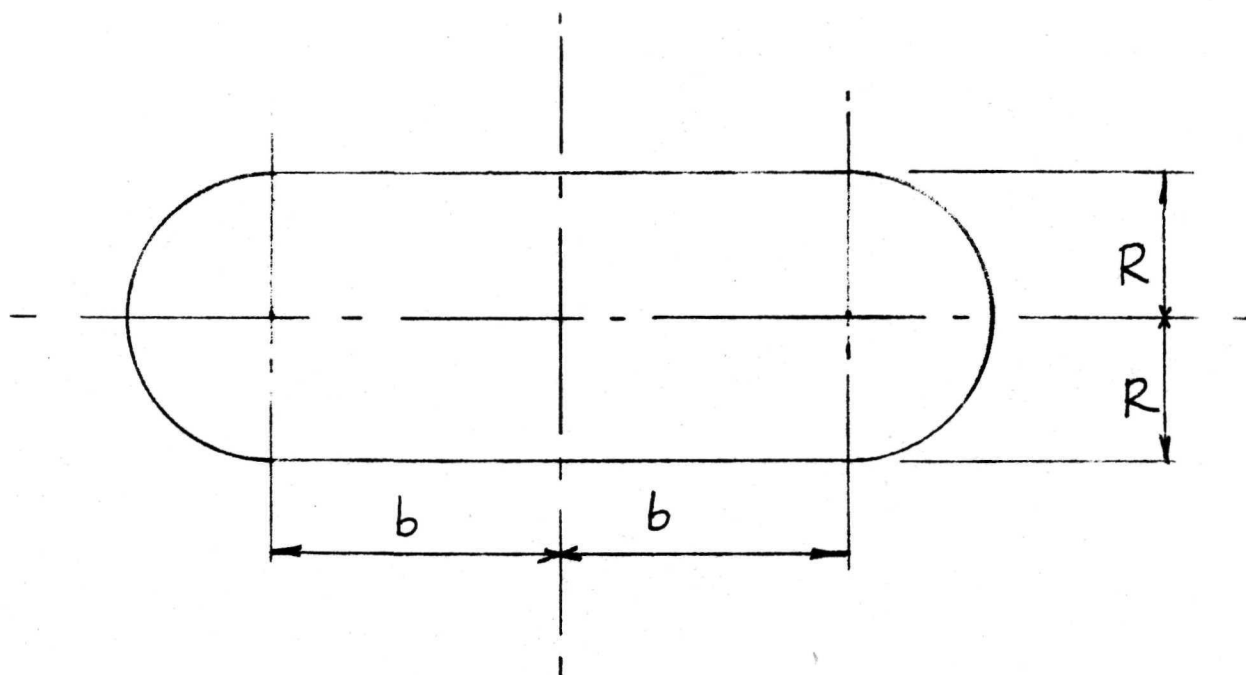
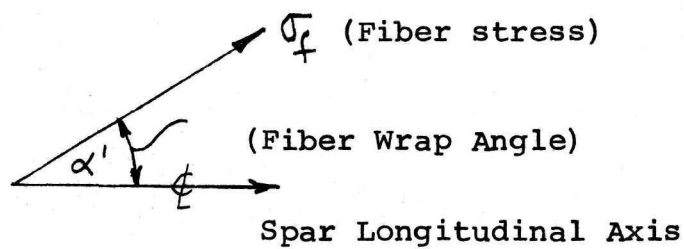
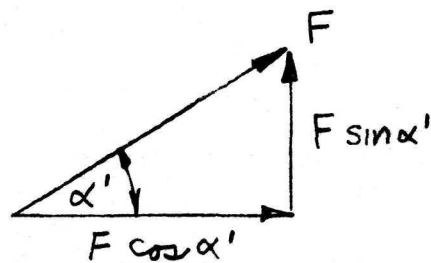


FIGURE A-1

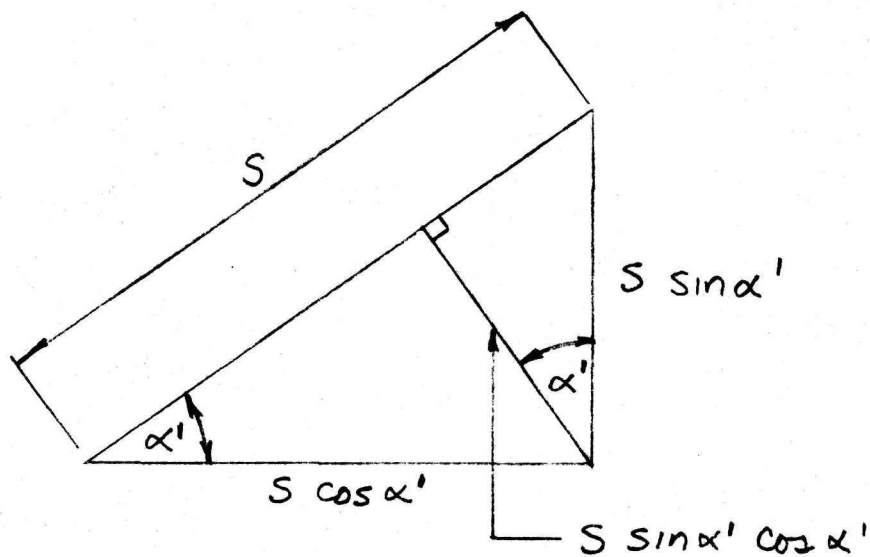
IDEALIZED SPAR CROSS-SECTION CONTOUR



a) Fiber Stress



b) Fiber Tensile Load Components



c) Fiber Widths

FIGURE A-2

FIBER GEOMETRY AND LOAD COMPONENTS

$$\sigma_{f\theta} = \text{fiber hoop stress} = \frac{T \sin \alpha'}{t_f s \cos \alpha'} \quad (\text{A-5})$$

$$\sigma_{fx} = \text{fiber longitudinal stress} = \frac{T \cos \alpha'}{t_f s \sin \alpha'} \quad (\text{A-6})$$

From (A-4) to (A-6) we obtain,

$$\sigma_{f\theta} = \sigma_f \sin^2 \alpha' \quad (\text{A-7})$$

$$\sigma_{fx} = \sigma_f \cos^2 \alpha' \quad (\text{A-8})$$

6.2.1.3 Strain Geometry

With metal and fiber element lengths before and after cryogenic stretch forming and strains as defined on Figure A-3, we have using the elementary geometric relation,

$$a^2 + b^2 = c^2 = a^2 (1 + \epsilon_x)^2 + b^2 (1 + \epsilon_\theta)^2 = c^2 (1 + \epsilon_f)^2 \quad (\text{A-9})$$

Noting that $a^2 + b^2 = c^2$ and $\sin \alpha = b/c$ we find from (A-9) after simplification,

$$\sin^2 \alpha' = \frac{(\epsilon_f - \epsilon_x) (2 + \epsilon_f + \epsilon_x)}{(\epsilon_\theta - \epsilon_x) (2 + \epsilon_\theta + \epsilon_x)} \quad (\text{A-10})$$

which defines the initial fiber wrap angle in terms of fiber and metal strains.

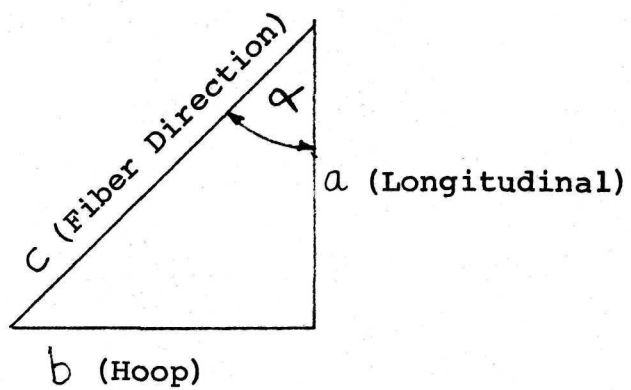
If the metal longitudinal strain, $\epsilon_x = 0$, we have the special case,

$$\sin^2 \alpha' = \frac{\epsilon_f (2 + \epsilon_f)}{\epsilon_\theta (2 + \epsilon_\theta)} \quad (\text{A-11})$$

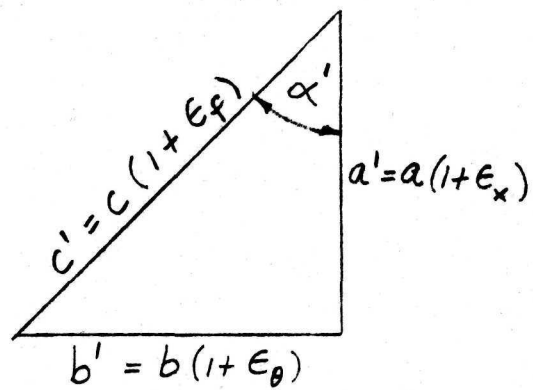
From geometry and definition (Figure A-3),

$$\sin \alpha' = \frac{b^1}{c^1} = \left(\frac{b}{c} \right) \frac{(1 + \epsilon_\theta)}{(1 + \epsilon_f)} = \sin \alpha \frac{(1 + \epsilon_\theta)}{(1 + \epsilon_f)} \quad (\text{A-12})$$

This relates the final to the initial fiber wrap angle.



a) Before Cryostretch



b) After Cryostretch

FIGURE A-3

SPAR STRAINS

6.2.1.4 Conditions at Cryostretch

(Pressure = P_s , Temperature = -320°F)

Design the metal liner to behave as a cylinder with true cryogenic stresses (see Section 3.1.1)

$$\sigma_{M\theta} = 250 \text{ ksi} \quad (\text{A-13})$$

$$\sigma_{Mx} = 125 \text{ ksi}$$

For Heat #76235 (See Figure 3)

this requires,

$$\epsilon_{\theta} = .142 \text{ in/in} \quad (\text{A-14})$$

$$\epsilon_x = 0 \text{ (See Section 3.1.1)}$$

Selecting as a design point a cryogenic fiber strain,

$$\epsilon_f = .01 \text{ (in/in)} \quad (\text{A-15})$$

and using Young's Modulus, $E_f \approx 12 \times 10^3 \text{ (ksi)}$ we have the cryogenic fiber stress,

$$\sigma_f = .01 \times 12 \times 10^3 = 120 \text{ ksi} \quad (\text{A-16})$$

From (A-11) and (A-12) using the numerical values of (A-14) to (A-16) we compute the initial and final fiber wrap angles,

$$\sin^2 \mathcal{L} = \frac{(.01)(2.01)}{(.142)(2.142)} = .0662; \sin \mathcal{L} = .258$$

$$\mathcal{L} = 14.95^\circ \approx 15^\circ \quad (\text{A-17})$$

(Initial fiber wrap angle)

$$\sin \mathcal{L}' = (.258) \frac{(1.142)}{1.01} = .292$$

$$\mathcal{L}' = 17^\circ \quad (\text{A-18})$$

(Final fiber wrap angle after cryo-stretch)

Using (A-7), (A-8), (A-18) we find,

$$\sigma_{f\theta} = (120) (\sin^2 17^\circ) = 10.23 \text{ ksi} \quad (\text{A-19})$$

$$\sigma_{fx} = (120) (\cos^2 17^\circ) = 109.4 \text{ ksi}$$

Imposing hoop and longitudinal equilibrium requirements at cryogenic condition, we have from (A-1), (A-3), (A-13) and (A-19),

$$N_{\theta} = P_s R = \sigma_{f\theta} t_f + \sigma_{M\theta} t_M = 10.23 t_f + 250 t_M$$

$$\frac{P_s R}{t_M} = 250 + 10.23 \left(\frac{t_f}{t_M} \right) \quad \text{and,} \quad (\text{A-20})$$

$$\frac{N_x}{t_M} = \frac{P_s R}{t_M} = \sigma_{Mx} + \sigma_{fx} \left(\frac{t_f}{t_M} \right) = 125 + 109.4 \left(\frac{t_f}{t_M} \right) \quad (\text{A-21})$$

From (A-20) and (A-21) we obtain the fiber to metal thickness ratio,

$$\frac{t_f}{t_M} = 1.26 \quad \text{and,} \quad (\text{A-22})$$

$$\left(\frac{P_s R}{t_M} \right) = 125 + (109.4) (1.26) = 263 \text{ ksi} \quad (\text{A-23})$$

The fiber to metal thickness ratio point above is plotted versus initial fiber wrap angle $\alpha = 15^\circ$ on the design graph of Figure 5.

6.2.1.5 Conditions at Prestressed State (pressure, $p = 0$, temperature = R.T.)

Using (A-7), (A-8), (A-18) we determine the hoop and longitudinal components of the fiber prestress as,

$$\begin{aligned} \sigma_{f\theta}^1 &= \sigma_f^1 (\sin^2 17^\circ) = .085 \sigma_f^1 \\ \sigma_{fx}^1 &= \sigma_f^1 (\cos^2 17^\circ) = .915 \sigma_f^1 \end{aligned} \quad (\text{A-24})$$

From equilibrium requirements at zero pressure, we have using (A-22) and (A-24),

$$\sigma_{M\theta}^1 t_M + \sigma_{f\theta}^1 t_f = 0 = \sigma_{M\theta}^1 + (.085 \sigma_f^1) \left(\frac{t_f}{t_M} \right)$$

$$0 = \sigma_{M\theta}^1 + (.085 \sigma_f^1) (1.26)$$

$$\sigma_{M\theta}^1 + .107 \sigma_f^1 = 0 \quad \text{and,} \quad (\text{A-25})$$

$$\begin{aligned}\sigma_{Mx}^1 t_M + \sigma_{fx}^1 t_f &= 0 = \sigma_{Mx}^1 + (.915 \times 1.26 \sigma_f^1) \\ \sigma_{Mx}^1 + 1.152 \sigma_f^1 &= 0\end{aligned}\tag{A-26}$$

Solving (A-25) and (A-26) simultaneously gives,

$$\left. \begin{aligned}\sigma_f^1 &= -.868 \sigma_{Mx}^1 \\ \sigma_{M\theta}^1 &= .0928 \sigma_{Mx}^1\end{aligned}\right\}\tag{A-27}$$

6.2.1.6 Strain Increments

(Elastic rebound from $P = P_s$,
 $T = -320^\circ\text{F}$ to $P = 0$, $T = \text{RT}$)

Using Hooke's Law, including thermal strains, we have for Poisson's ratio = .3 the strain increments,

$$\Delta \epsilon_\theta = \frac{\Delta \sigma_{M\theta} - .3 \Delta \sigma_{Mx}}{E_M} + \alpha_M \Delta T\tag{A-28}$$

$$\Delta \epsilon_x = \frac{\Delta \sigma_{Mx} - .3 \Delta \sigma_{M\theta}}{E_M} + \alpha_M \Delta T\tag{A-29}$$

$$\Delta \epsilon_f = \frac{\Delta \sigma_f}{E_f} + \alpha_f \Delta T\tag{A-30}$$

The stress increments from cryogenic state to prestressed state are (using A-13, A-27)

$$\left. \begin{aligned}\Delta \sigma_{Mx} &= 125 - \sigma_{Mx}^1 \\ \Delta \sigma_{M\theta} &= 250 - \sigma_{M\theta}^1 = 250 - .0928 \sigma_{Mx}^1 \\ \Delta \sigma_f &= 120 - \sigma_f^1 = 120 + .868 \sigma_{Mx}^1\end{aligned}\right\}\tag{A-31}$$

From Mohr's circle of strain, Figure A-4, we obtain the relation between fiber and metal strains,

$$\begin{aligned}\Delta \epsilon_f &= 1/2 (\Delta \epsilon_x + \Delta \epsilon_\theta) + 1/2 (\Delta \epsilon_\theta - \Delta \epsilon_x) \cos 2\alpha^1 \\ \Delta \epsilon_f &= \Delta \epsilon_\theta \left(\frac{1 + \cos 2\alpha^1}{2} \right) + \Delta \epsilon_x \left(\frac{1 - \cos 2\alpha^1}{2} \right)\end{aligned}\tag{A-32}$$

For $2\alpha^1 = 34^\circ$ from (A-18),

$$\Delta \epsilon_f = .9145 \Delta \epsilon_\theta + .0855 \Delta \epsilon_x\tag{A-33}$$

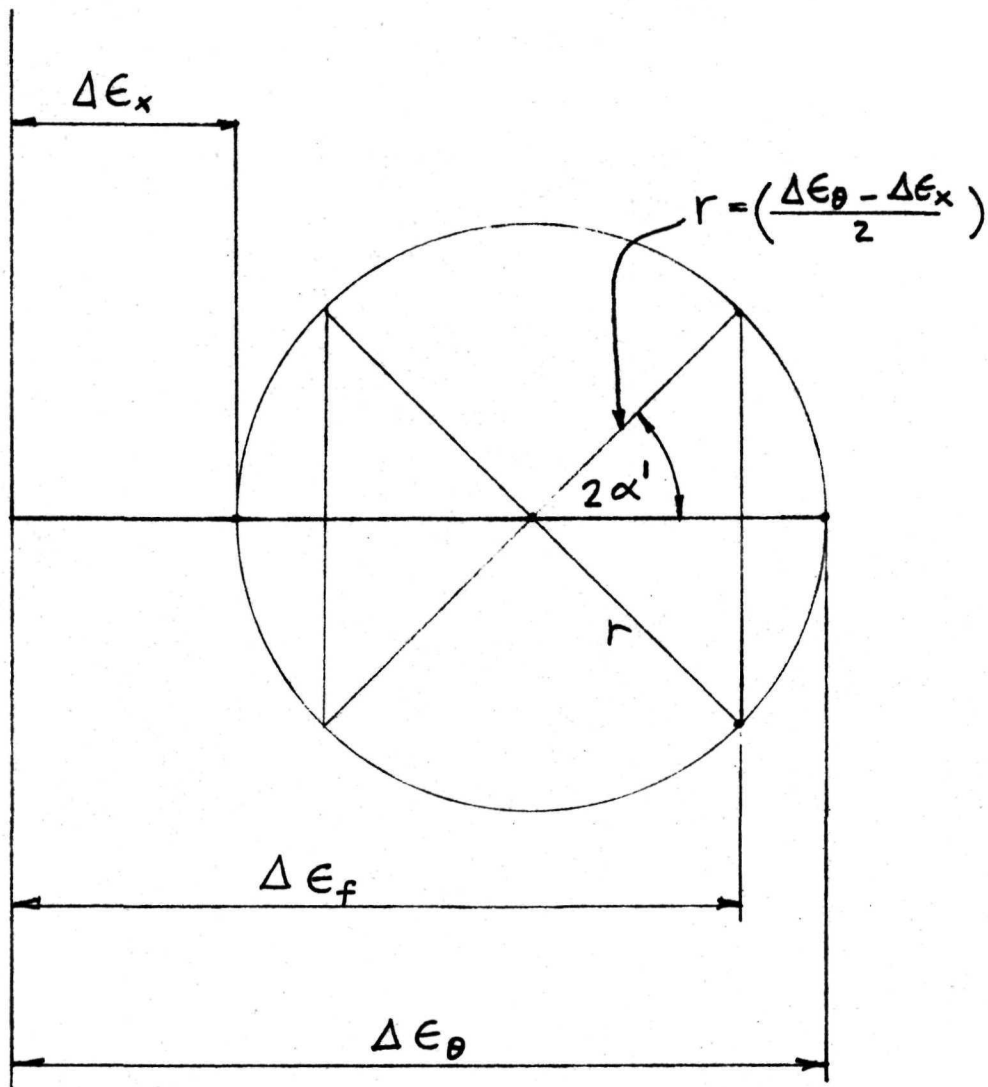


FIGURE A-4

MOHR'S CIRCLE OF STRAIN

Using (A-28), (A-29), (A-31) and taking $E_M = 27 \times 10^3$ ksi, $\alpha_M = 4.6 \times 10^{-6}$ in/in $^\circ$ F (R.T. to -320° F) and $\Delta T = 390^\circ$ F gives,

$$\Delta \epsilon_x = \frac{(125 - \sigma_{Mx}^1) - .3(250 - .0928 \sigma_{Mx}^1) + 4.6 \times 390 \times 10^{-6}}{27 \times 10^3}$$

$$(10^3) (\Delta \epsilon_x) = 3.643 - .036 \sigma_{Mx}^1 \quad (A-34)$$

$$\Delta \epsilon_{M\theta} = \frac{(250 - .0928 \sigma_{Mx}^1) - .3(125 - \sigma_{Mx}^1) + 4.6 \times 390 \times 10^{-6}}{27 \times 10^3}$$

$$(10^3) (\Delta \epsilon_{\theta}) = 9.633 + .00766 \sigma_{Mx}^1 \quad (A-35)$$

From (A-33) using (A-30), (A-34) and (A-35) using $E_f = 12 \times 10^3$ ksi, $\alpha_f = 2 \times 10^{-6}$ in/in $^\circ$ F (R. T. to -320° F) and $\Delta T = 390^\circ$ F we find,

$$\frac{(120 + .868 \sigma_{Mx}^1)}{12 \times 10^3} + 2 \times .390 \times 10^{-3} = 10^{-3} \left\{ \begin{array}{l} .9145(9.633 + .00766 \sigma_{Mx}^1) \\ + .0855(3.643 - .036 \sigma_{Mx}^1) \end{array} \right\}$$

Solving for σ_{Mx}^1 gives,

$$\sigma_{Mx}^1 = -24.45 \text{ ksi} \quad (A-36)$$

From (A-27) and (A-36),

$$\sigma_{M\theta} = .0928 (-24.45) = 2.27 \text{ ksi} \quad (A-37)$$

$$\sigma_f^1 = -.868 (24.45) = 21.25 \text{ ksi} \quad (A-38)$$

These prestress value points are plotted versus initial fiber wrap angle, $\alpha = 15^\circ$, on the design graph of Figure 5.

6.2.2 Bending, Axial and Torsional Load Effects for Composite Spar

6.2.2.1 Bending of Composite Spar

Mohr's circle of strain (see Figure A-4, Section 6.2.1.6) gives the relation between metal longitudinal and hoop strains and fiber strain as,

$$\epsilon_f = \left(\frac{\epsilon_x + \epsilon_\theta}{2} \right) + \left(\frac{\epsilon_x - \epsilon_\theta}{2} \right) \cos 2\alpha^1$$

Using trigonometric identities and simplifying one has,

$$\epsilon_f = \epsilon_x \cos^2 \alpha^1 + \epsilon_\theta \sin^2 \alpha^1 \quad (\text{A-39})$$

For bending effects, treat as "narrow beam", i.e., Poisson's ratio = 0, corresponding to hoop strain $\epsilon_\theta = 0$. Then from (A-39) fiber strain, for composite spar bending is,

$$\epsilon_f = \epsilon_x \cos^2 \alpha^1 \quad (\text{A-40})$$

Taking the metal longitudinal strain distribution as linear through the thickness we have,

$$\epsilon_x = \epsilon_0 z \quad (\text{A-41})$$

Then from Hooke's Law and (A-8), (A-41) we obtain the metal and fiber bending stresses,

$$\sigma_{Mb} = E_M \epsilon_x = E_M \epsilon_0 z \quad (\text{A-42})$$

$$\sigma_{fb} = \sigma_f \cos^2 \alpha^1 = (E_f \epsilon_f) \cos^2 \alpha^1 = E_f \cos^4 \alpha^1 \epsilon_0 z \quad (\text{A-43})$$

Since both the metal and the fibers resist part of the total moment we have the differential moments,

$$dM = dM_f + dM_M = \sigma_{fb} z dA_f + \sigma_{Mb} z dA_M$$

Using (A-42), (A-43) and integrating, yields the total moment

$$M = \int dM = \epsilon_0 \left\{ E_f \cos^4 \alpha^1 \int z^2 dA_f + E_M \int z^2 dA_M \right\}$$

Noting that the integrals represent fiber and metal moment of inertias, we have,

$$M = \epsilon_o \left\{ (E_f \cos^4 \alpha^1) I_f + E_M I_M \right\} \quad (A-44)$$

The bending strain parameter ϵ_o , is then defined from (A-44) as,

$$\epsilon_o = \frac{M}{E_M I_M + (E_f \cos^4 \alpha^1) I_f} = \frac{M}{(EI)_{\text{effective}}} = \frac{M}{EI} \quad (A-45)$$

For reference purposes, define now a datum homogeneous metal spar with thickness t_o , bending stiffness $E_M I_o$ and bending stress = σ_{bo} . For the same moment and cross-sectional perimeter and shape the composite and homogeneous spar bending stresses will be proportional to the bending stiffnesses. Using (A-45) one obtains,

$$\frac{\sigma_{Mb}}{\sigma_{bo}} = \frac{M/EI}{M/E_M I_o} = \frac{E_M I_o}{E_M I_M + (E_f \cos^4 \alpha^1) I_f} \quad (A-46)$$

For a thin-walled cross-section, the moment of inertia is, to good approximation, proportional to the wall thickness. Then we have from (A-46) the metal bending stress ratio,

$$\frac{\sigma_{Mb}}{\sigma_{bo}} = \frac{E_M t_o}{E_M t_M + (E_f \cos^4 \alpha^1) t_f} = \frac{(t_o/t_M)}{1 + \left(\frac{t_f}{t_M} \right) \left(\frac{E_f \cos^4 \alpha^1}{E_M} \right)} \quad (A-47)$$

Using (A-42), (A-43) and (A-47) we obtain the fiber bending stress ratio,

$$\frac{\sigma_{fb}}{\sigma_{bo}} = \left(\frac{\sigma_{Mb}}{\sigma_{bo}} \right) \left(\frac{E_f \cos^4 \alpha^1}{E_M} \right) \quad (A-48)$$

Blade mass is composed of spar mass plus non-structural mass, i.e.,

$$m_b = m_s + m_{ns} = m_s + \lambda m_b \quad (A-49)$$

with λ , the blade non-structural mass parameter (fraction of total blade mass that is non-structural)

Assuming the same non-structural mass when comparing the composite spar to the reference homogeneous metal spar, we obtain from (A-48) the blade masses,

$$m_{bo} = m_{so} + \lambda m_{bo}$$

$$m_{bc} = m_{sc} + \lambda m_{bo} = m_{sc} + \left(\frac{\lambda}{1 - \lambda} \right) m_{so}$$

The homogeneous to composite blade mass ratio then becomes after simplification,

$$\frac{m_{bo}}{m_{bc}} = \frac{\left(\frac{m_{so}}{1 - \lambda} \right)}{m_{sc} + \left(\frac{\lambda}{1 - \lambda} \right) m_{so}} = \frac{1}{\lambda + (1 - \lambda) \frac{m_{sc}}{m_{so}}}$$

For the same perimeter and length, the masses are proportional to the wall thickness times density. We then have,

$$\frac{m_{bo}}{m_{bc}} = \frac{1}{\lambda + (1 - \lambda) \frac{\rho_M t_M + \rho_{fc} t_{fc}}{\rho_M t_o}} = \frac{1}{\lambda + (1 - \lambda) \frac{t_M}{t_o} + \frac{\rho_{fc}}{\rho_M} \frac{t_{fc}}{t_o}} \quad (A-50)$$

Using (A-46), (A-47) and (A-50) we obtain, after simplification, the bending stiffness per unit mass ratio (composite to homogeneous)

$$\frac{\hat{k}_{bc}}{\hat{k}_{bo}} \equiv \frac{EI/m_{bc}}{EI_o/m_{bo}} = \frac{\left(\frac{t_M}{t_o} \right) + \left(\frac{t_f}{t_o} \right) \left(\frac{E_f \cos^4 \alpha^1}{E_M} \right)}{\lambda + (1 - \lambda) \left\{ \frac{t_M}{t_o} + \frac{\rho_{fc}}{\rho_M} \frac{t_{fc}}{t_o} \right\}} \quad (A-51)$$

From basic data on resin and glass density, we compute the composite fiber thickness and density as follows.

$$\text{resin density} = 1.16 \times \frac{62.4}{1728} = .0419 \text{ \#/in}^3$$

$$\text{S glass density} = 2.54 \times \frac{62.4}{1728} = .0917 \text{ \#/in}^3$$

If μ = resin fraction by weight, the density ρ_{fc} of the glass-resin composite is,

$$\rho_{fc} = \frac{1}{\frac{\mu}{.0419} + \frac{(1 - \mu)}{.0917}} = \frac{1}{10.9 + 12.96\mu} \quad (A-52)$$

Also, the volume ratio of glass fibers, $(VR)_f$, is obtained as,

$$(VR)_f = \frac{\frac{(1-\mu)}{.0917}}{\frac{\mu}{.0419} + \frac{(1-\mu)}{.0917}} = \frac{1-\mu}{1+1.19\mu} \quad (A-53)$$

Noting that $t_{fc} = t_f / (VR)_f$ and using (A-53) gives the fiber composite to structural thickness ratio,

$$\left(\frac{t_{fc}}{t_f} \right) = \frac{1+1.19\mu}{1-\mu} \quad (A-54)$$

6.2.2.2 Direct Axial Stresses in Composite Spar (Centrifugal Loading)

Using Hooke's Law, (A-8) and (A-40) we obtain,

$$\epsilon_f = \frac{\sigma_f}{E_f} = \left(\frac{\sigma_{fx} / \cos^2 \alpha^1}{E_f} \right) = \epsilon_x \cos^2 \alpha^1$$

Then,

$$\epsilon_x = \frac{\sigma_{fx}}{E_f \cos^4 \alpha^1} \quad (A-55)$$

From Hooke's Law using (A-55),

$$\epsilon_x = \frac{\sigma_{Mx}}{E_M} = \frac{\sigma_{fx}}{E_f \cos^4 \alpha^1}, \text{ or}$$

$$\frac{\sigma_{fx}}{\sigma_{Mx}} = \frac{\sigma_f \cos^2 \alpha^1}{\sigma_{Mx}} = \frac{E_f \cos^4 \alpha^1}{E_M}, \quad (A-56)$$

which gives ratio of fiber to metal stresses due to axial (centrifugal) loads.

From the definition of centrifugal force we have

$$dF = (\gamma'') dx \Omega^2 (a+x) \quad (A-57)$$

Since mass per unit length γ''

(including non-structural mass) is given by perimeter \times thickness \times density , we obtain from (A-57) after integrating the centrifugal force,

$$F = \int_g dF = \int_g \left[\int_M t_M + \int_{fc} t_{fc} + \int_{ns} t_{ns} \right] \Omega^2 \left[\int (a+x) dx \right] \Phi(x)$$

or,

$$F = \int_g \left[\int_M t_M + \int_{fc} t_{fc} + \int_{ns} t_{ns} \right] \Omega^2 \left[\Phi(x) \right] \quad (A-58)$$

From equilibrium considerations,

$$\Gamma \left[\sigma_{Mx} t_M + \sigma_{fx} t_f \right] = F \quad (A-59)$$

Using (A-56), (A-58) and (A-59), and solving for σ_{Mx} , the longitudinal membrane stress in the metal of the composite spar, gives

$$\sigma_{Mx} = \frac{\Omega^2}{g} \frac{(\int_M t_M + \int_{fc} t_{fc} + \int_{ns} t_{ns}) \Phi(x)}{\left(t_M + \frac{t_f E_f \cos^4 \alpha}{E_M} \right)} \quad (A-60)$$

Define now the centrifugal force, F_o , of the equivalent homogeneous metal spar of the same shape, perimeter, angular velocity, radius, but with thickness t_o and density, ρ_M as,

$$F_o = \Gamma \sigma_{ox} t_o = \left(\frac{\text{mass}}{\text{unit length}} \right) (\Omega^2) \times \text{radius}$$

$$F_o = \Gamma \sigma_{ox} t_o = \int_g (\int_M t_o + \int_{ns} t_{ns}) \Omega^2 \Phi(x)$$

As before, non-structural mass has been included.

Solving for σ_{ox} , the longitudinal membrane stress in the equivalent homogeneous metal spar yields,

$$\sigma_{ox} = \frac{\Omega^2 \Phi(x)}{g} \left\{ \rho_M + \frac{\int_{ns} t_{ns}}{t_o} \right\} \quad (A-61)$$

From (A-60) and (A-61), noting the definition of λ , the non-structural mass parameter, we obtain after simplification,

$$\left(\frac{\sigma_{Mx}}{\sigma_{ox}}\right) = \frac{1 + \frac{\int_{fc}}{\int_M} \left(\frac{t_{fc}}{t_M}\right) + \left(\frac{\lambda}{1-\lambda}\right) \left(\frac{t_o}{t_M}\right)}{1 + \left(\frac{t_{fc}}{t_M}\right) \left(\frac{E_f \cos^4 \alpha^1}{E_M}\right) \left(\frac{1}{1-\lambda}\right)} \quad (A-62)$$

6.2.2.3 Torsional Effects in Composite Spar

Both the metal liner and the fibers resist the applied torque. The metal liner twists and the pretensioned fibers undergo extensional strains which produce small changes in the fiber helix angle.

The resisting torque of the metal liner is related to the angle of twist per unit length by, reference 14,

$$T_M = \theta \left\{ (GJ)_M + \sigma_{Mx}^i I_{pM} \right\} \quad (A-63)$$

where, the conventional metal torsion stiffness parameter,

$$(GJ)_M = \frac{4 A^2 G_M}{\oint \frac{ds}{t_M}} \quad (A-64)$$

and the second term represents the effect of axial stresses.

If α^1 is the helix angle of the fiber wrap prior to loading in torsion and $d\alpha^1$ the angle change resulting from the applied torque as sketched in Figure A-5, we compute the fiber extensional strain, ϵ_f , from the fiber length changes as,

$$\epsilon_f = \frac{\left\{ \frac{x}{\cos(\alpha^1 + d\alpha^1)} \right\} - \left(\frac{x}{\cos \alpha^1} \right)}{\left(\frac{x}{\cos \alpha^1} \right)} = \frac{\cos \alpha^1}{\cos(\alpha^1 + d\alpha^1)} - 1$$

Using trigonometric identities and taking $\sin d\alpha^1 \approx d\alpha^1$, $\cos d\alpha^1 \approx 1$ appropriate for $d\alpha^1$ small, we have after simplification,

$$\epsilon_f \approx \frac{d\alpha^1}{\cot \alpha^1 - d\alpha^1} \approx \frac{d\alpha^1}{\cot \alpha^1} \quad \text{or,} \quad \epsilon_f \approx \tan \alpha^1 (d\alpha^1) \quad (A-65)$$

Using Hooke's Law, we obtain the change in fiber tension

$$dF = (E_f \epsilon_f) A_f = E_f A_f \tan \alpha^1 d\alpha^1 \quad (A-66)$$

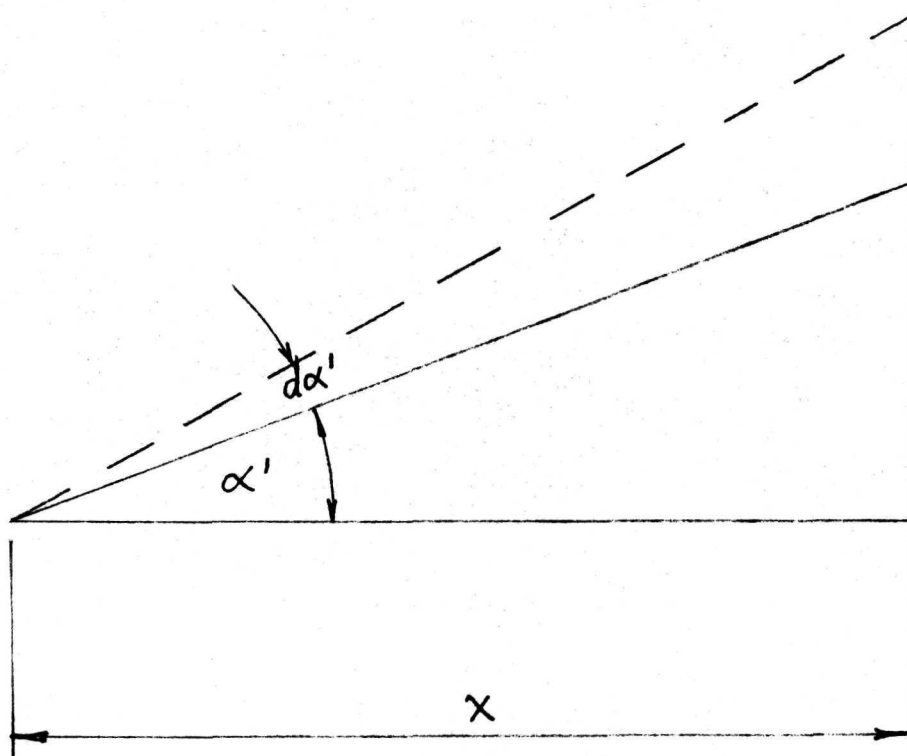


FIGURE A-5

FIBER WRAP ANGLE CHANGE

This fiber tension change either increases or decreases the fiber pretension depending on the direction of twist. The fiber torsional resistance results from the sum of tangential components of fiber tensions times their respective lever arms as sketched on Figure 6, Section 3.0.

The differential resisting torque for each pair of fibers is then,

$$dT_f = r \left\{ (F + dF) \sin (\alpha' + d\alpha') - (F - dF) \sin (\alpha' - d\alpha') \right\}$$

Simplifying, using trigonometric identities and the fact that $d\alpha'$ is small gives,

$$dT_f = 2r \left\{ dF \sin \alpha' + F \cos \alpha' d\alpha' \right\}$$

Noting that the change in fiber helix angle due to torsion is the twist per unit length times the radius to the cross-section shear center, i.e.,

$d\alpha' = r\theta$, and that dT_f is for each pair of fibers, we have, using (A-66) and summing up for all fibers,

$$T_f = \sum dT_f = \sum_{i=1}^{i=n} \left[E_f A_f r_i^2 \tan \alpha' \sin \alpha' + r_i^2 F \cos \alpha' \right]$$

Since fiber tension $F = A_f \sigma_f$ and the polar moment of inertia of the fibers,

$$I_{pf} = \sum_{i=1}^{i=n} A_f r_i^2 \quad (A-67)$$

we obtain finally the resisting fiber torque as,

$$T_f = \theta \left[E_f \tan \alpha' \sin \alpha' + \sigma_f \cos \alpha' \right] (I_{pf}) \quad (A-68)$$

Since the resisting torque of the composite spar, T_c , is the sum of metal and fiber resisting torques, i.e.,

$T_c = T_M + T_f$ and defining the composite spar torsional stiffness as,

$$k_{Tc} = \frac{T_c}{\theta}, \text{ noting that for thin-wall cross-sections, } \frac{I_{pf}}{I_{pM}} = \frac{t_f}{t_M},$$

we have, using (A-63) and (A-68),

$$k_{Tc} = (GJ)_M + I_{pM} \left[\sigma_{Mx} + \left(\frac{t_f}{t_M} \right) \left\{ E_f \tan \alpha' \sin \alpha' + \sigma_f \cos \alpha' \right\} \right] \quad (A-69)$$

blade, $\sigma_{Mx} = 0$. Then from (A-63) we have the reference torsional stiffness,

$$k_{T0} = (GJ) \quad (A-70)$$

Using now (A-50), (A-69), (A-70) we find the torsional stiffness per unit mass ratio,

$$\frac{(k_{Tc}/m_c)}{(k_{T0}/m_o)} = \frac{\hat{k}_{Tc}}{\hat{k}_{T0}} = \frac{\left\{ \left(\frac{t_M}{t_o} \right) + \left(\frac{I_{pM}}{GJ} \right) \left[\sigma_{Mx} + E_f \left(\frac{t_f}{t_M} \right) \left(\tan \alpha' \sin \alpha' + \frac{\sigma_f}{E_f} \cos \alpha' \right) \right] \right\}}{\left\{ \lambda + (1 - \lambda) \left[\left(\frac{t_M}{t_o} \right) + \left(\frac{\rho_{fc}}{\rho_M} \right) \left(\frac{t_{fc}}{t_o} \right) \right] \right\}} \quad (A-71)$$

Noting that in most cases, the term $\frac{\sigma_f}{E_f} \cos \alpha'$ (the order of the fiber strain) is small compared to

the other numerator terms, we obtain the approximate relation,

$$\frac{\hat{k}_{Tc}}{\hat{k}_{T0}} \approx \frac{\left\{ \left(\frac{t_M}{t_o} \right) + \left(\frac{I_{pM}}{GJ} \right) \left[\sigma_{Mx} + \frac{E_f t_f}{t_M} \tan \alpha' \sin \alpha' \right] \right\}}{\left\{ \lambda + (1 - \lambda) \left[\frac{t_M}{t_o} + \frac{\rho_{fc}}{\rho_M} \frac{t_{fc}}{t_o} \right] \right\}} \quad (A-72)$$

6.2.2.4 Composite Spar Design Point Calculations

Table 2, Section 3.1.6 gives composite spar design data for various initial fiber wrap angles. A typical design point calculation is presented in this section. In these computations, we use,

$$\frac{t_{fc}}{t_f} = 1.5, \frac{\rho_{fc}}{\rho_M} \approx 1/4 \text{ and } \frac{E_f}{E_M} = \frac{12.4}{25} = .497$$

Selecting for typical design point calculations initial fiber wrap angle, $\alpha = 17\frac{1}{2}^\circ$, with final wrap angle $\alpha' = 19.8^\circ$, we have from Figure 5 (see Section 6.2.1).

$$t_f/t_M = .987 = \text{fiber to metal thickness ratio}$$

$$\sigma_{Mx}^1 = -59 \text{ ksi} = \text{metal longitudinal compressive prestress}$$

$$\sigma_f^1 = 67 \text{ ksi} = \text{fiber tensile prestress}$$

If the allowable bending stress of the metal liner in composite is taken as twice the bending stress in homogeneous metal reference spar $\left(\frac{\sigma_{Mb}}{\sigma_{bo}} = 2\right)$ because the

composite spar metal liner is always in compression, we have from (A-47) and the above numerical values noting that $\cos^4(19.8^\circ) = .783$,

$$2 = \frac{\left(\frac{t_o}{t_M}\right)}{1 + .987 \times .497 \times .783} = \frac{\left(\frac{t_o}{t_M}\right)}{1.384}$$

$$\frac{t_M}{t_o} = .361 \text{ (relative metal thickness)}$$

For simplicity, we take non-structural mass parameter, $\lambda = 0$, and compute the relative weight (mass of spar from (A-50) as,

$$\frac{W_c}{W_o} = \frac{m_{bc}}{m_{bo}} = \left(\frac{t_M}{t_o}\right) \left[1 + \frac{\int_{fc}}{\int_M} \left(\frac{t_{fc}}{t_M}\right)\right] = .361 \left[1 + \frac{1}{4} \times 1.5 \times .987\right]$$

$$\frac{W_c}{W_o} = .496$$

Using (A-62) and appropriate numerical values gives,

$$\frac{\sigma_{Mx}}{\sigma_{ox}} = \frac{\left[1 + \frac{1}{4} \times 1.5 \times .987\right]}{1 + .987 (.497 \times .783)} = .989 \quad \text{and,}$$

$$\sigma_{Mx} = (.989) (24) = 23.7 \text{ ksi}$$

Using (A-56), (A-48) and above yields,

$$\sigma_{fx} = (23.7) (.497) (.783) = 9.2 \text{ ksi}$$

$$\sigma_{fb} = (\pm 34) (.497) (.783) = \pm 13.2 \text{ ksi}$$

Metal and fiber operating stress ranges are, therefore,

$$\sigma_M = (-59 + 23.7) \pm 34 = (-35.3 \pm 34) \text{ ksi}$$

$$\sigma_f = (67 + 9.2) \pm 13.2 = (76.2 \pm 13.2) \text{ ksi}$$

6.2.2.5 Composite Spar Stiffness Calculations

Table 3, Section 3.1.7 gives composite prestressed spar stiffness and stiffness versus weight trade-off data. Typical detailed calculations leading to these numerical results are presented herein.

For calculation purposes, we use the following numerical values (see Section 6.2.2.4) for the 17 1/2° initial fiber wrap angle composite spar selected design point:

$$\alpha' = 19.8^\circ, \sin \alpha' = .339, \tan \alpha' = .360, \cos^4 \alpha' = .783, \frac{t_f}{t_M} = .987,$$

$$\frac{t_{fc}}{t_f} = 1.5, \frac{t_M}{t_o} = .361$$

$$\frac{\int_{fc}}{\int_M} = 1/4, E_f/E_M = .497, \sigma_{Mx} = -35.3 \text{ ksi (net direct stress)}$$

For completeness in comparing a prestressed composite blade to a datum homogeneous metal blade, we take non-structural mass parameter, $\lambda = .23$ (reference 12).

a) Basic 17 1/2° Design Point Configuration

Using equations (A-50) and (A-51) and the above numerical values, we compute the composite to homogeneous spar mass and bending stiffness per unit mass ratios as follows:

$$(m_{bc}/m_{bo})_{\text{for } \lambda = 0} = .361 \left(1 + \frac{1}{4} \times 1.5 \times .987 \right) = .494 \text{ (structural ratio)}$$

$$\frac{m_{bc}}{m_{bo}} = .23 + .67 \times .361 \left(1 + \frac{1}{4} \times 1.5 \times .987 \right) = .561 \text{ (total blade ratio)}$$

$$\frac{k_{bc}}{k_{bo}} = \frac{\text{bending stiffness ratio}}{\text{mass ratio}} = \frac{.361 (1 + .987 \times .783)}{.561} = \frac{.50}{.561} = .892$$

For the computation of torsional stiffness properties, we idealize the cross-section as a thin-walled rectangular section of width, L four times its depth, d . The torsional stiffness factor of the metal alone, $(GJ)_M$ is given by,

$$(GJ)_M = \frac{4 A^2 G_M}{\oint \frac{ds}{t_M}} = \frac{4 d^2 L G_M t_M}{2 (L + d)}$$

The metal polar moment of inertia may be derived as,

$$I_{pM} = I_x + I_y = \frac{t_M d^3}{6} \left[\left\{ 1 + \left(\frac{L}{d} \right) \left[\left(\frac{t_M}{d} \right)^2 + 3 \right] \right\} + \left(\frac{L}{d} \right)^3 \left\{ 1 + \left(\frac{d}{L} \right) \left[\left(\frac{t_M}{L} \right)^2 + 3 \right] \right\} \right]$$

or,

$$I_{pM} \approx \frac{t_M d^3}{6} \left[1 + 3 \left(\frac{L}{d} \right) + \left(\frac{L}{d} \right)^3 \left\{ 1 + 3 \left(\frac{d}{L} \right) \right\} \right] \quad \left(\text{for } \frac{t_M}{L} \text{ and } \frac{t_M}{d} \ll 1 \right)$$

The ratio $\frac{I_{pM}}{(GJ)_M}$ is then given by,

$$\frac{I_{pM}}{(GJ)_M} \approx \frac{1}{12} \frac{d}{L} \left(1 + \frac{d}{L} \right) \left(\frac{1}{G_M} \right) \left[1 + 3 \frac{L}{d} + \left(\frac{L}{d} \right)^3 \left(1 + 3 \frac{d}{L} \right) \right] = \frac{1}{12} \left(\frac{1}{4} \right) \left(\frac{5}{4} \right) \left(\frac{1}{G_M} \right) \\ \times \left[1 + 3 \times 4 + (4)^3 \times \frac{7}{4} \right]$$

$$\frac{I_{pM}}{(GJ)_M} = \frac{3.23}{G_M}$$

Noting that for a thin-walled cross-section,

$$\frac{(GJ)_M}{(GJ)} = \left(\frac{t_M}{t_o} \right) \quad \text{we have,}$$

$$\frac{I_{pM}}{(GJ)} = \left(\frac{t_M}{t_o} \right) \left(\frac{3.23}{G_M} \right) = \left(\frac{t_M}{t_o} \right) \left(\frac{3.23}{E_M / 2.6} \right) = \frac{8.4}{E_M} \left(\frac{t_M}{t_o} \right)$$

Using the simplified relation (A-72) and the appropriate numerical values,

$$\frac{k_{Tc}}{k_{To}} = \frac{\text{torsional stiffness ratio}}{\text{mass ratio}} = \frac{.361 \left[1 + 8.4 \times .497 \left\{ \frac{-35.3}{12.4 \times 10^3} + .987 \times .339 \times .360 \right\} \right]}{.561}$$

$$\frac{k_{Tc}}{k_{To}} = \frac{.536}{.561} = .955 \approx .96$$

b) Added Fiber Configurations

Assume one adds 100% basic fiber thickness of 15° helix angle glass fibers and 30% basic fiber thickness of 45° helix angle glass fibers to enhance composite spar bending and torsional rigidities. Then using the above defined equations and numerical values, we compute the stiffness and mass increments as follows:

$$\Delta (m_{bc}/m_{bo})_{\lambda=0} = 1.0 \times (1.3 \times \frac{1}{4} \times 1.5 \times .987 \times .361) = .173$$

$$\Delta (m_{bc}/m_{bo})_{\lambda=.23} = .67 \times .173 = .116$$

The new structural and blade mass ratios then become,

$$(m_{bc}/m_{bo})_{\lambda=0} = .494 + .173 = .667 \approx .67 \text{ (structural mass ratio)}$$

$$(m_{bc}/m_{bo})_{\lambda=.23} = .561 + .116 = .677 \approx .68 \text{ (total blade mass ratio)}$$

Noting that $\cos^4(15^\circ) = .871$,

$\tan 15^\circ \sin 15^\circ = .268 \times .259$, $\cos^4(45^\circ) = .25$, $\tan 45^\circ \sin 45^\circ = 1 \times .707$, we have the stiffness ratio increments,

$$\Delta \left(\frac{k_{bc}}{k_{bo}} \right) = (.497) (.361) (.987) \left[1.0 \times .871 + .30 \times .25 \right] = .168$$

$$\Delta \left(\frac{k_{Tc}}{k_{To}} \right) = 8.4 \times .497 \times .361 \times .987 \left[1.0 \times .268 \times .259 + .30 \times 1.0 \times .707 \right] = .417$$

The new stiffness ratios then are,

$$\left(\frac{k_{bc}}{k_{bo}} \right) = .50 + .168 = .668 \approx .67 \text{ (bending stiffness ratio)}$$

$$\left(\frac{k_{Tc}}{k_{To}} \right) = .536 + .417 = .953 \approx .95 \text{ (torsional stiffness ratio)}$$

From which we obtain the stiffness ratios per unit mass,

$$\frac{\hat{k}_{bc}}{\hat{k}_{bo}} = \frac{.668}{.677} = .987 \approx .99$$

$$\frac{\hat{k}_{Tc}}{\hat{k}_{To}} = \frac{.953}{.677} = 1.41$$

If the added fibers are high modulus graphite with Young's modulus and density compared to glass fibers of $E_g/E_f \approx 4$ and $\frac{\rho_{gc}}{\rho_{fc}} \approx \frac{7}{8}$, we find the torsional

stiffness ratio increment as,

$$\Delta\left(\frac{k_{Tc}}{k_{To}}\right) = 4 \times .417 = 1.668 \quad \text{and then, the new torsional}$$

stiffness ratio is,

$$\left(\frac{k_{Tc}}{k_{To}}\right) = .536 + 1.668 \approx 2.20$$

In a similar manner, we compute the other stiffness and mass ratio results given in Table 3 which show the beneficial effect of the increased Young's modulus and reduced density of the added graphite fibers.

6.2.2.6 Flat Plate Buckling During Hydrostretch

Buckling of the unwrapped metal flat plate elements of the spar cross-section occurred during the room temperature hydrostretching operation as detailed in Section 3.3. If we take (conservatively) the boundary conditions of the flat plate as clamped all around due to the stiffening effect of the heads and curved cross-sectional members, we have the critical compressive strain (reference 15).

$$\epsilon_{cr} = \frac{\sigma_{cr}}{E} \approx 7 \left(\frac{t}{b}\right)^2$$

Using now thickness, $t = .025$, width, $b = 1.88$, we find the critical flat plate compressive strain as,

$$\epsilon_{cr} = 7 \left(\frac{.025}{1.88}\right)^2 = 1.24 \times 10^{-3} \text{ in/in.}$$

The curved members of the cross-section, hydrostretched plastically to a .2% diameter increase, will have a stress due to the forming pressure of about 45 ksi. Assuming as designed, that the curved members of the body section behave as cylinders, we compute their hoop elastic springback strain upon release of the forming pressure as,

$$\epsilon_{sp} = .85 \frac{\sigma}{E} = \frac{.85 \times 45}{25 \times 10^3} = 1.53 \times 10^{-3} \text{ in/in.}$$

Since the flat plate is attached to the curved members and $\epsilon_{sp} > \epsilon_{cr}$, the flat plate will buckle rather than shorten as a sheet.

6.3 Appendix 3 - Composite Spar Prestresses

This appendix details the computation of the prestresses in the two (2) composite prestressed spar specimens built during the program, part numbers D3819, serial numbers 4 and 5. This prestressed state at zero external load, compression in the metal liner and tension in the fiberglass, is determined by structural theory, geometric relations and spar inspection data taken prior and subsequent to cryogenic stretchforming the fiber wrapped metal lined spar.

6.3.1 Fiber Wrap Data for Spar Preforms

Measured fiber wrap data is given in Table 4.

TABLE 4 FIBER WRAP DATA FOR SPAR PREFORMS

Spar S/N	Fiber Wrap Angle (degrees)	Wt. Glass (gr.)	Wt. Resin (gr.)	Wt. Glass & resin (gr.)	Wt. Metal liner (gr.)	* Resin Fractions = wt. re- sin wt(glass & resin)	* Volume Ratio of glass (VR)g	* $\frac{t_{fc}}{t_f}$ = $\frac{1}{l}$ (VR)g	t_{fc} (for $t_f = 36$ Mils) (Mils)
2	17 3/4-19 1/2	425	117	542	1987	.216	.625	1.60	57.6
4	17 3/4-19 1/2	400	92	492	1977	.187	.664	1.505	54.2
5	17 3/4-19 1/2	403	75	478	1992	.157	.710	1.41	50.8
(composite fiber thickness)									↖

* See eq. (A-53), (A-54)

6.3.2 Estimate of Hoop Strain Based on Wrapped Spar Preform and Die Data

From Figure A-6 we note,

$$R = R_{\text{Die}} - (t_{\text{fc}} + W_{\text{sp}})$$

$$\Delta R = R - R_o$$

Then metal hoop strain = $\epsilon_{\theta} = \frac{\Delta R}{R_o}$, or

$$\epsilon_{\theta} = \left\{ \frac{R_{\text{Die}} - (t_{\text{fc}} + W_{\text{sp}})}{R_o} \right\} - R_o \quad (\text{A-73})$$

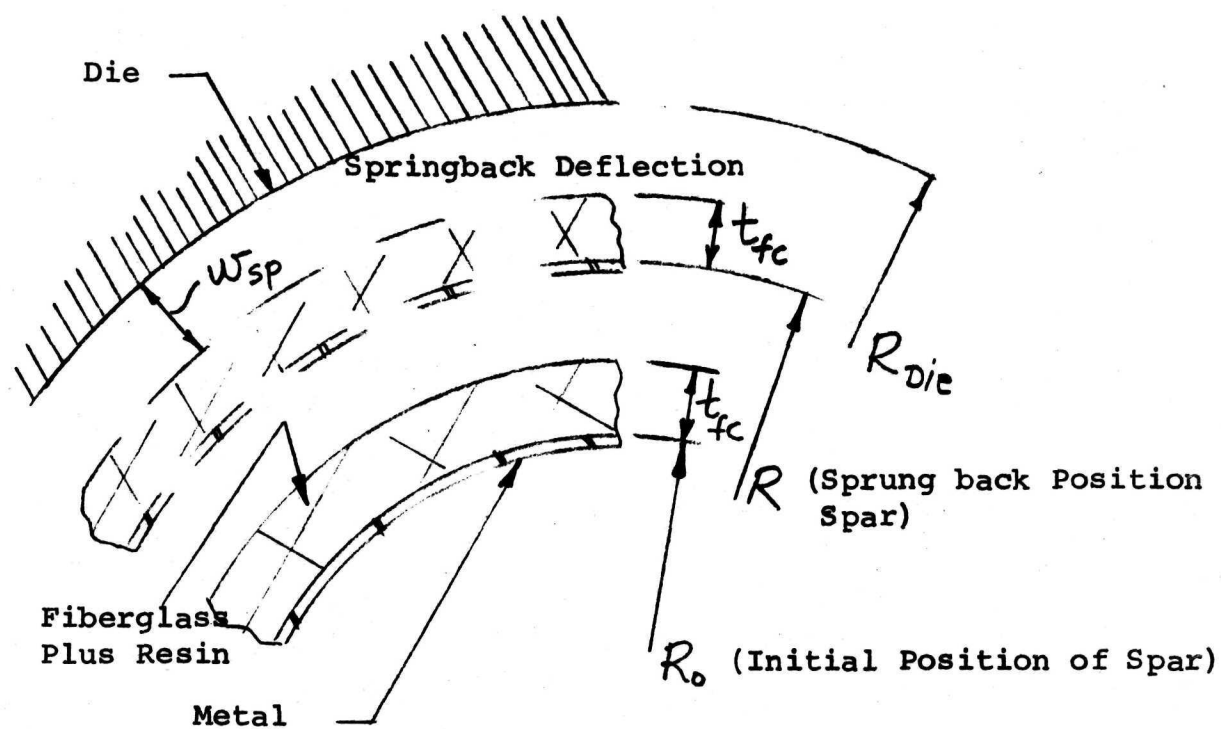


FIGURE A-6

SPAR DEFLECTION AND SPRINGBACK

For purposes of estimating the elastic springback take metal stresses at cryogenic and room temperature conditions as, $\sigma_{\theta c} = 230$ ksi, $\sigma_{xc} = 115$ ksi and $\sigma_{\theta i} \approx 0$, $\sigma_{xi} \approx -60$ ksi respectively. Then,

$$\Delta(\epsilon_{\theta}) = \frac{\Delta\sigma_{\theta} - .3 \Delta\sigma_x}{E_M} + \Delta(\alpha T)$$

$$\Delta\epsilon_{\theta} - \Delta(\alpha T) = \frac{(230 - 0) - .3 \{115 - (-60)\}}{25 \times 10^6} \approx 7 \times 10^{-3}$$

Now, $\Delta(\alpha T) \approx 10^{-3}$ thermal strain, so that

$\Delta\epsilon_{\theta} .008$ in/in. (hoop elastic springback strain

We compute the hoop strain, , from (A-73) and numerical data as shown in Table 5 below.

TABLE 5 - HOOP STRAIN CALCULATIONS

S/N	t_{fc} See Table 4	R_{Die}	R_o	$W_{sp} =$ $R_o \Delta\epsilon_{\theta}$	$\Delta = t_{fc}$ $+ W_{sp}$	$R =$ $R_{Die}^{-\Delta}$	$\Delta R =$ $R - \bar{R}_o$	$\epsilon =$ $\Delta R / R_o$	Estimated plastic hoop strain (metal) SAY $\approx .134$
		Basic Data							
4	.054	1.80	1.53	.012	.066	1.734	.204	.134	
4	.054	2.96	2.55	.020	.074	2.886	.336	.132	
5	.051	1.80	1.53	.012	.063	1.737	.207	.135	
5	.051	2.96	2.55	.020	.071	2.889	.339	.133	

at $1 + \epsilon = \frac{R_p}{R_o} = 1.134$, $\sigma_T \approx 225$ ksi (from cylinder design curve Heat #76235 Figure 3)

{O.K. close to 230 ksi hoop stress assumed above}

This checks consistency of assumed cryogenic stress state in metal with estimated plastic hoop strain, (See Figure 3).

6.3.3 Estimate of Hoop Strain Based on Diameter Measurements (Before & After Cryo-Stretch)

Strain compatibility at $\theta = 60^\circ$, see Figure A-7, forces "averaging" of strains. Symmetry and die force final body shape to be essentially similar to initial body shape. We, thus can define hoop strain as change in total perimeter divided by initial perimeter, i.e.,

$$\text{hoop strain} \equiv \epsilon_\theta = \frac{d\Gamma}{\Gamma} \quad (\text{A-74})$$

From geometry,

$$\Gamma = \text{perimeter} = 4 \left(R_A \frac{\eta}{3} + R_B \frac{\eta}{6} \right) = \frac{2}{3} \eta (2R_A + R_B) \quad (\text{A-75})$$

$$d\Gamma = \frac{2}{3} \eta (2dR_A + dR_B) \quad (\text{A-76})$$

$$\epsilon_\theta = \frac{(2 dR_A + dR_B)}{(2 R_A + R_B)} \quad \text{and from (A-74) to (A-76)} \quad (\text{A-77})$$

From geometric considerations we obtain expressions for "minor" and "major" diameters as,

$$\left. \begin{aligned} X &= R_A + R_B \\ X + dX &= (R_A + dR_A) + (R_B + dR_B) \end{aligned} \right\} \quad (\text{A-78})$$

$$\left. \begin{aligned} Y &= R_A (\sqrt{3}) + R_B (2 - \sqrt{3}) \\ Y + dY &= (R_A + dR_A) (\sqrt{3}) + (R_B + dR_B) (2 - \sqrt{3}) \end{aligned} \right\} \quad (\text{A-79})$$

and compute the hoop strain using (A-77) to (A-79) as detailed in Table 6.

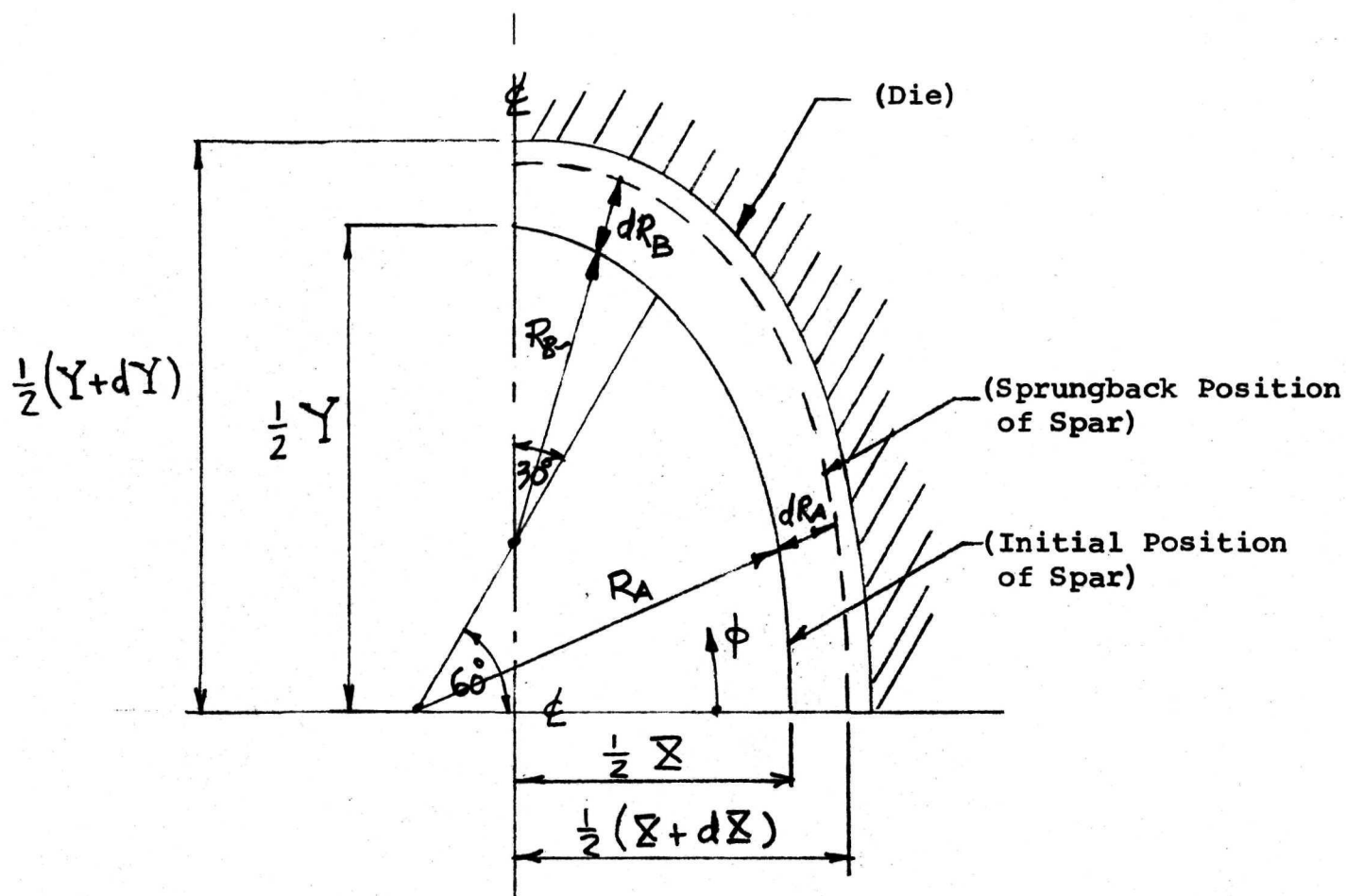


FIGURE A-7

SPAR AND DIE GEOMETRY

TABLE 6 SPAR MEASUREMENT DATA CORRELATION

S/N	t_c	t_{cx}^*	t_{cy}^*	\bar{X}_O^\oplus	\bar{Y}_O^\oplus	$\bar{X}_O^\oplus + dX_O$	$\bar{Y}_O^\oplus + dY_O$	\bar{X}	\bar{Y}	$\bar{X}+d\bar{X}$	$\bar{Y}+d\bar{Y}$	R_A	R_B
4	.054	.050	.024	4.180	4.875	4.835	5.421	4.080	4.827	4.735	5.373	2.55	1.53
5	.051	.053	.023	4.186	4.872	4.838	5.427	4.080	4.826	4.732	5.381	2.55	1.52

S/N	$R_A + dR_A$	$R_B + dR_B$	dR_A	dR_B	$2dR_A + dR_B$	$2R_A + R_B$	$\epsilon_\theta = \frac{2dR_A + dR_B}{2R_A + R_B}$ (See Figure A-7) (Hoop strain metal)
4	2.803	1.932	.253	.402	.908	6.63	.137
5	2.809	1.923	.259	.393	.911	6.63	.137

Agrees with estimate results based on preform & die data (See Table 5)

This checks consistency of hoop strain based on preform & die data with above results based on measured spar diameter data before and after cryostraining.

* \oplus Measurements (with subscript, 0) are to outside of fiber-glass. They include composite fiber thickness (glass & resin), i.e.,

$$\bar{X}_O = \bar{X} + 2t_{cx}; \quad \bar{Y}_O = \bar{Y} + 2t_{cy}$$

Composite thickness t_{cx} and t_{cy} are determined from initial spar diameter measurements prior to cryostretch, e.g.,

$$\bar{X}_O = 4.186 = \bar{X} + 2t_{cx} = (R_A + R_B) + 2t_{cx}$$

$$4.186 = (2.55 + 1.53) + 2t_{cx}; \quad t_{cx} = .053$$

6.3.4 Estimate of Fiber Strain Based on Measured Fiber Angles and Hoop and Longitudinal Strains

From Figure A-3 we have from geometry,

$$a^2 (1 + \epsilon_x)^2 + b^2 (1 + \epsilon_\theta)^2 = c^2 (1 + \epsilon_f)^2$$

$$a^2/c^2 (1 + \epsilon_x)^2 + \frac{b^2}{c^2} (1 + \epsilon_\theta)^2 = (1 + \epsilon_f)^2$$

Noting that $\sin \alpha = b/c$, $\cos \alpha = a/c$, we have,

$$\cos^2 \alpha (1 + \epsilon_x)^2 + \sin^2 \alpha (1 + \epsilon_\theta)^2 = (1 + \epsilon_f)^2 \quad (A-80)$$

which defines relation between strains and original fiber angle.

Using (A-12) in (A-80) gives,

$$\cos^2 \alpha (1 + \epsilon_x)^2 + \sin^2 \alpha (1 + \epsilon_\theta)^2 = (1 + \epsilon_\theta)^2 \frac{\sin^2 \alpha}{\sin^2 \alpha'}$$

After simplification we obtain,

$$(1 + \epsilon_x) = \tan \alpha \cot \alpha' (1 + \epsilon_\theta) \quad (A-81)$$

which defines metal longitudinal and hoop strains in terms of initial and final fiber angles.

For S/N 4 and 5

$$(1 + \epsilon_\theta) = 1.137 \quad (\text{See Table 6})$$

Take now,

$$\alpha' = 20.5^\circ \quad (\text{measured fiber angle, after cryostretch and spring-back to R. T. See Table 8}).$$

$$\alpha = 18^\circ \quad (\text{approximate average angle over large radius region at middle area of spar})$$

$$\frac{\sin \alpha}{\sin \alpha'} = \frac{.0390}{.3502} \quad , \text{ From (A-12) we have,}$$

$$(1 + \epsilon_x) = 1.137 \times \frac{.3090}{.3502} = 1.00323$$

$$\epsilon_f = .00323 \quad (\text{in/in}) \quad \text{fiber prestrain}$$

$$\tan \alpha \cot \alpha' = .869$$

Then from (A-81),

$$(1 + \epsilon_x) = .869 \times 1.137 = .988, \text{ or we have}$$

$$\epsilon_x = -.012 \text{ (in/in)}$$

as the metal longitudinal compressive prestrain which is compatible with hoop strain and fiber angles above. This should now be compared with measured longitudinal strain data to check consistency of results.

Measured axial strain and fiber angle data are given in Tables 7 and 8. Figure A-8 defines the gage points for axial strain.

Hoop strain magnitudes based on "selected" axial strain data (See Table 9) appear to agree reasonably well with computed values based on diameter measurements and wrapped preform and die data. However, improved measurement techniques are needed primarily for axial strain determination and less so for fiber angle measurements. Spar diameter measurement accuracy is considered adequate (micrometer measurement technique used).

The axial strain data is suspect due to measurement difficulties and influence of head strain (See Figure A-8).

- (1) Gage marks were irregular and of variable width due to difficulty of marking fiberglass surface. This posed length measurement problems.
- (2) Gage lengths C and D were short and near head region.
- (3) Overall length reduction (gage length, E) probably correct, but significant shortening is due to heads.
- (4) For data correlation, therefore, rely on measurements taken at gage lengths A and B as detailed in Table 9 using $\alpha = 18^\circ, \alpha' = 20.5^\circ$ for correlation).

6.3.5 Estimate of Spar Prestress State Based on Strain Data and Equilibrium Requirements

Using Hooke's Law, the fiber prestress is obtained as,

$$\sigma_f' = E_f \epsilon_f \quad (\text{A-82})$$

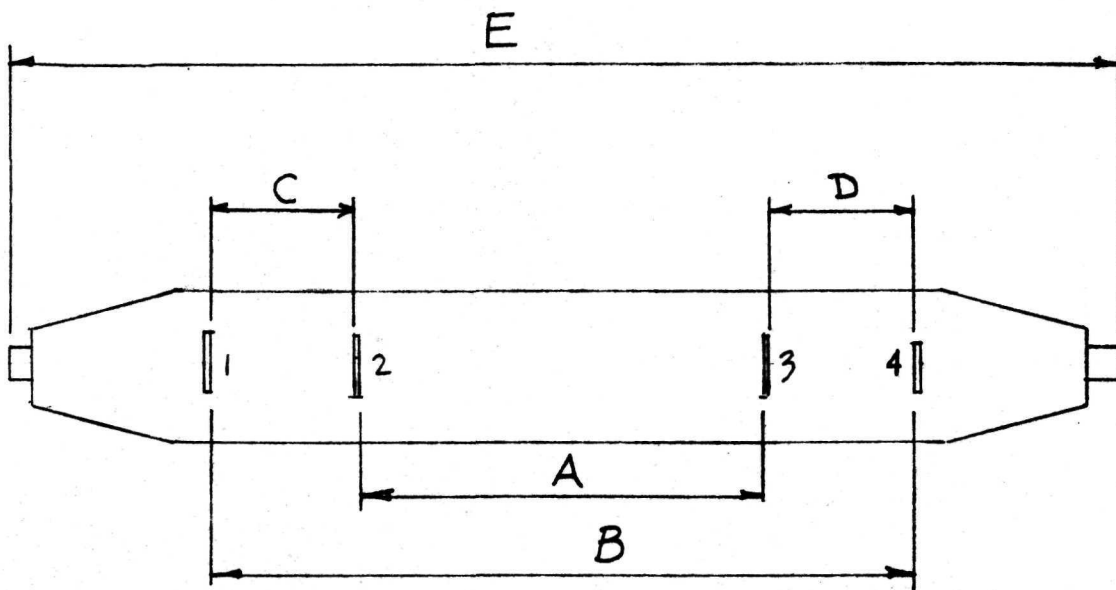


FIGURE A-8

GAGE POINTS FOR AXIAL STRAIN

TABLE 7 - AXIAL STRAIN MEASUREMENT DATA

	S/N	A	B	C	D	E	Remarks
L (in)	5	12.767	19.690	3.250	3.700	33.900	Before cryostretch
	5	(12.580)	(19.490)	(3.190)	(3.610)	(33.272)	After cryostretch
ΔL (in)		-.187	-.200	-.060	-.090	-.718	(Measured near middle of large radius portion of cross-section)
$\frac{\Delta L}{L} = \epsilon_x$		-.0146	-.0102	-.0185	-.0243	-.0211	
L	4	13.747	19.125	2.570	2.770	33.990	Before cryostretch
	4	(13.532)	(18.865)	(2.560)	(2.690)	(33.300)	After cryostretch
ΔL		-.215	-.260	-.010	-.080	-.690	(Measured near middle of large radius portion of cross-section)
$\frac{\Delta L}{L} = \epsilon_x$		-.0156	-.0136	-.0039	-.0289	-.0203	

TABLE 8 - MEASURED FIBER ANGLES
AFTER CRYOSTRETCH & SPRINGBACK TO ROOM TEMPERATURE

S/N	$(2\alpha')^*$	
4	}	$41 \rightarrow 42^\circ$
5		$41 \rightarrow 41.5^\circ$
		$2\alpha' \text{ average } \approx 41^\circ \text{ at large radius region at spar middle section}$
		$\alpha' = 20.5^\circ$

*Fiber directions traced on tracing paper and angles determined by intersection of lines joining traced points.

TABLE 9 - STRAIN DATA CORRELATION

S/N	$(1 + \epsilon_x)$ See Table 7	$\tan \theta \cot \theta$	$(1 + \epsilon_\theta)$ (See A-81)	ϵ_θ	ϵ_θ (See Table 6)	ϵ_θ (See Table 5)
4	A .9854	.869	1.134	.134	.137	.132
4	B .9898		1.139	.139		to
4	$(\frac{A+B}{2})$.9876		1.136	.136		.134
5	A .9844		1.133	.133		.133
5	B .9864		1.135	.135		to
5	$(\frac{A+B}{2})$.9854	.869	1.134	.134	.137	.135

Here, E_f = Young's Modulus of Fiberglass
 $= 12.4 \times 10^6 \text{ \#/in}^2$ at room temperature

Take now $\epsilon_f = .00323 \text{ in/in}$ (See Section 6.3.4)
as most probable value for fiber strain. This yields from
(A-82),

$\sigma_f' = 12.4 \times 10^6 \times .00323 = 40.3 \text{ ksi}$ spar fiberglass
tensile prestress.

Using equations (A-7) and (A-8) with the
equilibrium requirements at the prestressed (zero external
load state) we obtain (see Section 6.2.1.5),

$$\Sigma F_{\text{hoop}} = 0 = \sigma_{f\theta}' t_f + \sigma_{M\theta}' t_M = \sigma_f' \sin^2 \alpha' t_f + \sigma_{M\theta}' t_M \quad (\text{A-83})$$

$$\Sigma F_{\text{longitudinal}} = 0 = \sigma_{fx}' t_f + \sigma_{Mx}' t_M = \sigma_f' \cos^2 \alpha' t_f + \sigma_{Mx}' t_M \quad (\text{A-84})$$

Taking $\alpha' = 20.5^\circ$, $t_f = 36 \text{ mils}$, $t_M = 25.5 \text{ mils}$
and $\sigma_f' = 40.3 \text{ ksi}$ (see Tables 4, 8 and above) we have from
(A-83) and (A-84),

$$\sigma_{M\theta}' = -\sigma_f' \sin^2 \alpha' \frac{t_f}{t_M} = -40.3 (.350)^2 \times \frac{36}{25.5} = -7.0 \text{ ksi} \left. \vphantom{\sigma_{M\theta}'} \right\} \begin{array}{l} \text{metal hoop} \\ \text{compressive} \\ \text{prestress} \end{array}$$

$$\sigma_{Mx}' = -\sigma_f' \cos^2 \alpha' \frac{t_f}{t_M} = -40.3 (.937)^2 \times \frac{36}{25.5} = -50 \text{ ksi} \left. \vphantom{\sigma_{Mx}'} \right\} \begin{array}{l} \text{metal} \\ \text{longitudinal} \\ \text{compressive} \\ \text{prestress} \end{array}$$

6.4 Appendix 4 - Composite Spar Test Specification

ARDE, INC. Test Specification ATS-100, "Composite Metallic Fiberglass Prestressed Spar Structural Model Tests", is contained in this section.

ARDE TEST SPECIFICATION (ATS-100)

Composite Metallic - Fiberglass Prestressed Spar

Structural Model Tests

NASA Contract NAS 1-10028

ARDE J/N 41003-1

1. Objective

The objective of this specification is to define the requirements for testing prestressed composite metallic-fiberglass spar structural models.

2. Purpose of Tests

The purpose of the tests is to provide information regarding prestressed composite spar structural and materials properties which may be compared to data on homogeneous material spars without prestress.

3. Reference Documents

Arde Drawings:

D 3817	Weldment Assembly, Preform Spar-Composite
C 104624	Boss
D 104622	Head
D 104623	Body
D 3818	Preform Assembly, Fiber Wrapped Spar-Composite
D 3819	Spar-Composite Assembly

4. Description of Tests

4.1 General

Two basic types of tests are required, static and cyclic load tests. A constant axial tensile force, Q , shall be applied to the composite spar in all tests. The preferred method for

axial loading is to apply and react the axial force, Q, through the threaded central bosses on each composite spar head. The magnitude of axial force Q is approximately 10,000 lbs.

A description of the number and type of tests, as well as specimen type and identification is given in Table I below. Arde will provide the specimens complete with inspection data.

TABLE I

Type of Test	No. of Tests	Type of Specimen	No. of Specimens Required
Static } Bending	1	Smooth prestressed composite spar	1
	1	Smooth prestressed composite spar	1
Cyclic Loading } Bending Fatigue	2	Smooth prestressed composite spar	2
	2	Precracked prestressed composite spar	2
	1	Precracked homogeneous metal spar (without prestress) metal to be the same and processed the same as metal liners for composite spar specimens	1

4.2 Static Load Tests

Two types of static load tests are required, bending and torsion, both combined with axial tension loading (see 4.1 above). The loading and support methods used must insure that specimen failure occurs in the constant cross-section region of the composite spar, far away from load or support regions so as to eliminate edge effects. Shear, bending and torsion loads may be applied to the composite spar heads inboard of the boss to head girth weld provided that such loads are distributed in a manner which will prevent failure or excessive distortion of the heads.

4.2.1 Static Bending Test

The spar specimen shall be tested as an axially and transversely loaded beam. The preferred method of loading and support is that which produces a constant bending moment over the central composite spar body region.

The bending moments shall be applied first about the strong axis of the composite spar and after completion of this test, the moments then shall be applied about the weak axis of the composite spar. The magnitude of the maximum bending moment applied about the strong axis of the spar shall be limited to a value which will not yield, buckle or significantly distort the spar. The magnitude of the bending moment applied about the weak axis of the spar shall be continuously increased until spar failure occurs. Spar transverse deflections and axial strains both shall be monitored independently as a function of applied bending moment in such a way as to provide for check measurements and to permit determination of both bending and direct axial strains.

Data required from the prestressed composite spar static bending (plus axial load) test are as follows:

- a) Bending rigidities of the composite spar as a function of applied moment for bending about both the weak and strong composite spar axes.
- b) Axial (extensional) rigidity of the composite spar.
- c) Initial axial stresses in the composite spar at zero external load.

4.2.2 Static Torsion Test

The composite spar shall be tested as an axially loaded beam subjected to an applied torque. Both spar torsional angle of rotation and fiber extensional strains shall be monitored as a function of applied torque in such a manner as to provide check measurements and to permit determination of axial stresses in the composite spar. The applied torque shall be continuously increased until failure occurs. Data required from the pre-stressed composite spar static torsion (plus axial load) test are as follows:

- a) Torsional rigidity of the composite spar as a function of applied torque.
- b) Initial axial stresses in the composite spar at zero external load.

4.3 Cyclic Load Tests

4.3.1 General

Two types of cyclic bending load tests shall be performed, fatigue and crack propagation. The spar specimens shall be supported and loaded in the manner described for the static bending (plus axial load) tests (Sections 4.2, 4.2.1), except that the bending moments shall be applied only about the spar weak axis and the moments shall be cyclic in nature, cycling about zero mean values from positive maximums to identical magnitude negative maximum values. The magnitude of the maximum bending moment to be applied to the spar specimens is approximately 20,000 inch lbs. The frequency of the applied moments shall be in the range of 20 - 30cps. The cyclic tests shall be run for a total of 10^7 cycles, or failure, whichever occurs first. Cyclic bending testing shall be halted at intervals

for specimen inspection and/or performance of other tests as described below.

4.3.2 Cyclic Bending Fatigue Test

a) Natural Frequency and Damping Factor

Spar specimen fundamental natural frequency in bending and damping factor shall be determined prior to fatigue testing and at two (2) times during fatigue testing. The bending fatigue testing shall be halted as required to permit this data to be obtained.

b) Fatigue Testing

The applied loads, loading frequency and specimen condition shall be monitored. The number of cycles required to produce a fatigue failure in the composite spar shall be determined. The specimen shall be visually inspected after test (or failure) and at test halt intervals for natural frequency determinations.

4.3.3 Cyclic Bending Crack Growth Test

The applied loads, loading frequency and specimen condition shall be monitored. The metal liner of the composite spar specimen will have a partial thickness crack located on the flat portion of the spar constant cross-section region at the spar center. The crack length shall be in the hoop direction (so far as is possible). A suitable small gap in the composite spar specimen fiberglass wrap will be provided to facilitate initial crack forming and subsequent monitoring of crack growth. The cyclic bending moments shall be applied so that the crack will be subjected to tensile bending loads. Data required is crack length at discreet values of number of cycles. Four (4) such data points, including crack length at initiation of fatigue crack extension, are required. Cyclic loading shall be stopped

to facilitate monitoring of crack length and spar specimen inspection.

5. Documentation and Data

5.1 Test Plan and Procedures

A document describing the proposed test plan and procedures shall be submitted to Arde for approval prior to testing. Three (3) copies of this documentation are required.

5.2 Test Report

Three (3) copies of a test report shall be submitted to Arde within thirty (30) days following completion of testing. The report shall include a summary of the test results, complete test data, a description of the tests, test methods and test equipment as well as appropriate 3" x 5" black and white photographs and other sketches and illustrative material required to adequately document the testing.

7.0 DISTRIBUTION LIST FOR FINAL REPORT - NASA CR-112191
Contract NAS 1-10028
ARDE, INC.

No. of Pages

National Aeronautics & Space Administration	
Langley Research Center	
Hampton, Virginia 23365	
Attention: 122/Report & Manuscript Control Office	1
115/Raymond L. Zavasky	1
139A/Technology Utilization Office	1
249/John F. Ward	5

National Aeronautics & Space Administration	
Ames Research Center	
Moffett Field, California 94035	
Attention: 202-3/Library	1

National Aeronautics & Space Administration	
Flight Research Center	
P. O. Box 273	
Edwards, California 93523	
Attention: Library	1

Jet Propulsion Laboratory	
4800 Oak Grove Drive	
Pasadena, California 91103	
Attention: 111-113/Library	1

National Aeronautics & Space Administration	
Manned Spacecraft Center	
2101 Webster Seabrook Road	
Houston, Texas 77058	
Attention: JM6/Library	1

National Aeronautics & Space Administration	
Marshall Space Flight Center	
Huntsville, Alabama 35812	
Attention: Library	1

National Aeronautics & Space Administration	
Lewis Research Center	
21000 Brookpark Road	
Cleveland, Ohio 44135	
Attention: 60-3/Library	1
49-1/Raymond F. Lark	1

National Aeronautics & Space Administration
Goddard Space Flight Center
Glen Dale Road
Greenbelt, Maryland 20771
Attention: Library 1

National Aeronautics & Space Administration
John F. Kennedy Space Center
Kennedy Space Center, Florida 32899
Attention: IS-DOC-12L/Library 1

National Aeronautics & Space Administration
Washington, DC 20546
Attention: KSS-10/Library 1
RA/NASA Headquarters 1

Union Carbide Corporation
Carbon Products Division
P. O. Box 6116
Cleveland, Ohio 44101
Attention: Director, Research & Advanced Technology 1

HITCO
P. O. Box 1097
Gardena, California 90249
Attention: Librarian, Materials Science Center 1

U. S. Army Air Mobility Research & Development Lab.
Eustis Directorate
Structures Division
Fort Eustis, Virginia 23604 1

Bell Helicopter Company
P. O. Box 482
Fort Worth, Texas 76101 1

The Boeing Company
Vertol Division
P. O. Box 16858
Philadelphia, Pennsylvania 19142
Attention: Librarian 1

Doman Helicopters, Inc.
P. O. Box 609
Danbury, Connecticut 06810
Attention: Director of Research & Development 1

No. of Pages

Fairchild-Hiller Corporation Helicopter Development Center Farmingdale, New York 11735	1
Gyrodyne Company of America, Inc. Flowerfield, St. James, New York 11780	1
Hughes Tool Company Aircraft Division Culver City, California 90230	1
Kaman Aircraft Division Kaman Corporation Old Windsor Road Bloomfield, Connecticut 06002	1
Attention: Mr. Donald W. Robinson, Jr.	1
Kellett Aircraft Corporation Central Airport Camden, New Jersey 08109	1
Lockheed Aircraft Corporation Lockheed-California Company Burbank, California 91503	1
United Aircraft Corporation Research Laboratories East Hartford, Connecticut 06108	1
United Aircraft Corporation Sikorsky Aircraft Division Stratford, Connecticut 06497	1
National Aeronautics & Space Administration Scientific & Technical Information Facility P. O. Box 33 College Park, Maryland 20740	11 plus 01 reproducible